STUDY OF THE HIGH FIELD Q-SLOPE USING THERMOMETRY

A Dissertation
Presented to the Faculty of the Graduate School
of Cornell University
in Partial Fulfillment of the Requirements for the Degree of
Doctor of Philosophy

by
Grigory Victorovich Eremeev
August 2008

STUDY OF THE HIGH FIELD Q-SLOPE USING THERMOMETRY

Grigory Victorovich Eremeev, Ph.D.

Cornell University 2008

The high field Q-slope and the mild baking effect in 1.5 GHz superconducting radio frequency niobium cavities were studied experimentally within the framework of current models, which are the interface tunnel exchange, the magnetic field enhancement and the modified oxygen pollution models.

Regarding the high field Q-slope, we found that the high field Q-slope in 1.5 GHz superconducting niobium cavities starts at 105±5 mT in all cavities after chemical treatment. The thermometry system indicated that the high field Q-slope is a magnetic field effect. It also showed that it is not a local effect, i.e. all thermometers in the magnetic field region show non-quadratic losses at fields above 105±5 mT, the high field Q-slope. The slope in a given region depends on the strength of magnetic field, i.e. it is bigger, where the magnetic field is stronger.

Regarding the mild baking effect, we discovered that the mild baking effect in the case of 100° C baking for 48 hours occurred to the depth of about 20 nm for cavities, treated by EP and by BCP.

Regarding the present models for studied effects, we conclude that neither of them give a satisfactory explanation of the data collected: the interface tunnel exchange failed to account for the preferential heating in the magnetic field regions, the magnetic field enhancement model failed to account for high-field-Q-slope's heating in areas without grain boundaries, the modified oxygen pollution model failed to account for the high temperature baking. As an alternative

we propose a new model for the mild baking effect, an oxide-purifier model.

BIOGRAPHICAL SKETCH

Grigory Victorovich Eremeev was born on February 28, 1981, in Moscow, Russia. In 1998 he entered the Moscow Institute for Physics and Technology, from which he graduated in May, 2002, with Bachelor of Science in applied physics and mathematics. The same year he entered the graduate program in physics at Cornell University. He graduated from Cornell University in 2008.

ACKNOWLEDGMENTS

Due to Graduate School requirements this chapter was modified from its original length of 27 pages to a mere page. I deeply apologize to all people, whom I unwillingly do not mention in the shortened version. I do acknowledge you and your help. Thank you!

First, in this short version I, though being agnostic, would like to acknowledge God: for I am finally finishing writing this thesis. Of course, I would not have done that, or would not have done that on time, or would not have done that properly, without the persistent guidance of my supervisor, Hasan Padamsee. Most of all I deeply appreciate his patience without which my graduate studies might have been terminated unhappily on a few occasions.

Second, I appreciate all scientists, not-so-scientists and non-scientists, I have been communicating with and have learned so much from during my study at Cornell University, during conferences, workshops and schools, and during occasional visits to different places.

Finally, I am grateful to my family and friends, and friends, and friends.

TABLE OF CONTENTS

LIST OF FIGURES

LIST OF TABLES

CHAPTER 1

INTRODUCTION

Success of science and technology helps us to understand how unsuccessful we are in understanding the Universe. Currently, it is agreed that we understand about 5 percent of the matter and energy composing the Universe. The rest, 95 percent, is something we know very little about. We call this 95 percent of unknown land ”dark energy” and ”dark matter”.

An experiment is about to start this year, 2008, in CERN, which, as many believe, will explore the new territory. But to map out this land an even more sophisticated tool is proposed, the International Linear Collider(ILC). If dark-matter particles have masses in the TeV scale, they will be found in LHC, but to verify that these particles are indeed related to ”dark matter” postulated, a precise measurement of their properties, i.e. mass, spin, parity, will be needed.

Feasibility of many ILC components is being studied now in many universities and laboratories around the world. On 20 August 2004 the International Technology Recommendation Panel recommended superconducting technology for the main linac design. Many kilometers of superconducting cavities must be built, installed and operated continuously in ILC.

In 2005, when this thesis was first proposed, a good estimate for linac construction was 100.000 dollars per meter. Using this value, we describe the relation between total construction cost of a superconducting linac and the accelerating gradient of the cavity:

$$Construction\ cost = 100000 \cdot \frac{2E_{beam}}{E_{acc}} \tag{1.1}$$

, where E_{beam} is energy of beam, which is proposed to be 250 GeV for ILC and E_{acc} is operating gradient of the cavity. So one would like to have as high as

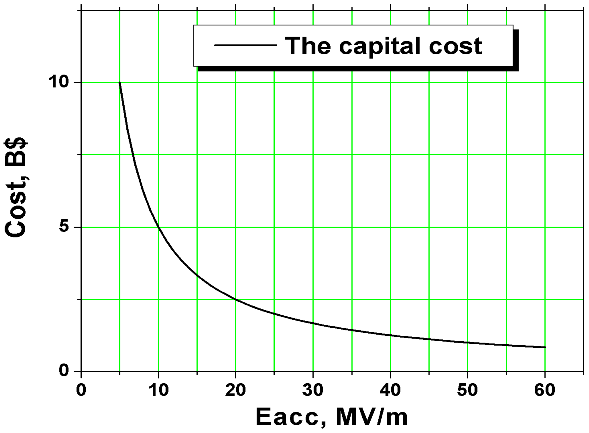

Figure 1.1: Construction cost.

possible an accelerating gradient in superconducting cavities. This goal posses interesting physical questions about the superconducting properties of niobium at high RF fields.

Also, once the linac is installed, the quality factor of the cavity at high fields must be high in order to keep operating costs under control. Our goal is to understand why RF losses increase exponentially at high RF fields. We study different cavity materials and preparation procedures to determine their influence on cavity losses. Our physics goal therefore is to learn the mechanisms that cause excessive losses at high RF fields. Such understanding will eventually create paths toward high performance cavities. The physics behavior of superconducting niobium cavities at high RF fields is the main topic of this thesis.

The thesis is organized as follows, in the following Chapter we introduce RF cavity terminology by presenting a well-known, but necessary, outline of superconductivity and RF cavity basics. Chapter 3 is devoted to experimental setups and techniques. In the fourth chapter we review models for the high field performance of superconducting cavities and related literature, and lay out the plan of experimental work. In the fifth and sixth Chapters we summarize RF and thermometry diagnostics general results for high field behavior of superconducting cavities. We present anodizing experiments in Chapter 7. In the Chapter 8 the results with large grain cavities and contribution to losses from grain boundaries are discussed. Experimental results related to contribution of niobium oxide to losses at high field is discussed in Chapter 9. The conclusions are drawn in Chapter 10.

CHAPTER 2

RADIO FREQUENCY CAVITIES AND SUPERCONDUCTIVITY

2.1 Superconductivity

On July 10^{th}, 1908 H. Kamerlingh Onnes became the first who succeeded in liquefying helium and thus extended available temperature range below liquid hydrogen temperatures. As it is usual in experimental physics, fun began after regular working hours:"*The surface of the liquid was soon made clearly visible by reflection of light from below, and that unmistakably because it was clearly pierced by the two wires of the thermoelement. This was at 7.30 p.m.*" [1].

One of experiments, which were carried out with newly acquired liquid helium, was designed to test a then-modern theory of resistance of metals at low temperatures. Contrary to expectations they found out that resistance of pure metals such as gold and platinum decreases as a function of temperature down to 1.5 °K:"*In view of this result, then, we must abandon the theory that has served for years as a guide in our Leiden researches upon the resistance of metals at low temperature, according to which it was imagined that the resistance would attain a minimum as the temperature was lowered and would become infinitely great at T=0, in consequence of the assumption that the electrons which are actual conductors in metals would, as was expressed by me in 1904, begin to precipitate on the atoms as a vapour on being cooled to hydrogen temperatures, or as Koenigsberger - in a manner leading to a similar dependence upon temperature - explains the phenomenon that was then supposed to exist, by the recombination of the electrons that had been freed by dissociation*" [2]. A greater surprise lay ahead in experiments with mercury: they failed to measure the resistance of mercury at temperatures below 4.2 °K :"*These measurements* *showed that from the melting point hydrogen to the neighbourhood of the boiling point of helium the curve exhibited the ordinary gradual lessening of the rate of diminution of resistance, practically the same as given by the formula of Comm. N.119. A little above and a little below the boiling point, from 4.29 ^{0}K. to 4.21 ^{0}K. the same gradual change was clearly evident(cf. the fig.), but between 4.21 ^{0}K. to 4.19 ^{0}K. the resistance diminished very rapidly and disappeared at 4.19 ^{0}K.(Temperature measurements are here given with 4.25 ^{0}K. as the boiling point of helium)"* 2.1 [3]. The infinite conductivity, which was discovered in the search for infinite resistance, is called superconductivity. The temperature, at which resistance becomes immeasurable, is called critical temperature of superconductor, T_c.

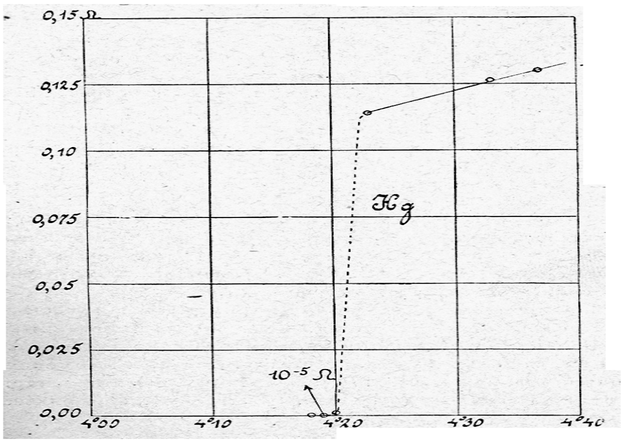

Figure 2.1: The original plot by H. Kamerlingh Onnes shows absence of resistance below 4.20^{0} K.

Later H. Kamerlingh Onnes found a loss of resistance for tin below 3^{0} K and an absence of resistance for lead in the whole range of liquid helium temperatures [4]. Considering a future use of superconductors he set out on investigating magnetic properties of these materials in the superconducting state and discovered that he can measure the resistance of lead brought into a magnetic field of 1000 Gauss. The transition between normal and superconducting states occurred at a certain magnetic field for given temperature similarly to the transition at critical temperature in zero magnetic field 2.2 [5]. The magnetic field was called critical field of superconductor. We will refer to the critical field, at which the bulk of a superconductor transits to normal conducting state as thermodynamic critical field, H_c. H. Kamerlingh Onnes also proposed an

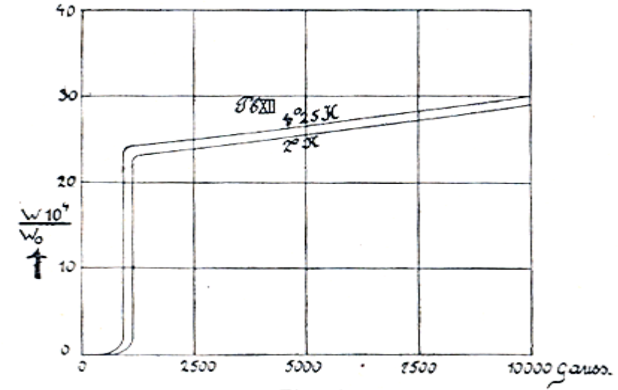

Fig. 1.

Figure 2.2: The original plot by H. Kamerlingh Onnes shows appearance of resistance for elevated magnetic fields.

experiment that would extend the sensitivity of resistance measurement in superconducting materials:*"If a current is generated in a closed supraconductor, from which no other work is required than what is necessary to overcome the possible remaining micro-residual resistance of the conductor, it follows, from the small value that the micro-residual resistance can have the most, that the current will continue for a considerable time after the electromotive force that set it in motion has ceased to work"* [6]. From the outcome of the experiment he placed the upper limit of resistance to $2 \cdot 10^{-11}$ of the ordinary resistance at room temperature. At present, on the same basis on which electron-nuclei system is considered absolutely stable, the resistance of superconductor is considered to be exactly zero.

Leiden held a monopoly on liquid helium until 1923, when a helium liquefier was installed at University of Toronto. In 1927 a helium liquefier capable of 10 liters per hour started at the Physikalisch-Technische Reichsanstalt near Berlin.

This group led by W. Meissner reported in 1930 the discovery of superconductivity in niobium with T_c=9.2 °K [7]. Niobium, which is the main topic of this thesis, is the pure element with the highest T_c under normal conditions. The critical temperature measured in monocrystal high purity niobium(RRR=5000) was reported to be 9.2877 °K [8]. The critical field H_c measured in monocrystal high purity niobium(RRR=4000) was reported to be 2061 Gauss [9].

In 1933 W. Meissner and R. Ochsenfeld performed an experiment, that triggered development of theories of superconductivity [10]. In their experiment they researched a magnetic field distribution near two cylinders that are cooled down below T_c. At temperatures above the transition temperatures the magnetic field is almost undisturbed by the specimens(they used lead and tin in their experiment, which are weak diamagnetic and paramagnetic respectively). As they reduced the temperature, the magnetic field was altered in such a way, as if it was completely expelled from the interior of the superconductor, which was contrary to the existing view, i.e. magnetic field is frozen in the superconductor. One may express surprise that it took more than twenty years to realize that superconductors are perfect diamagnetic materials. Firstly this fact was hindered by early experiments of H. Kamerlingh Onnes, in which he put a superconductor in magnetic field above the transition temperature; then below transition he turned the field off and saw that the superconductor creates magnetic field. Only in his experiments he used a superconducting loop, to see how low the resistance of the superconductor is, and therefore the magnetic field was contained in the loop, but not in the superconductor itself. Secondly due to a poor quality of the samples some flux indeed was pinned on the impurities.

After W. Meissner and R. Ochsenfeld's discovery it was realized that superconducting state is a thermodynamic state, i.e. the state of a superconductor is determined by external parameters and does not dependent on history. And shortly after C.J.Gorter and H.Casimir put forward a theory that accounted for some superconducting phenomena and that presented a clear picture of superconductivity. They suggested that upon superconducting transition a number of electrons turn ″super″ and these, now ″super″ electrons, can carry a small current without losses. As the temperature goes closer to absolute zero the number of ″super″ electrons increases and the number on normal electrons decreases. In order to explain experimental results, C.J.Gorter and H.Casimir argued that the free energy of the electrons gas in the superconductor takes a rather peculiar form [11]:

$$F(n,T) = \sqrt{n} \cdot f_n(T) + (1-n) \cdot f_s(T)$$

, where n represented the fraction of normal conducting electrons, and

$$f_n(T) = -\frac{1}{2}\gamma T^2$$

$$f_s(T) = -\beta = const$$

Here $f_n(T)$ represents the electronic free energy in normal metal, so that the free energy of superconducting and normal phases agree when $(1-n) \rightarrow 0$. Then by minimizing $F(n,T)$ with respect to n for fixed T, one finds that the fraction n of ″normal″ electrons at a temperature T is given by

$$n = \Big(\frac{T}{T_c}\Big)^4$$

, where $T_c = \sqrt{\frac{4 \cdot \beta}{\gamma}}$. From the thermodynamic relation:

$$\frac{H_c^2(T)}{8\pi} = F_n(T) - F_s(T)$$

one can derive the temperature dependence of the thermodynamic critical field:

$$H_c(T) = H_0\Big(1 - \Big(\frac{T}{T_c}\Big)^2\Big)$$

for critical field, which is in agreement with experiment.

In the framework of the Gorter-Casimir theory H. London and F. London introduced two equations for ”superelectrons” in order to explain the Meissner effect. Since ”superelectrons” move without friction through the material, Newton’s second law is:

$$m\frac{\partial \vec{v}}{\partial t} = -e\vec{E}$$

By multiplying both sides by $\frac{n_s e}{m}$ they got, what is now called the first London equation:

$$\frac{\partial \vec{J_s}}{\partial t} = \frac{n_s e^2 \vec{E}}{m}, J_s = n_s e v \tag{2.1}$$

By taking curl on both sides of equation 2.1 and using Maxwell’s equation for $\nabla \times E$, they got:

$$\frac{\partial}{\partial t}(\frac{m}{n_s e^2}\vec{\nabla} \times \vec{J_s} + \vec{B}) = 0$$

The expression in brackets does not depend on time and is therefore only a function of coordinates. This equation is general and valid for electrons moving without friction. But to explain the Meissner effect, London and London suggested that the function is identically zero. Therefore the so-called second London equation is:

$$\frac{m}{n_s e^2}\vec{\nabla} \times \vec{J_s} = -\vec{B}$$

If we use another Maxwell equation:

$$\vec{\nabla} \times \vec{B} = \mu_0 \vec{J}$$

We get:

$$\nabla^2 \vec{B} = \frac{\mu_0 n_s e^2}{m}\vec{B}$$

Here, following originators of this equation, we define λ as:

$$\lambda_L = \sqrt{\frac{m}{\mu_0 n_s e^2}}$$

If we now restrict to a one-dimensional geometry, where the half-space is filled with superconductor and put the boundary conditions that the field is $B = B_0$ at $x = 0$, $B = 0$ at $x = \inf$, the field distribution in superconductor is governed by:

$$B(x) = B_0 e^{-\frac{x}{\lambda_L}}$$

Thus we come to the conclusion that the field penetrates into superconductor at characteristic length λ_L, London penetration depth. The penetration depth forms an important length scale for this thesis. This length is one of the parameters that characterize materials in the superconducting state. Because it depends on the concentration of superconducting electrons, it depends on temperature. Now if we make use of Gorter-Casimir's result:

$$\frac{n_s(T)}{n} = 1 - \left(\frac{T}{T_c}\right)^4$$

We get the temperature dependence of the penetration depth:

$$\lambda = \frac{\lambda(0)}{\sqrt{1 - (T/T_c)^4}}$$

And this result is in good agreement with experiment. Experimentally it was shown that the penetration depth value λ_L^0 depends on the material and the temperature dependence can be fairly approximated by:

$$\lambda_L = \frac{\lambda_L^0}{\sqrt{1 - (\frac{T}{T_C})^4}}$$

, where T_C is the transition temperature. The London penetration depth λ_L^0 was reported to be 39.7±1 nm for polycrystalline high purity niobium(RRR=2000) [12]

The equations derived above are only correct for weak fields, as can be understood from the existence of the critical field. Since the superconducting state ceases at a certain field, the presence of the magnetic field should alter the amount of superconducting electrons and therefore the penetration depth. This effect is neglected in Londons' theory.

The drawback of Londons' theory is that the superconducting and normal conducting phases cannot coexist macroscopically, whereas a number of experiments following Shubnikov showed that the magnetic field seemed to be trapped in even the most pure superconductors. A theory that fixed the drawback was introduced by V.L. Ginzburg and L.D. Landau in 1950. It is also a phenomenological theory. The theory starts with the introduction of an "order parameter" $\psi(r)$: a quantity that characterizes a degree of superconductivity in the superconductor. The order parameter is defined to be zero for normal conducting regions and unity for a pure superconductor, i.e. a superconductor in zero magnetic field and at zero temperature. With the Gorter-Casimir model in mind, one relates the order parameter to the superfluid fraction in a two-fluid model. $\psi(r)$ is taken to be complex function and is treated as a wave function of "superconducting electrons". Then the density of "superconducting electrons" is:

$$n(r) = |\psi(r)|^2 \tag{2.2}$$

After introduction of the "order parameter" the G-L theory suggests that near the superconducting transition, the free energy of a superconductor can be expanded in powers of the "order parameter":

$$\begin{aligned} F = F_n + \int \bigg\{ & \frac{(H-H_a)^2}{8\pi} + \frac{\hbar^2}{2m^*}\bigg|\bigg(\nabla - \frac{ie^*}{\hbar c}A\bigg)\psi\bigg|^2 \\ & - a|\psi|^2 - \frac{b}{2}|\psi|^4 \bigg\} dV \end{aligned} \tag{2.3}$$

In the equation above F_n - free energy in a normal conducting state(n_s=0), the first term under the integral represents an increase in free energy due to expulsion of magnetic field from the superconducting regions, the second term represents an increase due to a flow of a supercurrent and a "stiffness" against spatial variation in the "order parameter", the last two terms are an energy benefit due to the existence of a superconducting phase below the transition temperature, where b was suggested to be a positive coefficient, independent on temperature, and a to decrease linearly with temperature, vanishing at $T = T_C$: $a = \alpha(T - T_c)$, where $\alpha > 0$. Minimizing free energy with respect to $\psi^*(r)$ and $A(r)$ Ginzburg and Landau derived two equations, which are, not surprisingly, called the Ginzburg-Landau equations:

$$\begin{aligned} &-\frac{\hbar^2}{2m^*}\left(\nabla + \frac{ie^*}{\hbar c}A\right)^2\psi - a\psi - b|\psi|^2\psi = 0 \\ &-\frac{rotH}{4\pi} = \\ &\frac{i\hbar e^*}{2m^* c}\left(\psi^*\left(\nabla - \frac{ie^*}{\hbar c}A\right)\psi - \psi\left(\nabla + \frac{ie^*}{\hbar c}A\right)\psi^*\right) \end{aligned} \tag{2.4}$$

In the absence of a magnetic field it is reasonable to assume that $\psi(r)$ does not vary in space. In this case the density of the superconducting fluid is:

$$|\psi_0|^2 = -\frac{a}{b} = \frac{a}{b}(T_c - T) \tag{2.5}$$

Now if ψ in the first equation, 2.4, is normalized with respect to this value, $\psi = \varphi\psi_0$:

$$-\frac{\hbar^2}{2m^* a}\left(\nabla + \frac{ie^*}{\hbar c}A\right)^2\varphi - \varphi - |\varphi|^2\varphi = 0 \tag{2.6}$$

Then the coefficient at the first term characterizes fluctuations of φ according to the equation, and it has the dimension of length. It is called the coherence length:

$$\xi(T) = \frac{\hbar}{2\sqrt{m|a|}} = \frac{\hbar}{2\sqrt{m\alpha(T_c - T)}} \tag{2.7}$$

The second G-L equation gives an important length under assumption of the weak magnetic field. In this case we take ψ to be constant and equal to its value at zero field. Then we get the second London equation:

$$\nabla \times H = \frac{8\pi e^2}{mc^2} |\psi_0| A \tag{2.8}$$

with the penetration depth:

$$\lambda = \left[\frac{mc^2 b}{8\pi e^2 |a|} \right]^{1/2} = \left[\frac{mc^2 b}{8\pi e^2 \alpha (T_c - T)} \right]^{1/2} \tag{2.9}$$

The ratio of coherence length and penetration depth is a dimensionless parameter:

$$\kappa = \frac{\lambda(T)}{\xi(T)} = \frac{mcb^{1/2}}{(2\pi)^{1/2} |e| \hbar} \tag{2.10}$$

This parameter is called the Ginzburg-Landau parameter κ. The coherence length for niobium $\xi(0)$ was reported to be 39±1.5 nm [12]. Thus the Ginzburg-Landau parameter is very close to unity. For ultra high monocrystal niobium samples(RRR=34000) the Ginzburg-Landau parameter is 0.702, very close to magic number $\frac{1}{\sqrt{2}}$ [13], which separates type I and type II superconductors.

In the framework of the G-L theory A.A. Abrikosov considered the contribution of the superconducting boundary to the free energy. He showed that the surface energy becomes negative for superconductors with $\kappa > \frac{1}{\sqrt{2}}$ at fields less than the thermodynamical critical field [14]. So the behavior of the superconductors with $\kappa > \frac{1}{\sqrt{2}}$(Type II) is different from the behavior of superconductors with $\kappa < \frac{1}{\sqrt{2}}$(Type I) in the magnetic field.

A long cylindric slab of a type-I superconductor stays completely in the Meissner state on increasing external field, and becomes normal conducting once the external field reaches the thermodynamical critical field of the superconductor.

In the case of a type-II superconductor it can be thermodynamically advantageous to have normal conducting regions with negative surface energy of the normal-superconducting interface. These surfaces have negative energy and compensate the increase in total energy due to normal-conducting core. The lowest field when such a situation occurs is called the lower superconducting field, or H_{c1}. In the same way one may argue that on decreasing the field from very high values, at a certain field above thermodynamical critical field the appearance of superconducting regions becomes favorable. The highest field when this happens is called the upper critical field or H_{c2}.

Superconductors of the second type, exposed to the external magnetic field between the two values $H_{c1} < H < H_{c2}$, are in the mixed or Shubnikov state. Since the G-L parameter for niobium is higher than $\frac{1}{\sqrt{2}}$, niobium is a type-II superconductor. The lower critical field for high purity niobium(RRR=2000) was reported to be $H_{c1}=1.8\cdot10^3$ Gauss. The high critical field of niobium was reported to be $H_{c2}=3.9\cdot10^3$ Gauss [12].

It is possible to find H_{c2} within the G-L model from general considerations. When the external field is close to H_{c2} we can drop a non-linear term in ψ in the G-L equation, because at this field $\psi \to 0$:

$$\frac{1}{4m}\left(-i\hbar\nabla - \frac{2e}{c}A\right)^2 \psi = |a|\psi \tag{2.11}$$

, where A is a vector potential for uniform field $H \to H_{c2}$, when $\psi = 0$. The equation above is the Shroedinger equation for a particle with mass $2m$ and charge $2e$ moving in constant magnetic field with energy $|a|$. The boundary conditions are also the same: $\psi = 0$ for $r \to \pm\infty$. The ground state energy for such particle is $E_0 = \frac{\hbar|e|H}{2mc}$. Thus the critical field will be $H_{c2} = \frac{2mc|a|}{|e|\hbar}$. This field can be expressed through the G-L parameter and the thermodynamic critical field $H_{c2} = \sqrt{2}\kappa H_c$.

The lower critical field can also be found with this theory. Considering the energy contribution of one single normal conducting vortex line, one can calculate the lower critical field in case of large G-L parameter $\kappa >> 1$: $H_{c1} = H_c\frac{ln\kappa+0.081}{\sqrt{2}\kappa}$.

The calculations that lead to bulk superconducting fields are only valid in an infinite medium and they neglect boundary effects, whereas for an ideal sample a nucleation of superconductivity always takes place first on the surface [15]. The analysis based on Ginzburg-Landau equations shows, that for the infinite perfectly flat boundary between superconductor and insulator the nucleation of the superconducting surface takes place at a magnetic field H_{c3}:

$$H_{c3} = 1.7 \cdot H_{c2} = 2.4 \cdot \kappa \cdot H_c \tag{2.12}$$

, where $\kappa = \frac{\lambda(T)}{\xi(T)}$ is the G-L parameter of the substance. This effect is called surface superconductivity.

Finally a so-called superheating critical field must be introduced. For type I superconductors above H_c a vortex has to form at the surface of superconductor. Due to the vacuum-superconductor boundary, currents that circumvent the vortex have no normal component at the surface. This condition forces currents to be distributed in such a way as to create a force that pushes the vortex to the surface. At H = H_c this attraction force overcomes pressure from the ambient magnetic field, that pushes the vortex in the superconductor. This is called surface-barrier and such a situation in a superconductor exists up to the so-called superheating critical field H_{sh}. So superconductivity may exist metastably above H_c up to H_{sh}. The superheating field, calculated within G-L theory, depends on G-L parameter and the whole range of κ can be split into three groups:$\kappa <<$1,$\kappa \approx$1,$\kappa >>$1:

$$\begin{aligned} H_{sh} &= 0.75 H_c \; for \; \kappa >> 1 \\ H_{sh} &= 1.2 H_c \; for \; \kappa \approx 1 \\ H_{sh} &= \frac{H_c}{\sqrt{\kappa}} \; for \; \kappa << 1 \end{aligned} \tag{2.13}$$

The G-L parameter of niobium is close to unity, so the superheating field of niobium is $H_{sh} \approx$2500 Gauss.

In 1957 the successful microscopic theory of superconductivity was presented by J. Bardeen, L.N. Cooper and J.R. Schrieffer [16]. Superconductivity was explained by a bound state formed of two electrons through their interaction with the lattice. The bound state, called a Cooper pair, is separated from the Fermi level by a so-called energy gap, Δ. Cooper pairs do not dissipate energy, but they have mass, and so they cannot move with the phase velocity of RF field. The resulting RF field, the sum of the one produced by external source and the one produced by the motion of Cooper pairs, is acting on normal electrons. Normal electron then dissipate the consumed energy. The temperature dependence of RF surface resistance was derived from the BCS theory by D.C. Mattis and J. Bardeen [17]. The dependence is rather complex, involving different material parameters, but a convenient fit to the experimental data for T$< T_c/2$ and for frequencies much lower than $\frac{2\Delta}{h}$ is given by:

$$R_{BCS} = A\Big(\frac{f}{1.5}\Big)^2 \frac{exp\big(-\frac{\Delta}{kT}\big)}{T} \tag{2.14}$$

Where A depends on the material properties(one of the important material parameters is the electron mean free path, related to niobium purity), f is a frequency in GHz and Δ is an energy gap.

Besides BCS resistance the resistance of niobium cavities was found to have a temperature independent component, a so-called residual resistance. Some mechanisms that are contributing to the temperature-independent residual resistance are not related to niobium. Among these are residual losses from the joints at the cavity flanges, bad welds, etc. But some mechanisms are related to niobium. An external DC magnetic field is trapped on the lattice defects and inhomogeneities during the cool-down, causing additional temperature-independent losses. Therefore it is important to shield niobium cavities from the Earth's magnetic field [18]. Another niobium-related contribution to residual losses comes from the niobium hydrides [19]. When the bulk hydrogen concentration in niobium exceeds 2 ppm by weight, there is a danger of hydride formation at the niobium surface. Hydrides can increase the residual surface resistance to hundreds nanoohms, therefore precautions are taken during the cavity preparation to keep the hydrogen concentration under control.

Having introduced all the critical parameters, we may ask what is the critical field for 1.5 GHz niobium superconducting cavity at T=$1.5°$K. The answer is: there is no such thing as perfect superconductivity in RF fields. By definition superconductivity is the absence of resistance and the perfect diamagnetism, but superconducting materials are lossy in RF fields of any amplitude. Though formally it is meaningless to talk about the RF critical field within a classical definition, we may redefine the RF critical field as the field at which there is discontinuity in resistance of the material and ask about such fields. The best hint toward the answer comes so far from experimental work. First, in 1970 T. Yogi et al. [20] measured resistance of In, Sn, Pb and some alloys in 90-300 MHz RF fields. They found that near T_C the data suggests a discontinuity in conductivity occurs at the superheating critical field. Recent experiments with niobium also suggest that niobium is not limited by lower critical field [21]. The current record for magnetic field in the cavity was reached with re-entrant 1.3 GHz cavity and is 2059 Oe [22].

Parameter	Value
T_c	9.29 °K
H_c	2061 Gauss
H_{c1}	1800 Gauss
H_{c2}	3900 Gauss

2.2 Superconducting cavities

The simplest cavity one can consider is a rectangular box. But, since modern cavities, discussed in this thesis, have cylindrical symmetry, we shall consider a pill-box cavity, because it will be easier to translate results on modern cavities later. Inside the cavity, in a source-free, homogeneous vacuum, Maxwell's equations can be reduced to the wave equations for electric and magnetic fields:

$$\left(\nabla - \frac{1}{c^2}\frac{\partial}{\partial t}\right)\begin{pmatrix} E \\ H \end{pmatrix} = 0 \tag{2.15}$$

If we assume that that a superconductor has infinite conductivity, so that electric and magnetic fields inside the superconductor are zero, and that the superconductor fills the whole space except the cavity, the boundary conditions are:

$$\begin{aligned} \hat{n} \cdot D_2 &= \rho_s \\ \hat{n} \cdot B_2 &= 0 \\ \hat{n} \times E_2 &= 0 \\ \hat{n} \times H_2 &= J_s \end{aligned} \tag{2.16}$$

The solution of these equations with boundary condition for a pill-box yields two different types of modes. One type of mode has no longitudinal, i.e. along axis of symmetry, component of magnetic field, therefore these modes are called transverse magnetic, TM, modes. Another class of modes has no longitudinal component of electric field, therefore these modes are called transverse electric modes. Since we are interested in accelerating electrons and positrons in ILC, TM modes are of most interest to us, in particular TM_{010}, which is used for acceleration. We particularly are interested in the electric field on the axis of symmetry, because this field accelerates electrons, and in the magnetic field on the surface, because it defines the critical field at which superconductivity(and so the good properties of the cavity) ceases. If we assume that the pill-box has longitudinal length d, and diameter 2R, we can look up solutions in [18]:

$$E_z = E_0 J_0\Big(\frac{u_0\rho}{R}\Big)e^{-\omega_0 t} H_\phi = -i\frac{E_0}{\eta}J_1\Big(\frac{u_0\rho}{R}\Big)e^{-\omega_0 t} \tag{2.17}$$

Where ρ is the distance from the axis of symmetry, $\eta = \frac{\mu_0}{\epsilon_0} = 377\ \Omega$, $\omega_0 = \frac{u_0 c}{R}$ is resonant frequency, J_0 and J_1 are zero- and first-order Bessel's functions, $u_0 \cong 2.405$ first root of zero-order Bessel's function. From these solution we find that the peak electric field is $E_z^{peak} \equiv E_{pk} = E_0$ and the peak magnetic field is $H_\phi^{peak} \equiv H_{pk} = \frac{E_0}{\eta}J_1(1.84) = \frac{E_0}{647\ \Omega}$. Thus 1 V/m peak electric field in the cavity leads to 1/647 A/m peak magnetic field on the cavity surface. So for a pill-box cavity we conclude that the ratio of peak magnetic field to peak electric field is 19.42 $\frac{Oe}{MV/m}$.

Next we derive how much energy a charged particle gains gains, while moving through the pillbox:

$$Energy = \Big|\int_0^d eE_z(\rho = 0)e^{i\omega_0 z/v}dz\Big| = eE_0\frac{sin\Big(\frac{\omega_0 d}{2v}\Big)}{\frac{\omega_0}{2v}} \tag{2.18}$$

If we assume that the particle moves with a speed of light, then for a charged particle to gain most energy, the particle should enter the cavity, when the electric field is zero, and the length of the pill-box should be $d = \frac{\pi c}{\omega_0} = \frac{\lambda}{2}$. Then the energy gain per unit length and unit charge is $\frac{2E_0}{\pi}$. This value is specific for each shape and defines how much can be delivered to a particle moving with the speed of light through the cavity. This energy gain divided by the electron charge and by the cavity length is called the accelerating electric field, E_{acc}. One can see that E_{acc} is proportional to E_0, which is proportional to H_{pk}. Therefore the higher the magnetic field a superconducting cavity can sustain the more energy can be delivered to charged particles for the same cavity length. For a pill-box the ratios of fields are:

$$\begin{aligned}\frac{E_{peak}}{E_{acc}} &= \frac{\pi}{2} \\ \frac{H_{peak}}{E_{acc}} &\cong 30.5\frac{Oe}{MV/m}\end{aligned} \tag{2.19}$$

The second important parameter is the cryogenic loss in the superconducting cavity walls, which is given by:

$$P_{diss} = \int_s \frac{1}{2} R_s H^2(r) ds \tag{2.20}$$

Instead of using dissipated power, which is field dependent, it is convenient to introduce the quality factor, denoted Q, which, theoretically, should be field independent. So superconducting radio frequency cavities are typically characterized by presenting their quality factor as a function of field. The quality factor is the amount of energy stored in the cavity divided by the power dissipated in the surface of the cavity per RF cycle.

$$Q = \frac{U}{P/\omega} \tag{2.21}$$

The total energy in the cavity is a volume integral over the electromagnetic energy density in the cavity:

$$U = \int^V \frac{1}{2}\mu_0 H^2(r) d^3r \tag{2.22}$$

These relations can be simplified by introduction of the mean surface resistance according to:

$$\bar{R} = \frac{\int^S \frac{R(r)H^2(r)}{2} d^2r}{\int^S \frac{H^2(r)}{2} d^2r} \tag{2.23}$$

Then the quality factor of the cavity is:

$$Q = \frac{1}{\bar{R}} \cdot \omega\mu_0 \frac{\int^V \frac{H^2(r)}{2} d^3r}{\int^S \frac{H(r)^2}{2} d^2r} \tag{2.24}$$

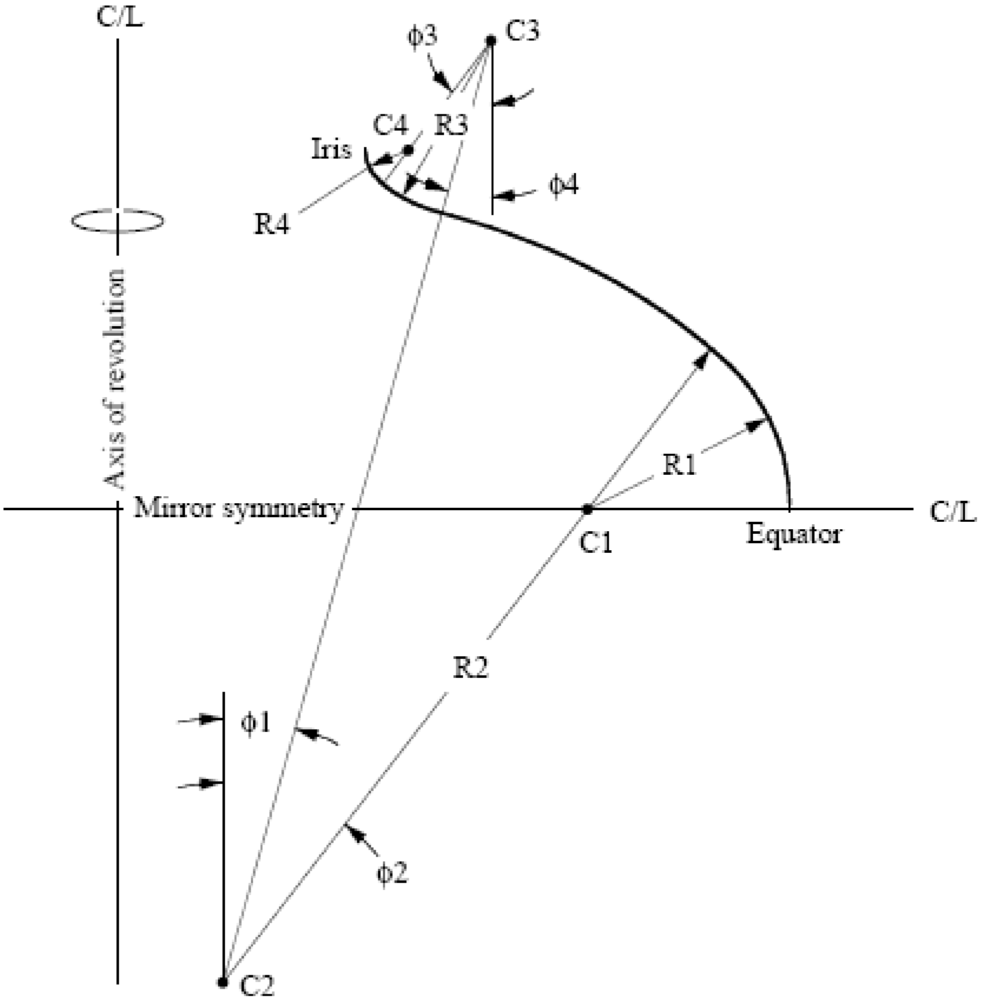

Figure 2.3: Elliptical cavity shape MARK-III

Since $H(r) = A \cdot f(r)$, the amplitude of the field cancels out and the second term in equation 2.24 does not depend on the field level, but only on the field distribution in the cavity. This factor is called a geometry factor,G, and it is a constant of the cavity shape. By introduction of the mean surface resistance and geometric factor of the cavity the quality factor of the cavity can be reduced to:

$$Q = \frac{G}{\bar{R}} \tag{2.25}$$

The geometric factor of the pill-box cavity is 257 Ω. The real shape of cavities, discussed in this thesis, was modified to introduce beam aperture and a rounded wall shape in order to eliminate multipacting [23], [24]. The shape and parameters of the shape are reproduced from [25] in Fig. 2.3 and in Table. 2.2.

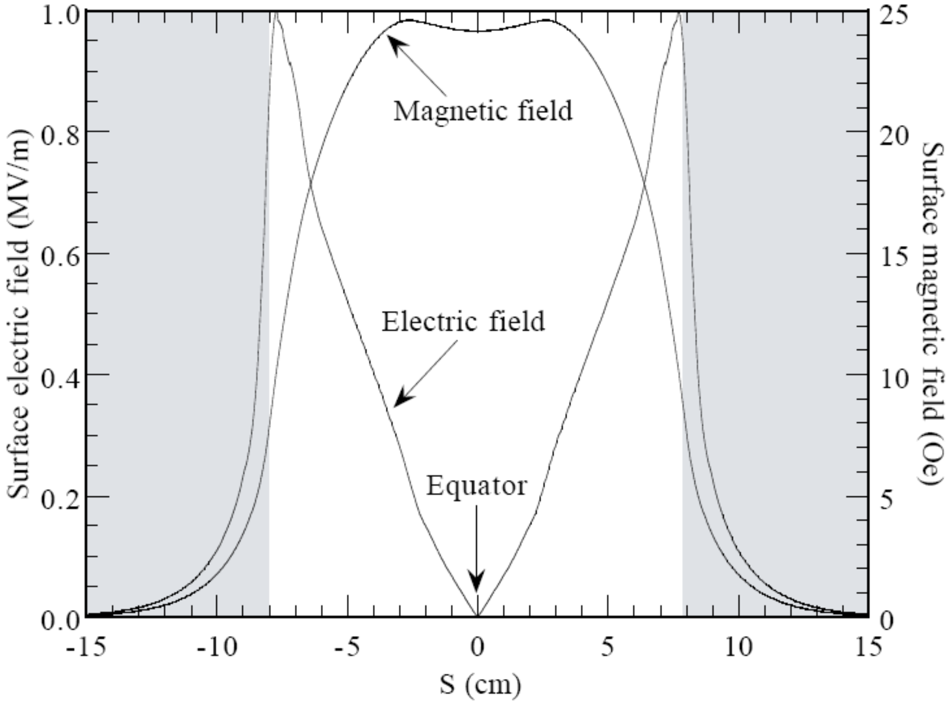

Figure 2.4: Field distribution on the cavity surface. The peak electric field here is 1 MV/m. The light area marks the cell region of the cavity.

Parameter	Value	Param.	Val.	Param.	Val.	Param.	Val.
R1	2.892	C1X	6.422	C1Y	0.000	R2	10.646
C2X	1.658	C2Y	-6.118	R3	2.498	C3X	5.249
C3Y	6.526	R4	0.590	C4X	4.095	C4Y	5.006
$\phi1$	15.89°	$\phi2$	37.58°	$\phi3$	37.22°	$\phi4$	15.97°

The analytic solution of the wave equation for such a shape is very hard, if possible at all, so typically numerical codes are used to calculate the field distribution. We calculated parameters of the MARK-III shape, using SLANS. The geometric constant G was found to be 273 Ω. The field ratios are:

$$\begin{aligned}\frac{E_{peak}}{E_{acc}} &\cong 1.83\\ \frac{H_{peak}}{E_{acc}} &\cong 44.98\frac{Oe}{MV/m}\end{aligned} \tag{2.26}$$

The electric and magnetic field distributions on the cavity surface are reproduced from [25] in Fig. 2.4.

CHAPTER 3

EXPERIMENTAL

3.1 Cavity preparation

In this chapter we discuss all preparation steps taken prior to testing a cavity. The standard preparation of the niobium cavity consists of the following procedures:

∗ Chemistry, chemical etching and electrochemical etching.
∗ High pressure water rinsing.
∗ Assembly in the dust-free cleanroom class 100 (less then 1 particle of size 5 mum, 10 particle of size 1 mum, 100 particles of size 0.5 mum, 300 particles of size .3 mum, 750 particles of size .2 mum per cubic foot of air).

In our studies we developed and additionally applied following treatments:

∗ Anodizing with various voltages.
∗ Mild baking at different temperatures for 48 hours.
∗ 400 °C heat treatment.
∗ Air exposures of cavity baked at high temperature.

Chemistry

A niobium cavity has to be chemically etched in order to remove possible surface damage or residues due to cavity production, or effects of previous treatments. In the course of development of niobium cavities two techniques of chemical polishing were empirically found to produce best results. The one, applied in the majority of tests reported in this work, is a buffered chemical polishing, so-called BCP(1:1:2), which consists of HF(48%), HNO_3(68%),H_3PO_4(85%) acids in the volume ratios 1:1:2 respectively. The schematic of chemical etching is presented in Fig. 3.1. The cavity initially is filled with BCP(1:1:2) at about -7 °C. Usually it takes about 40 minutes till the temperature of the solution reaches 15 °C. At this point the cavity is emptied and new cold acid is put in. About 40-50 μm is removed per step as it is measured on a sample placed inside the cavity, i.e. the removal rate is about 1 μm/min. In cases, when no more than 10-20 μm are to be removed, the chemical etching is done without magnetic stirring and ice cooling. After chemistry, the cavity is rinsed with ultrapure water and is either placed in the bucket with water or sealed in a plastic bag and carried into the cleanroom, class 100.

The essential component of this chemical solution is hydrofluoric acid, which is responsible for etching niobium pentoxide off the niobium surface. The bare niobium surface oxidizes via reaction with NO_3^-. The mixture solely of HF(48%), HNO_3(68%) reacts with niobium at room temperature very violently and heats up quickly. In order to have better control over the reaction, H_3PO_4 is added to the solution to dilute and to increase viscosity of solution, thereby slowing down the reaction.

The reaction of niobium pentoxide with hydrofluoric acid is exothermic, and the product of reaction depends on the concentration of the hydrofluoric acid. For solution with high concentration of hydrofluoric acid a heptafluoroniobic acid, H_2NbF_7, is formed, for diluted solutions oxipentafluoroniobic acid, H_2NbOF_5 [26]. During BCP treatment the niobium stripped of its oxide reacts with nitric acid, HNO_3. The reaction is also exothermic with brown gas, NO_2, being released. It was found empirically that the temperature of solution must always be below 15 °C, in order to avoid hydrogen contamination of niobium.

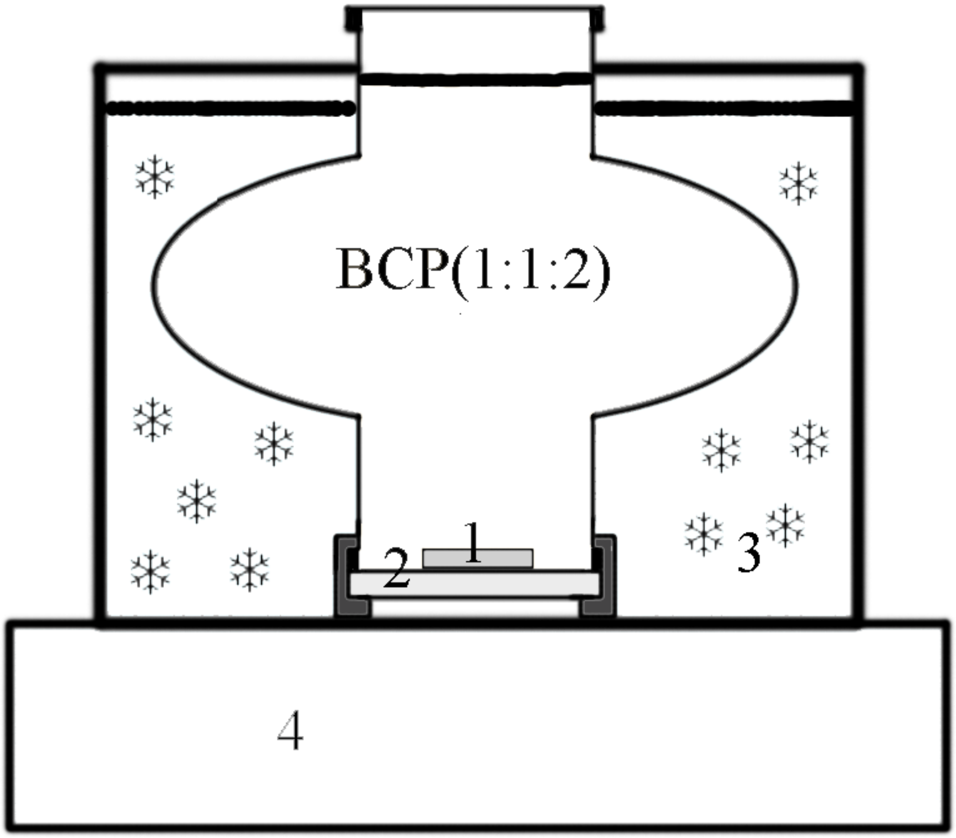

Figure 3.1: Schematic of BCP setup. 1. Stir bar; 2. Teflon cap; 3. Ice and water; 4. Magnetic stirrer.

An alternative technique is electropolishing. During electropolishing the oxidation of the niobium surface is enhanced by applying a positive potential to the cavity surface. Thus electropolishing can be considered as a continuous oxidation(anodizing) and HF etching. The acid mixture is usually made of HF(48%), H_2SO_4(95%) acids in volume ratios 1:9 [27]. A complex horizontal electroplishing setup, in which the cavity is half-filled with acid and rotates during electropolishing, was developed by K. Saito [28]. A simpler version of vertical electropolishing was developed at Cornell University [29]. The schematic of the setup is presented in Fig. 3.2. In this case the acid should be agitated gently in order to electropolish the surface effectively. Therefore agitation arms are

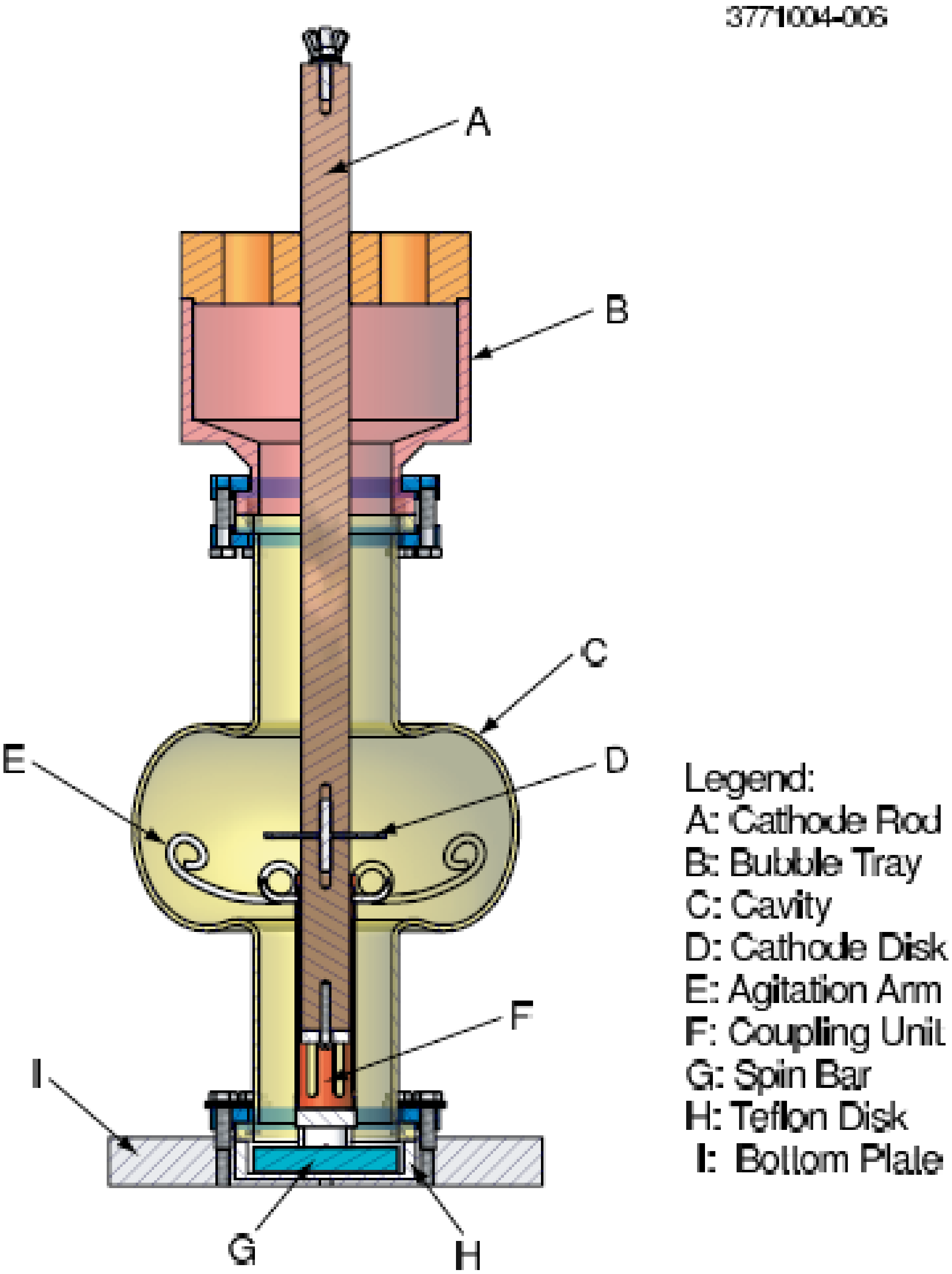

Figure 3.2: Schematic of vertical EP setup.

coupled to a magnetic strirring bar on the bottom of the cavity. These agitation arms increase agitation of the acid near the cell's inner surface significantly. Otherwise, when only a magnetic stirring bar on the bottom is applied, almost no etching takes place at the equator. The typical removal rate for this setup is 0.3-0.5 μm/min.

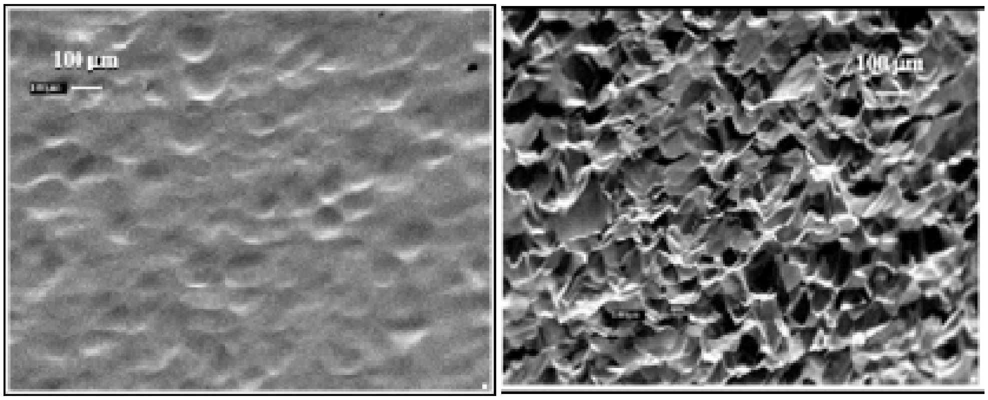

Figure 3.3: Niobium surface etched by EP[left] and BCP[right] [30].

Studies of the niobium surface showed that the surface of electropolished samples is more smooth than that of BCPed samples, Fig. 3.3. The typical steps between adjacent grains are less than 0.5 μm for electropolishing, and are about 5 μm for BCP.

Anodizing

Anodizing is a well-known technique of growing oxide films on certain metals. Metals, which can be anodized, react readily in air and are covered by a thin oxide film under normal conditions. In the process of anodizing, a sample is connected to the positive terminal of a DC supply. Another conductor is connected to the negative terminal of the DC supply. It is preferable that both conductors are made of the same material in order to avoid contamination of the sample. Both anode and cathode are then placed in the electrolyte to close the circuit. The oxide formed on the sample should be insoluble in the electrolyte or, at least, dissolve slower than it grows. After the circuit has been closed no current will flow until the voltage reaches a few volts. Once the voltage exceeds a certain limit, the natural oxide can no longer sustain the induced electrical field. Kovacs et al. [31], who anodized niobium in $H_3PO_4(1\%)$, found via X-ray photoelectron spectroscopy that on the electrolyte-oxide interface PO_4^{-3} ions were incorporated in the oxide during oxide formation. Secondary ion mass spectrometry studies showed that PO_4^{-3} ions are incorporated in first 30% of oxide grown at 40 Volts. One of the possible explanations is that oxide is formed on both, electrolyte-oxide and oxide-metal interfaces. On the oxide-metal interface negative oxygen ions from the electrolyte diffuse through the oxide to the metal to form oxide and on the electrolyte-oxide interface positive metal ions from the metal diffuse through the oxide to electrolyte. The ratio of oxide thickness to applied voltage weakly depends on oxide thickness, current density and temperature of electrolyte.

To niobium cavities this treatment was first applied by H.Martens et al. in the late 70's. The motivation was to protect the surface and to avoid the drop in quality factor because of surface impurities. They used NH_4OH solution at 20^0C with a current density of 2 mA/cm^2 in order to grow .1 μm thick oxide films. Their first results were encouraging: the quality factor improved [32] by a factor of two and a maximum achievable field increased by 50%. But later experiments did not support these findings.

Today anodizing is not a part of standard cavity preparation in any of the labs worldwide, because this treatment complicates preparation of the cavity without any obvious advantage. We used anodizing to do depth profiling(see chapter 7).

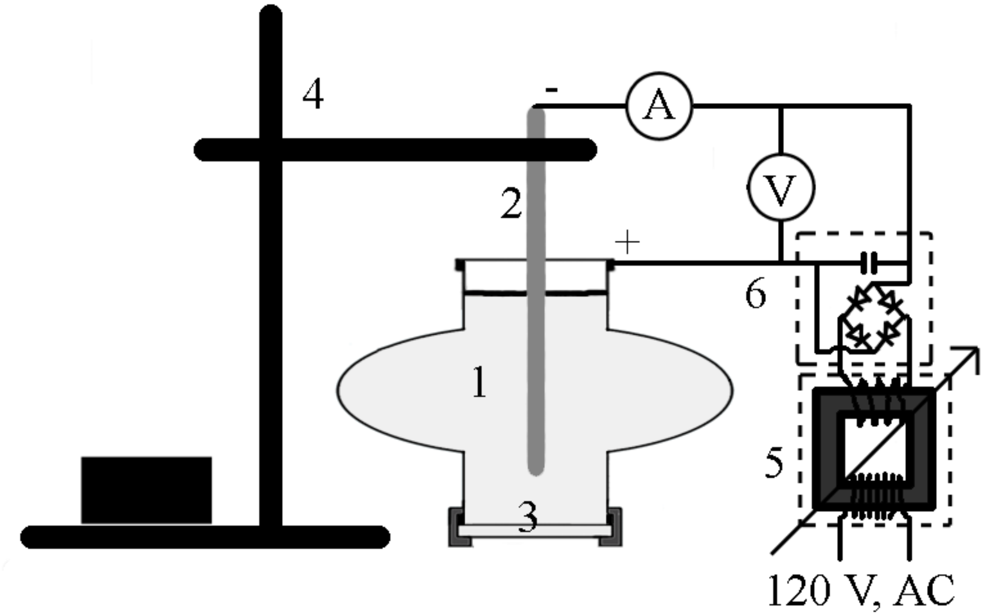

Figure 3.4: Schematic of anodizing setup. 1. Aqueous solution; 2.Niobium rod; 3. Teflon disk; 4. Holder; 5. Variable transformer; 6. Rectifier.

Typically at Cornell we use NH_4OH(28%)(diluted to 15%) as the electrolyte. The schematic of the anodizing setup is presented in Fig. 3.4. The resulting thickness of niobium oxide mainly depends on applied voltage, but varies with such parameters as current density and electrolyte temperature. As it can be seen from the table below the oxide thickness per volt is of the order 2 nm/V.

Thickness	Electrolyte	Temperature	Current density	Reference
3 nm/V	H_3PO_4	65^0C	0.01-0.067 mA/cm^2	[31]
1.5-1.7 nm/V	H_3PO_4	20-50^0C	0.0075-0.0165 mA/cm^2	[33]
2.0 nm/V	H_2SO_4	25.8^0C	10 mA/cm^2	[34]

High Pressure Rinsing

Particles on the niobium surface cause field emission(explained later in Chapter 5). The effective way to remove dust particles from the cavity inner surface is to rinse the inner surface with ultra-pure de-ionized water under 1000 psi pressure. In order to reduce the handling time of the cavity after high pressure rinsing, a top flange with transmission coupler is placed onto the cavity prior to rinsing. After that the cavity is placed on the holder of the high pressure rinsing stand, which allows to move the cavity up and down at speed specified by computer. Usually two up/down cycles are done, where each cycle takes about one hour. The high pressure rinsing setup involves also a turn table, so that rinsing jets cover the whole surface. Typical rotation speed of the turn table is about 3-5 turns per minute, and it is changed after each up/down cycle, so that the water jets do not follow the same path on niobium surface.

Cleanroom assembly

After high pressure rinsing the cavity is normally left drying for two days. After drying, the cavity is removed from the high pressure rinsing setup and is mounted onto the test stand in the cleanroom class 100. Following assembly the pumping line to a roughing/turbo pump is connected, and cavity is pumped down to $2\cdot 10^{-7}$ torr as indicated by cold cathode gauge on the pump. The initial pumping is done at a slow rate, so that the gas flow in the vacuum system stays laminar. Pumping down to the final pressure usually takes several hours. After the ultimate pressure is reached, the vacuum is leak-checked to ensure absence of leaks. Upon successful completion the cavity's vacuum is isolated, the pumping line is disconnected and the test stand is carried out of the cleanroom. Outside the cleanroom the ion pump is turned on and the valve that isolates the cavity vacuum from ion pump vacuum is opened. Usually the cavity is pumped down for a few hours before the vacuum reaches about 10^{-7} torr as indicated

Figure 3.5: Cornell high-pressure-rinsing system.

by the current in the ion pump.

Mild baking setup

In the quest for high-gradient cavities it was found that heat treatment at low temperatures, 100-120 °C, for 48 hours(mild baking treatment) improves the performance of cavities(this effect will be discussed in chapter 4). Therefore one of the necessary setups to study the high field Q-slope is the mild baking setup. Two different setups were used at Cornell University.

One setup utilized heat tapes. The cavity is covered with several layers of aluminum foil, on top of which two heat tapes are wrapped. Tapes in turn are covered with aluminum foils. The advantage of this setup is simplicity, the disadvantage is a relatively large temperature spread across the cavity surface, ± 5 °C.

A different setup was developed in order to improve the temperature distribution on the cavity surface. A thermal insulation box is assembled around the cavity and hot air is blown in the box. This setup allowed to improve the temperature distribution during baking to ± 2 °C, Fig. 3.6. In the beginning of mild baking the pressure in the system rises to about 10^{-6}-10^{-5} torr, and then in the course of two days drops down to about 10^{-8} torr, Fig. 3.7.

High temperature 'in-situ' treatment setup

Studies discussed in chapter 9 show that heating the niobium surface to 400 °C destroys most of the niobium oxide layer. Therefore a new 400 °C setup was designed to heat the cavity above 400 °C, in order to study the effect of oxides on losses at high fields. For the heat treatment a steel box was put around the cavity and pressurized with argon, preheated to 250°C, to avoid oxidation of the outer surface of the cavity during the heat treatment. The inside of the cavity was kept under UHV. The heating elements were two 1.5 kW band heaters placed

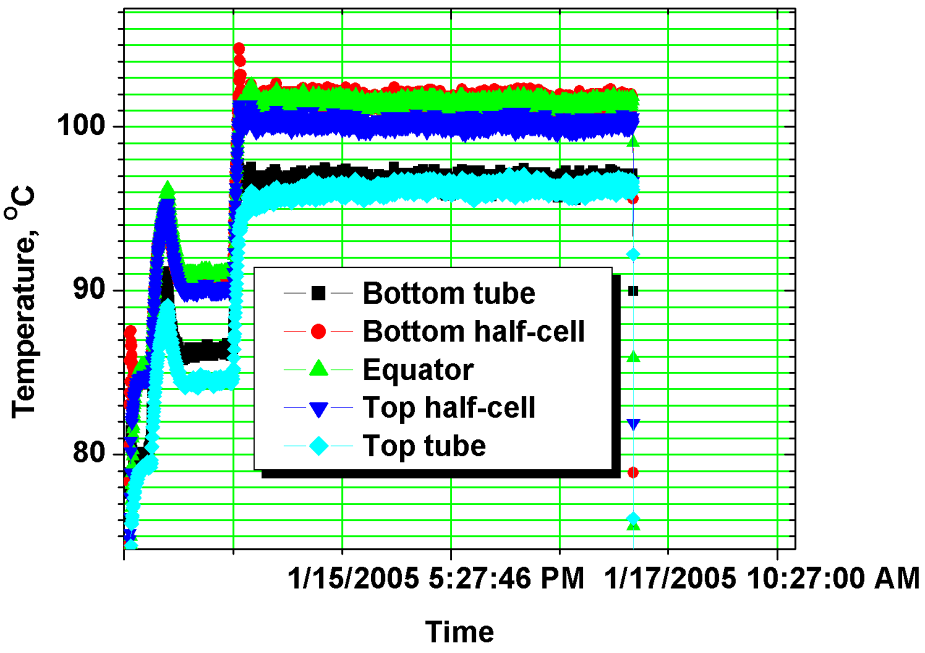

Figure 3.6: Temperature distribution during mild baking at 100 °C.

on copper rings, which were contoured to follow the shape of the cavity. Copper foils were used to improve the temperature distribution. Only the cell itself was heat treated, the rest of the cavity (beam tubes) was kept at a room temperature by water-cooling clamps on beam pipes, so that the temperature at indium seals was below 100 °C, see Fig. 3.8. The pressure during the heat treatment was $4.5 \cdot 10^{-7}$ Torr. The main constituents were water($2 \cdot 10^{-7}$ Torr) and CO($3 \cdot 10^{-8}$ Torr) as indicated by residual gas analyzer. The oxygen partial pressure was $8 \cdot 10^{-11}$ Torr. Three runs were performed. During the third run the cavity's temperature reached 500 °C with temperature spread of about 30 °C around the cavity, Fig. 3.9.

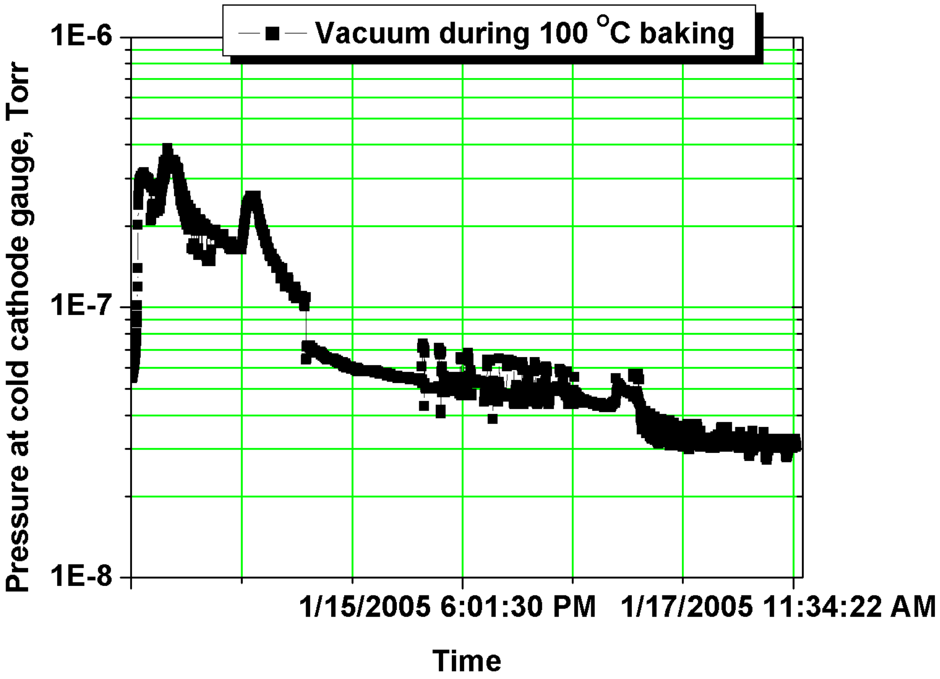

Figure 3.7: Pressure during mild baking at 100 °C as read by the cold cathode gauge.

Air exposures

After 400 °C heat treatment the cavity was controllably exposed to different pressures of air in an attempt to re-grow the oxide layer. The air was let in through a precision valve with air filter. VOC Zero Grade Air from Airgas was used. After air exposures the cavity was pumped down to 10^{-7} Torr. In Fig. 3.10 the schematic of the cavity in cryostat is presented [25].

Post-purification of niobium

In order to improve RRR, niobium cavities and manufactured half-cells are often "post-purified". "Post-purification" is heat treatment at 1300-1400 °C for several hours in the presence titanium foil. During heat treatment a titanium layer forms of niobium surface via vapor deposition. This layer serves as a solid

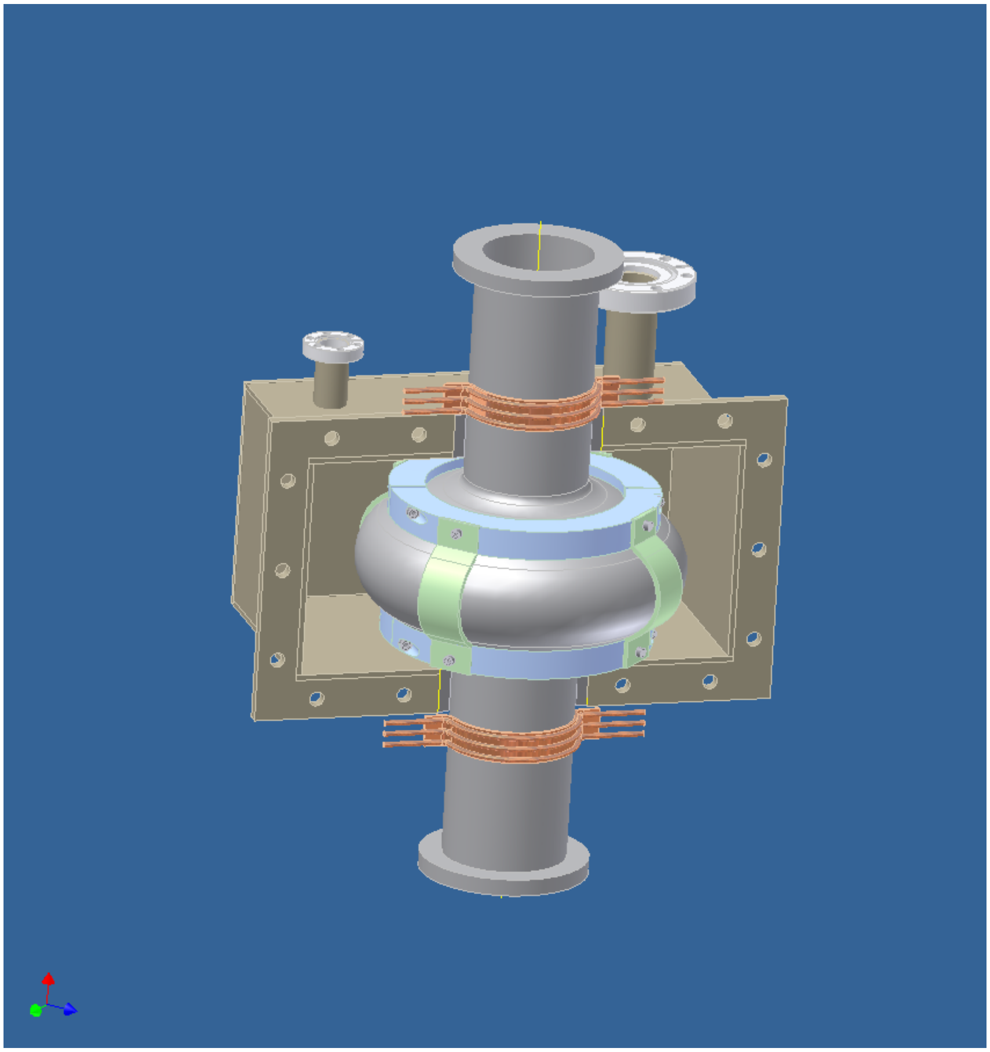

Figure 3.8: A sketch of the setup for high temperature baking of a one-cell 1.5 GHz cavity.

state getter, absorbing impurities from niobium. After heat treatment titanium layer is easily removed by chemistry.

Hydrogen degassing

High concentration of hydrogen causes a hydrogen Q-disease in niobium cavities. The solubility of hydrogen in niobium drops rapidly with temperature, so, when hydrogen Q-disease is suspected, niobium cavities are degassed at

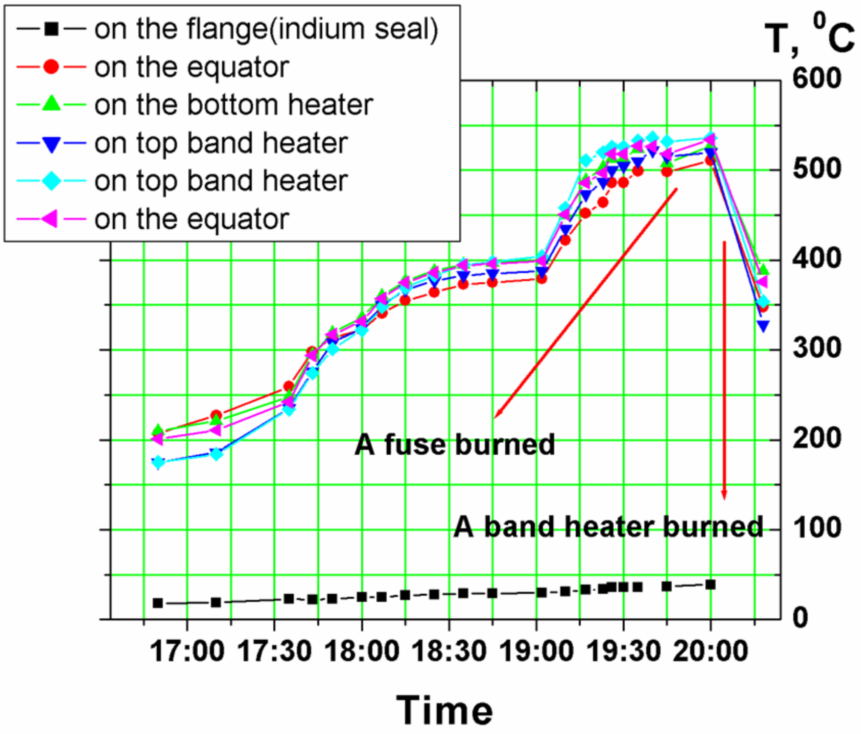

Figure 3.9: Temperature distribution during 400 °C heat treatment.

600-900 °C for several hours in vacuum.

3.2 RF measurements

The RF setup is designed to measure two important values for accelerator applications: quality factor of the cavity and field in the cavity. The schematic of RF setup is presented in Fig. 3.11. To provide the cavity with power a 50 Ω transmission line is connected. The coupling strength, β, is defined as a ration of the power emitted into the line, P_e, to the power dissipated in the cavity, P_d, when there is no incident power and only power of electromagnetic field is dissipated into the coupled line and cavity wall. Since $P_e = \frac{V_0^2}{2Z_0}$, where Z_0 is transmission line impedance as seen from coupling point, and $P_d = \frac{V_0^2}{2Z_1}$, where Z_1 is

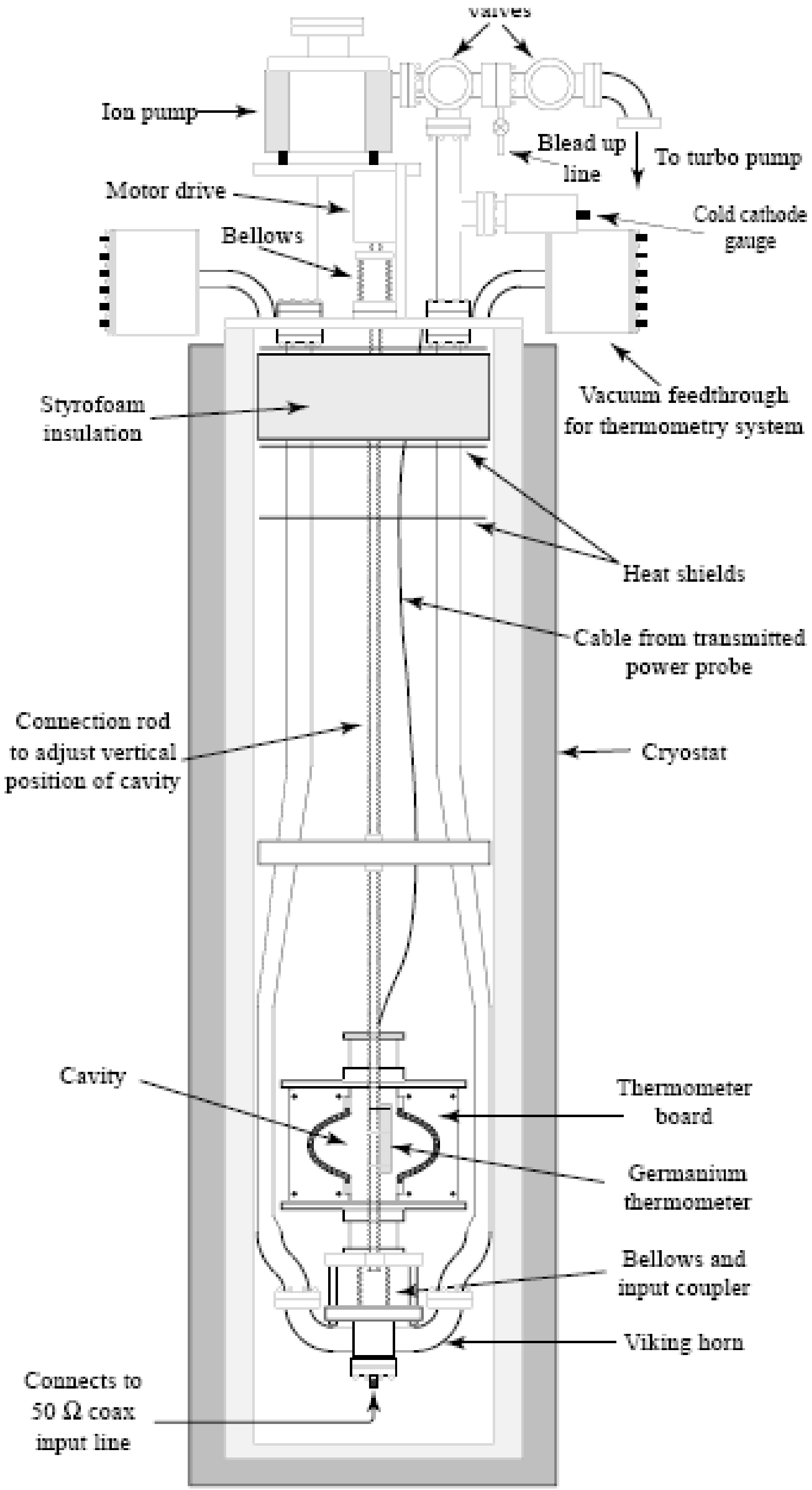

Figure 3.10: Sketch of the cavity in the cryostat [25].

load impedance as seen from coupling point, so $\beta = \frac{Z_0}{Z_1}$. If there is an incident power from the transmission line, then due to mismatch reflected power will appear. First, we shall consider a steady-state. The incident voltage can be presented as $V^{in} = V_0^+ e^{-ikx}$. Since generally $Z_1 \neq Z_0$, there will be a reflected wave $V^{ref} = V_0^- e^{ikx}$ with the same wave-vector, k. The total voltage in transmission line is $V = V_0^+ e^{-ikx} + V_0^- e^{ikx}$. The total current is $I = \frac{V_0^+ e^{-ikx} - V_0^- e^{ikx}}{Z_0}$. On the load Z_1 at x=0, the boundary condition must be met:

$$Z_1 = \frac{V(x=0)}{I(x=0)} = \frac{V_0^+ + V_0^-}{V_0^+ - V_0^-} Z_0 \tag{3.1}$$

, which relates V_0^+ and V_0^-:

$$V_0^- = \frac{Z_1 - Z_0}{Z_1 + Z_0} V_0^+ \tag{3.2}$$

The ratio of voltages is called voltage reflection coefficient, Γ:

$$\Gamma = \frac{Z_1 - Z_0}{Z_1 + Z_0} \tag{3.3}$$

or in terms of β:

$$\Gamma = \frac{1-\beta}{1+\beta} \tag{3.4}$$

The voltage and current in line can thus be rewritten in following form:

$$\begin{aligned} V &= V_0^+ (e^{-ikx} + \Gamma e^{ikx}) \\ I &= \frac{V_0^+}{Z_0} (e^{-ikx} - \Gamma e^{ikx}) \end{aligned} \tag{3.5}$$

The average power flowing through the line and dissipated in the load is:

$$\begin{aligned} P_d &= \frac{1}{2} Re(VI^*) = \frac{1}{2} \frac{|V_0^+|^2}{Z_0} Re(1 - \Gamma^* e^{-2ikx} + \Gamma e e^{2ikx} - |\Gamma|^2) \\ &= \frac{1}{2} \frac{|V_0^+|^2}{Z_0} (1 - |\Gamma|^2) = \frac{1}{2} \frac{|V_0^+|^2}{Z_0} \frac{4\beta}{(1+\beta)^2} \end{aligned} \tag{3.6}$$

The reflected and incident powers are following:

$$\begin{aligned} P_{in} &= \frac{1}{2} \frac{|V_0^+|^2}{Z_0} \\ P_{ref} &= \frac{1}{2} \frac{|V_0^+|^2}{\Gamma}^{2} = \frac{1}{2} \frac{|V_0^+|^2}{Z_0} \left(\frac{1-\beta}{1+\beta} \right) \end{aligned} \tag{3.7}$$

The first step during the measurement is to calibrate the system for a particular test. The forward, reflected and transmitted powers are measured. Then

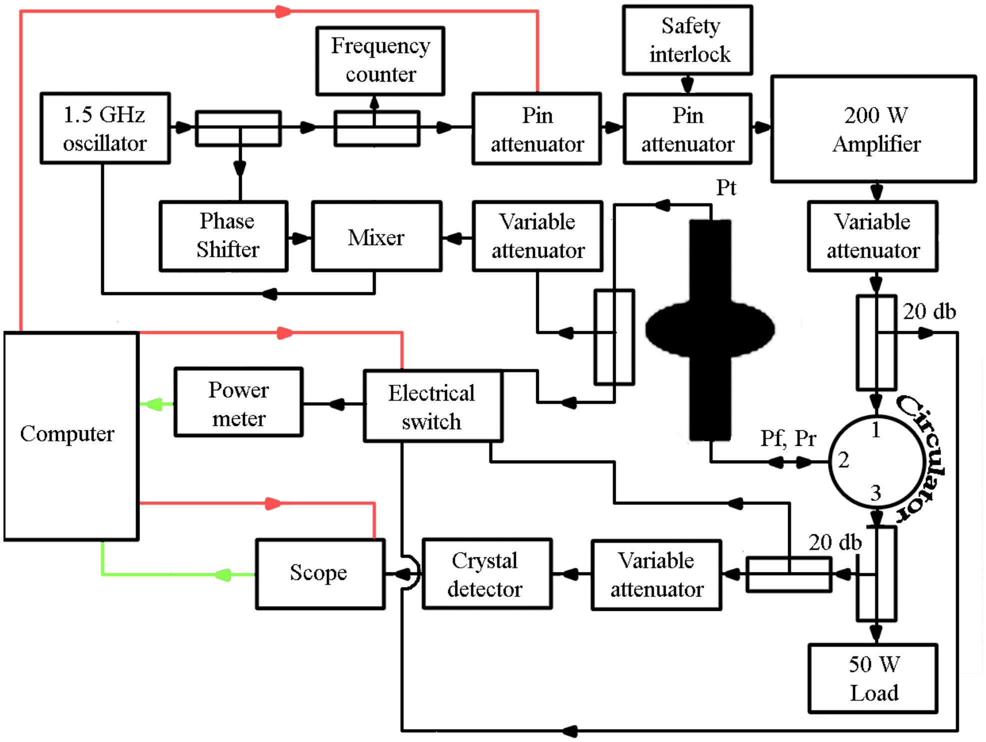

Figure 3.11: Sketch of RF setup at Cornell for testing a one-cell 1.5 GHz cavity

the power is switched off and the trace from the oscilloscope is saved to the computer. From the oscilloscope trace the decay time, τ, is calculated, and forward, reflected and emitted powers are measured in relative units. From this measurement a coupling strength is determined via two formulas:

$$\beta_1 = \frac{1}{2\sqrt{\frac{P_f}{P_e}} - 1} \tag{3.8}$$

$$\beta_2 = \frac{1 \pm \sqrt{\frac{P_r}{P_f}}}{1 \mp \sqrt{\frac{P_r}{P_f}}} \tag{3.9}$$

In the later formula the upper sign holds if $\beta > 1$ and the lower one otherwise. Here the user can pick either of the calculated β's, their mean, or enter a different value. With known β the quality factor of the cavity, the dissipated power, and the stored energy are calculated:

$$Q_0 = 2\pi f\tau(1+\beta) \tag{3.10}$$

$$P_{diss} = \frac{4P_f\beta^{\,2}}{1+\beta} \tag{3.11}$$

$$U = P_{diss}\tau(1+\beta) \tag{3.12}$$

Now the field level in the cavity can be calculated using an external calibration constant, ratio of stored energy to field level in the cavity, which is known from numerical calculation with electromagnetic field calculating code SLANS and was determined to be 16.90 MV/$\sqrt{J}$ for all cavities discussed in this thesis.

$$E_{peak} = Ke \cdot \sqrt{U} \tag{3.13}$$

The final step during the calibration is to determine coupling constants for transmission coupler:

$$CE = \frac{E_{peak}}{\sqrt{P_t}} \tag{3.14}$$

$$CU = \frac{U}{P_t} \tag{3.15}$$

After the transmission coupler is calibrated the peak electric field and energy stored in the cavity is determined by transmitted power throughout the whole measurement:

$$E^i_{peak} = CE \cdot \sqrt{P^i_t} \tag{3.16}$$

$$U^i = CU \cdot P^i_t \tag{3.17}$$

The β is determined again by relative values of incident, reflected and emitted powers calculated from oscilloscope trace. Finally, the dissipated power and the quality factor of the cavity can be found by forward power:

$$P^i_{diss} = \frac{4\beta^i P^i_f}{(1+\beta^i)^2} \tag{3.18}$$

$$Q_0^i = \frac{2\pi f U^i}{P_{diss}^i} \tag{3.19}$$

3.3 Thermometry measurements

From the RF point of view, the cavity is a simple impedance on the end of the transmission line. The RF setup permits the measurement of this impedance, but it does not provide any insight to the distribution of losses, the understanding of which is essential if the development and improvement of the cavity's surface properties are the objectives. Ideally, since the quality factor, and thus resistance, is of most interest, one would want to have an instrument measuring resistance locally at every point. Fortunately to me, such a device was available at Cornell.

The device is called thermometry system. It is an array of thermometers that measure a local temperature on the outer surface. Since the temperature on the outer surface is determined by the dissipated power on the inner surface, via the known field on the inner surface, the resistance of the inner surface may be determined. The complete description of the thermometer design and general setup can be found in [25]. The computer software for the data acquisition was updated recently, but all the major parts and general approach were kept intact.

To perform a successful measurement the temperature mapping system must be calibrated. During the cool down the resistance of each thermometer as a function of helium bath temperature is measured. Once the data is acquired the data points for each thermometer are fit with a polynomial. Though the resistive element is carbon, a semiconductor, and thus one would expect an exponential decrease of resistance with increasing temperature, the data is fit with polynomial of third order or fourth order:

$$T = \frac{1}{a_0 + a_1 R + a_2 R^2 + a_3 R^3 (+a_4 R^4)} \tag{3.20}$$

For each thermometer, five calibration values and mean squared error are calculated. In order to measure the temperature increase on the cavity outer surface due to dissipated power on the inner surface, the resistance is measured for the field-on and field-off settings. The difference in measured values correspond to power flowing from the niobium surface into the helium bath multiplied by Kapitza resistance. Therefore the measurement permits the calculation of dissipated power on the inner surface.

Calculation of the cavity's quality factor from thermometry

The thermometry system measures local dissipated power(after calibration), so it is possible by summation over all thermometers to calculate the total dissipated power. The dissipated power calculated in this way would be proportional to the real total dissipated power. The coefficient of proportionality depends on:bath temperature, thickness of the niobium wall and other parameters. Therefore the usual procedure is to calculate the proportionality coefficient as a ratio of the known dissipated power, from RF measurement, and the total dissipated power, calculated from thermometry, at a single field value. This calibration constant is then applied for the whole test.

CHAPTER 4

Q-SLOPES IN NIOBIUM CAVITIES

In real RF superconducting niobium cavities due to various mechanisms the quality factor may be field-dependent virtually at any field, signifying field-dependent resistance and therefore non-quadratic losses. The excitation curve of a real cavity is presented in Fig. 4.1 and it is typically divided into three regions: low field Q-slope, medium field Q-slope and high field Q-slope, attributed to different loss mechanisms.

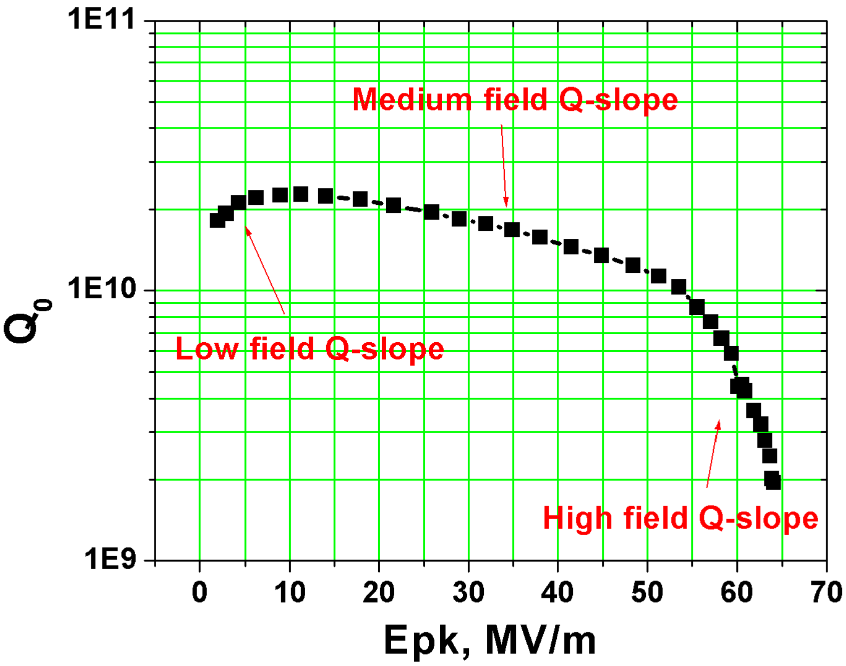

Figure 4.1: A typical excitation Curve

The low field Q-slope is an increase in quality factor as a function of field at low fields, which was observed in many experiments throughout the world. But, since this phenomenon does not present any limitation to fulfillment of

ILC, it will not be discussed further in this work.

The second region, which is usually distinguished, is a so-called medium field Q-slope. The medium field Q-slope is a steady decrease in the quality factor with field. The medium field Q-slope is typically attributed to a thermal feedback effect, which is caused by a positive feedback between temperature of the niobium surface and power dissipated in it, i.e. resistance is a function of temperature, but the temperature itself is a function of dissipated power:

$$\bar{R}(T) = \bar{R}(T(P)) \approx R_{T_0} + \left.\frac{\partial R}{\partial T}\right|_{T=T_0} \left.\frac{\partial R}{\partial T}\right|_{P=0} \bar{R}(T) H^2 \approx \bar{R}_{T_0} + \gamma H^2 \bar{R}(T) \tag{4.1}$$

Thus

$$\bar{R} \approx \frac{\bar{R}_0}{1 - \gamma \cdot H^2} \approx \bar{R}_0 (1 + \gamma \cdot H^2) \tag{4.2}$$

The temperature in the equations above is the temperature of the inner surface. In fact, the temperature of inner surface is not only the function of the power dissipated in the inner surface, but also a function of temperature of the outer surface, which is in thermal contact with helium bath. The temperature of the helium bath is constant across the bath, because tests are carried out at temperatures below 2.17 °K, the He-II point. One can imagine two heat flow conditions, one, in which the helium bath temperature is kept constant during the test, and second, in which the temperature of the helium bath is allowed to increase with dissipated power. If the thermal feedback effect is responsible for the medium field Q-slope, one would expect a stronger medium field Q-slope in latter case, because then there will be another positive quadratic term in eq. 4.2. Indeed this effect was observed in our experiments. In Fig. 4.2 the result for an experiment, in which the bath temperature is constant, is presented. The quality factor drops by 20-25 percent from its value at $B_{peak} = 40$ mT to its value at $B_{peak} = 90$ mT. In Fig. 4.3 the result is presented for an experiment, in which the bath temperature is not constant. Here the quality factor at $B_{peak} = 90$ mT is a half of its value at

$B_{peak} = 40$ mT. These plots illustrate the effect of the thermal feedback on the medium field Q-slope. Therefore it is important to control the bath temperature effect in medium-field-Q-slope studies. The thermal feedback effect gives a stronger medium field Q-slope, when the dependence of the surface resistance on the magnetic field is included [35], [36]. However in many cases the combined effect gives a stronger medium field Q-slope than observed. Hence the medium field Q-slope does not have yet a complete explanation.

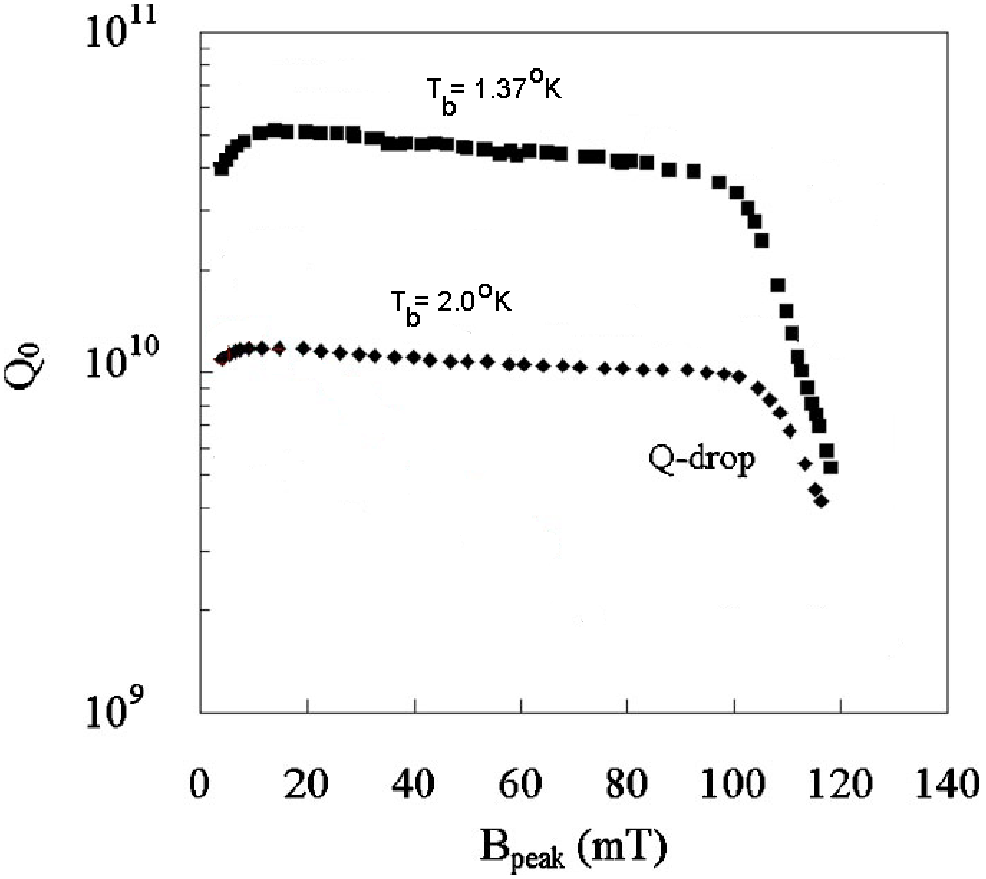

Figure 4.2: Typical medium field Q-slope from SRF group at JLab.

Finally, at $B_{peak} \approx 100$ mT the so-called high field Q-slope starts and it is usually the final limitation for niobium cavities after chemical treatment. The major part of this work presents experimental results related to this phenomenon.

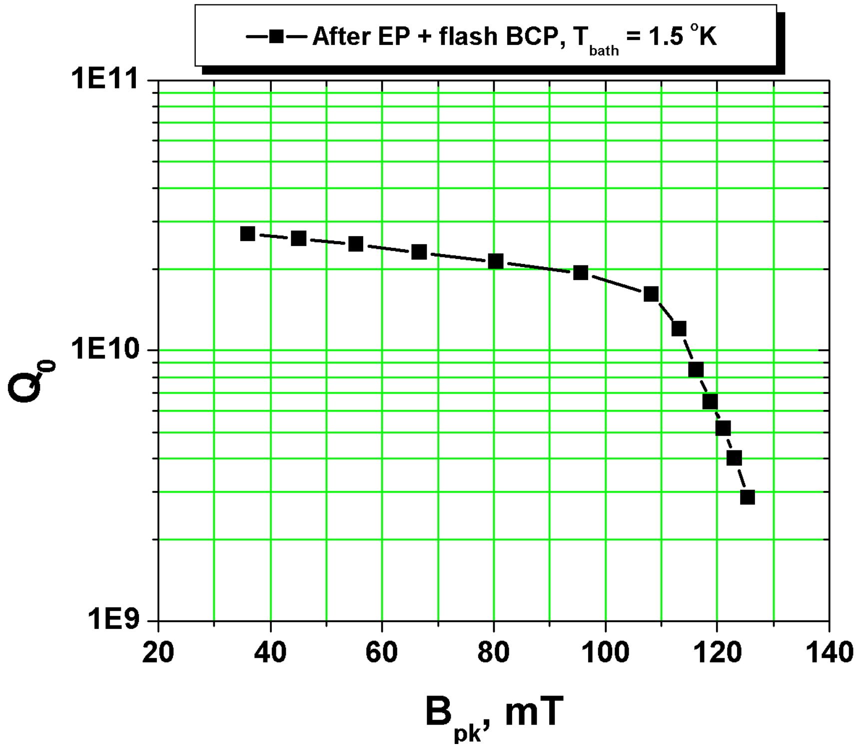

Figure 4.3: Typical medium field Q-slope from SRF group at Cornell University.

Below several models are presented that are typically discussed in relation to the high field Q-slope and that form basis for the experimental investigation of the high field Q-slope.

4.1 Models for the high field Q-slope

Roughness

The roughness of the inner surface was suspected to worsen the properties of superconducting material from the very beginning of superconducting RF studies. When the high-field-Q-slope effect was established, the roughness was looked upon as a possible candidate for the high field Q-slope. Knobloch et al., at Cornell University, developed a quantitative model that explained degradation of the quality factor observed in the experiment [37].

The surface magnetic field is enhanced at surface irregularities. Enhanced magnetic field penetrates into irregularities at fields lower than niobium critical field due to local field enhancement. The granularity of niobium constitutes the main part of such irregularities. Since the typical niobium grain size is 50 μm, there are 20 grain boundaries per millimeter, at which the field is enhanced. When magnetic field penetrates into the grain edge, the grain edge becomes normal-conducting, and the resistance of the grain edge increases by a several orders of magnitude, Fig. 4.4.

In the paper, the power dissipated by each quenched grain edge was given by:

$$P_{diss}^{gb} = \frac{1}{2} R_{nc} L_{nc} w_{nc} (\beta_m H)^2 \tag{4.3}$$

Where R_{nc} was assumed to be $1.35 m\Omega$, cf. $0.01 \mu\Omega$ of superconductor, L_{nc} is a length of the quenched edge, w_{nc} is the width of the quenched edge, β_m is a magnetic-field-enhancement factor and H is applied field.

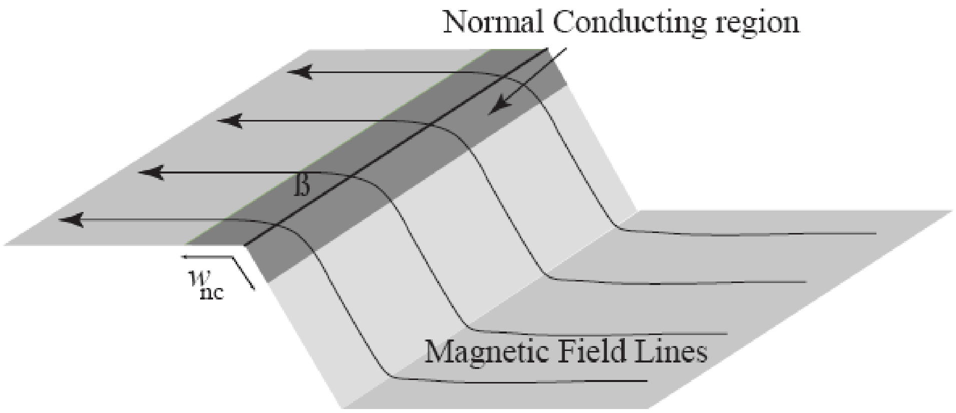

Figure 4.4: This plot illustrates the magnetic field enhancement.

β_m depends not only on angle of the step, but also on the radius of the edge.

From the profilometry measurements it was concluded that the radius of the edge is smaller than the radius of stylus tip, 5μm. SEM contrast pictures suggested that the radius is a fraction of the micron. In order to calculate the field enhancement as a function of the grain boundary angle, the radius of the edge was assumed to be 1 micron in SLANS simulation. This numerical simulation gave β_m as a function of angle. The number of grain boundaries that have a given field-enhancement factor was assumed to have exponential dependence:

$$n(\beta_m)d\beta_m = exp(-\frac{|\beta_m - \beta_0|^{0.5}}{\sigma^{0.5}})d\beta_m \tag{4.4}$$

Finally, the width of the quenched edge was also assumed independent of field and to be 1 μm. The authors verified via numerical simulation with the ANSYS code, that quenched edges do not cause thermal breakdown. They also studied the effect of the quenched edge on the surrounding niobium. In simulations they found that the power increase in the surrounding niobium due to normal-conducting grain-boundary edge would be only 15 percent(even at the highest field) of what is dissipated by the quenched edge itself. Therefore, they neglected this contribution and that the total losses in the cavity are:

$$P_{total} = P_{gb} + P_{sc} \tag{4.5}$$

Where P_{sc} are losses due to RF resistance of a superconductor without quenched grain-boundary edges, and P_{gb} are losses due to quenched grain-boundary edges. With a known distribution of the number of quenched edges as a function of β_m the losses at a given field are given by:

$$P_{gb} = \int_0^\infty \theta(\beta_m H - H_{crit}) P_{diss}^{gb}(H, \beta m) n(\beta_m) d\beta_m \tag{4.6}$$

In the paper the authors also took into account a random orientation of the grain boundaries, which would lead to a different field enhancement factor for grains parallel and perpendicular to field line. The model gave a good fit to their experimental curve, Fig. 4.5.

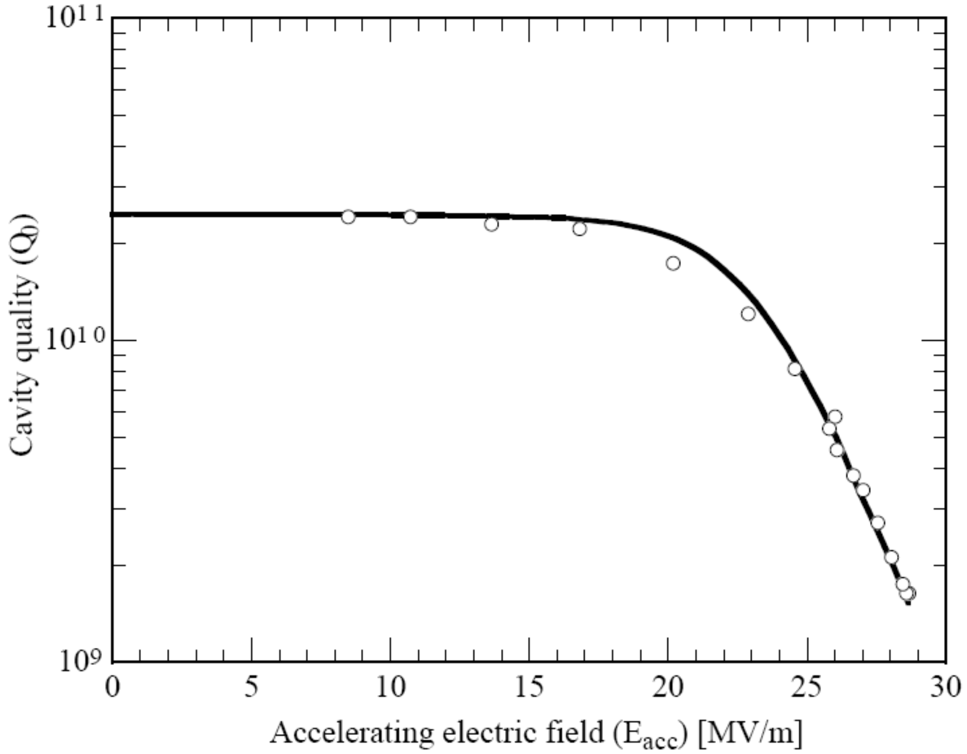

Figure 4.5: Comparison of experimental data and numerical simulation with the framework of magnetic field enhancement model developed by Knobloch et al. The picture shows a very good quantitative agreement between model and experiment.

There are several points in the paper that are not elucidated significantly.

First, it is questionable whether measurement of hundred grain boundaries with stylus is sufficient to make simulation with 10^8 grain boundaries.

Second, the argument for the area of the quenched region seemed to be particularly weak. The speculation, which is put forward, is only valid for a 90 degree grain boundaries. For a more typical 20 degree grain boundaries the same calculation will give an order of magnitude bigger area.

Third, in the paper it is shown via ANSYS simulation that heating of niobium adjacent to quench site will contribute 30 percent at most to heating from grain boundaries, but a possible overlap of heating zones from two different quenched site is not discussed.

Although the grain-boundary enhancement model can explain the high field Q-slope in rough-surface cavities, it cannot account for a similar high field Q-slope found in single-crystal niobium cavities(no grain boundaries) as well as a similar high field Q-slope in cavities prepared by electropolishing, which have smoother surfaces.

Interface tunnel exchange

A model, based on existence of localized states in niobium pentoxides, was proposed by J. Halbritter. This model is a variation of field emission model(Chapter 5), in which it is assumed that besides vacuum there are also states in oxide to which electrons can be extracted by electric field, which is lower than the one needed to cause field emission. The model suggests that there is a Fowler-Nordheim(F-N) current flowing from the metal into localized states in niobium pentoxide. In this model the energy dissipated due to this current is

$$P_E^{Halbritter} \approx e^{-\frac{const}{\beta_E E}} \tag{4.7}$$

, where β_E is a local field enhancement factor. Halbritter suggested that in the F-N formula the energy gap of superconductor(~ 1 meV) should be substituted instead of metal work function(~ 1 eV) and that density of localized states in niobium oxide is very high, $n_L \approx 10^{19}\ 1/cm^3$. Thus appreciable currents will flow and energy will be dissipated at $\beta_E E$ values hundred times lower than those for standard field emission.

Nonlinear BCS

Alex Gurevich calculated a correction to BCS resistance due to magnetic field, which is present even at relatively low fields and which enhances the thermal feedback effect. He introduced a field-dependent correction to BCS formula:

$$R_{s,BCS}^{nlin}(T,B) = \frac{8R_{s,BCS}^{lin}(T)}{\pi\beta^2(T)h^2}\left(\int_0^{\pi} sinh^2\Big(\frac{\beta(T)h}{2}cos(t)\Big)tanh^2(t)dt\right) \tag{4.8}$$

, where $\beta(T) = \frac{\pi}{2^{3/2}}\frac{\Delta}{k_bT}$, $h = \frac{H_{rf}}{H_{crit}}$, $R_{s,BCS}^{lin}(T) = \frac{A\omega^2}{T}e^{-\frac{\Delta}{k_bT}}$. This dependence for low fields, $\beta h << 1$, can be reduced to a quadratic dependence of resistance on the magnetic field:

$$R_{s,BCS}^{nlin}(T,H) = R_{s,BCS}^{lin}(T)\left[1 + \frac{\beta^2}{48}\left(\frac{H_{rf}}{H_{c,0}}\right)^2\right] \tag{4.9}$$

This formula was derived under the assumption that niobium is pure, i.e. electron mean free path is much longer than coherence length, but it was argued that the general field dependence will hold for all cases:

$$R_{s,BCS}^{nlin}(T) = R_{s,BCS}^{lin}(T)\left[1 + C(l,\omega,T)\left(\frac{H_{rf}}{H_{c,0}}\right)^2\right] \tag{4.10}$$

This equation is then used in the thermal feedback model. In order to compare the predictions of this model with results from superconducting cavities, Pierre Bauer solved the problem numerically for simplified geometry, Fig. 4.6. The equation of continuity of power flow in this case is:

$$\frac{1}{2}R_{s,BCS}^{nlin}(T,H)H_{rf}^2 = \int_{T_s}^{T_m} k(t)dt = h_{Kap}(T_s,T_0)(T_s - T_0)d \tag{4.11}$$

, where $k(t) = 0.7e^{1.65t-0.1t^2}\ \frac{W}{m\cdot K}$ is thermal conductivity of niobium as a function of temperature, $h_{Kap}(T,T_0) = 200\cdot T^{4.65}\left[1 + 1.5\left(\frac{T-T_0}{T_0}\right) + 1.5\left(\frac{T-T_0}{T_0}\right)^2 + 0.25\left(\frac{T-T_0}{T_0}\right)^3\right]\ \frac{W}{K\cdot m^2}$ is the Kapitza conductance on the niobium-He II interface as a function of temperature. The results of this simulation were compared with

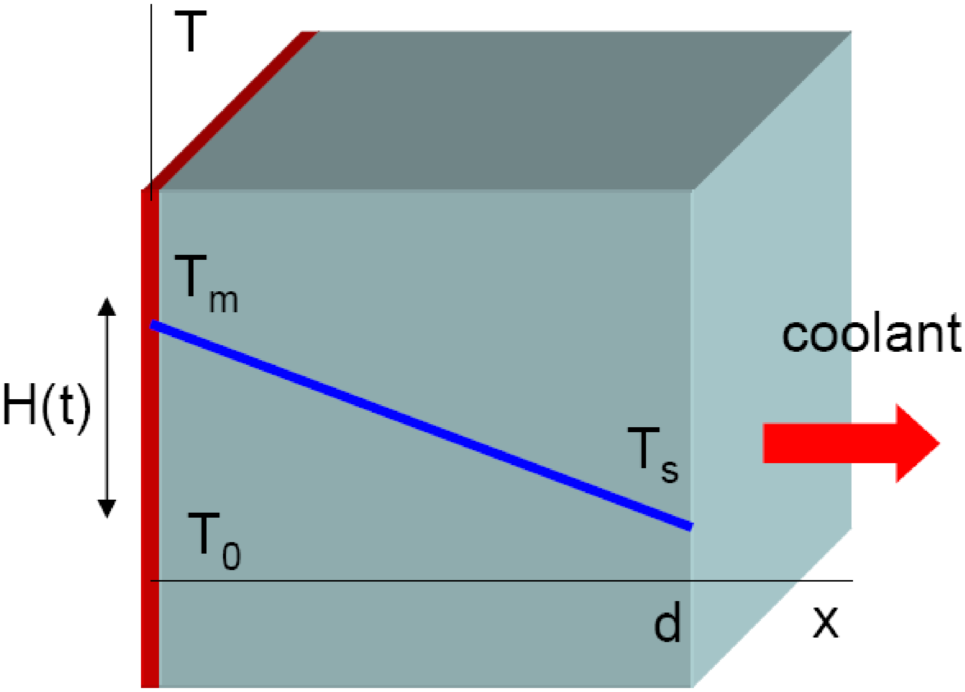

Figure 4.6: Schematic of thermal feedback model that was used to calculate contribution of nonlinear BCS to losses.

typical excitation curves for different cavities at different laboratories around the world. It was found that the high field Q-slope cannot be accounted by this quadratic nonlinearity in resistance, but that this nonlinearity may contribute to medium field Q-slope, as mentioned earlier.

4.2 Mild baking effect

B. Visentin et al [38] reported that the BCS resistance of a niobium cavity, which was chemically polished with BCP, decreased after an "in-situ"(in place) low-temperature ($100°C$ and 170°C) heat treatment was applied for about two days. The BCS resistance of the post-purified 1.3 GHz niobium cavity decreased almost by 50% after heat treatment at 170°C for 70 hours, Fig. 4.7. The high-field performance of the cavity also showed improvement, Fig. 4.8. They confirmed

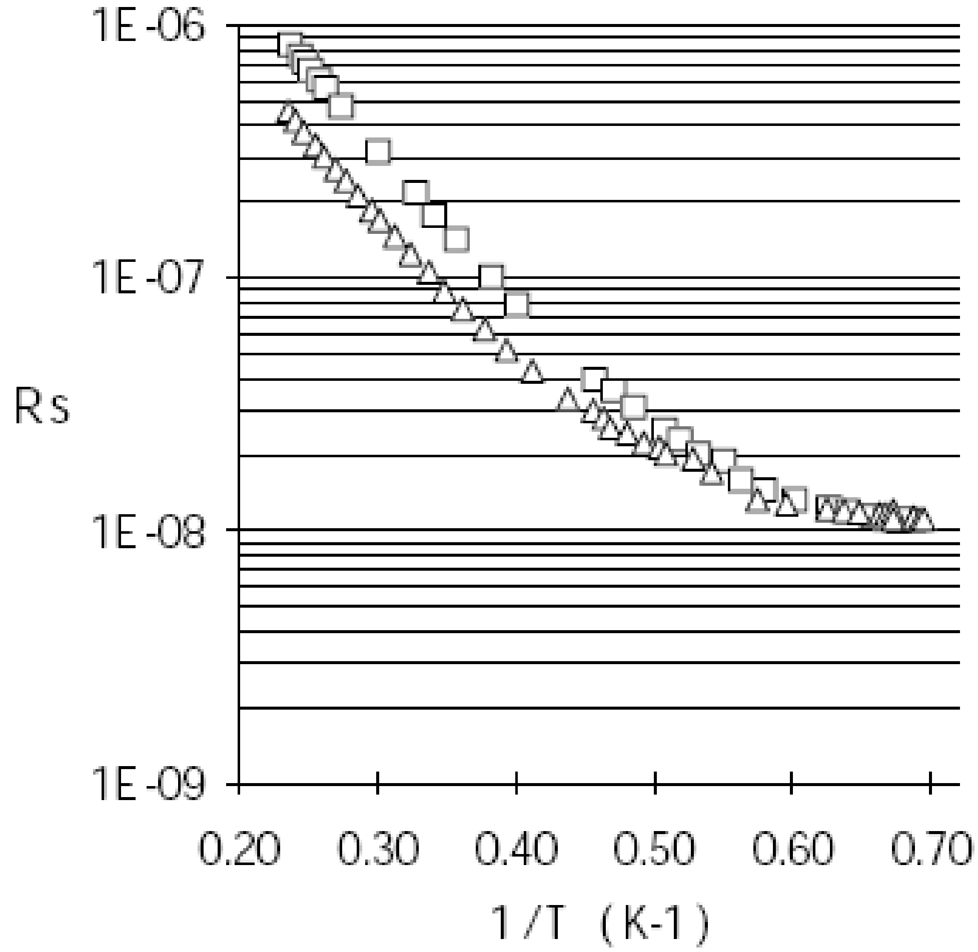

Figure 4.7: Results from [38]. Plot presents the change in BCS resistance before[squares] and after[triangles] low-temperature heat treatment.

the improvement after the low-temperature heat-treatment with a different non-post-purified cavity from another manufacturer. They also found that the improvement is preserved after several weeks in vacuum, but is removed by 20 μm BCP. Finally, in one of the experiments an oxidation of outer surface was allowed, but the performance still improved. Based on the results they concluded that the improvement is not related to the thermal conductivity or Kapitza resistance, but is related only to inner surface of niobium cavity. Their hypothesis

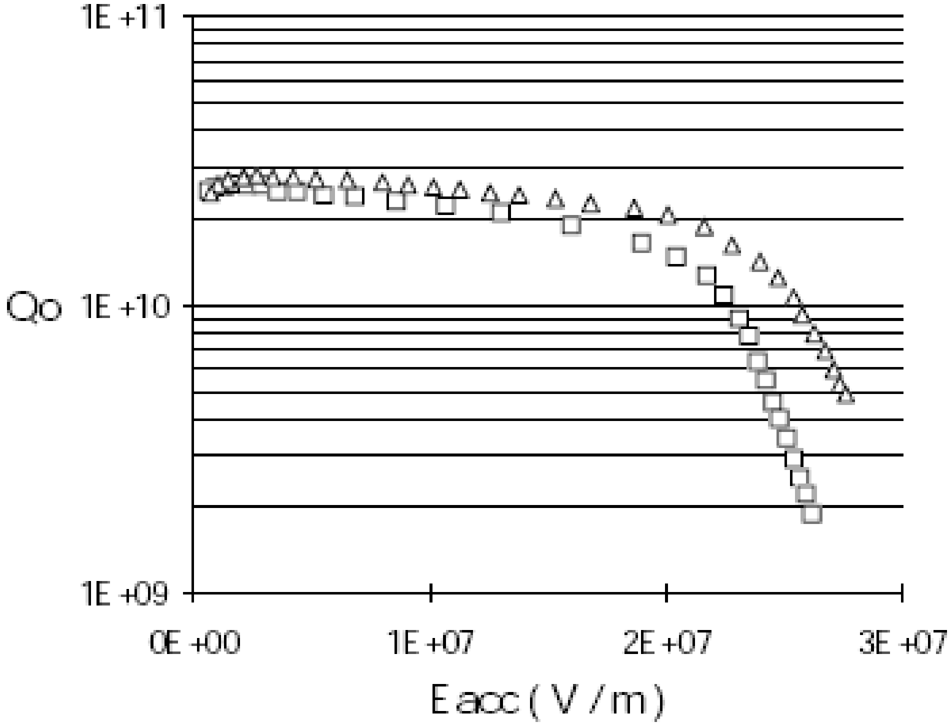

Figure 4.8: Results from [38]. Plot presents the improvement in the quality factor before[squares] and after[triangles] low-temperature heat treatment.

was that the improvement in BCS resistance of niobium and the improvement in high-field performance are related phenomena. The improvement in the BCS resistance was explained by reduction of the mean free path due to the oxygen diffusion, which as they pointed out is not negligible at 100°C.

It turned out that KEK electropolished cavities, which reached routinely higher fields than chemically polished cavities, also underwent mild baking at 90°C for 48 hours as a part of preparation procedure, which had been introduced to improve vacuum in the cavity. So as previously mentioned the high field Q-slope exists in both electropolished and chemically polished cavities, but it persists in chemically polished cavity after baking and is routinely removed in electropolished cavities after mild baking.

4.3 Oxygen pollution model

In order to explain improvement in the high field Q-slope after mild baking H. Safa proposed an oxygen pollution model [39]. In this model he assumed that niobium close to the oxide is rich in oxygen, the so-called oxygen pollution layer. The superconducting properties of niobium have been found to vary significantly with oxygen concentration, e.g. T_c decrease by about .93°K [40] or 1.23°K [41] per atomic percent of oxygen for low oxygen concentrations. According to Safa, before mild baking there are two layers of niobium, one is the oxygen polluted layer, that has a poor superconducting properties, and the other is pure niobium, Fig. 4.9. The oxygen-polluted layer has superconducting prop-

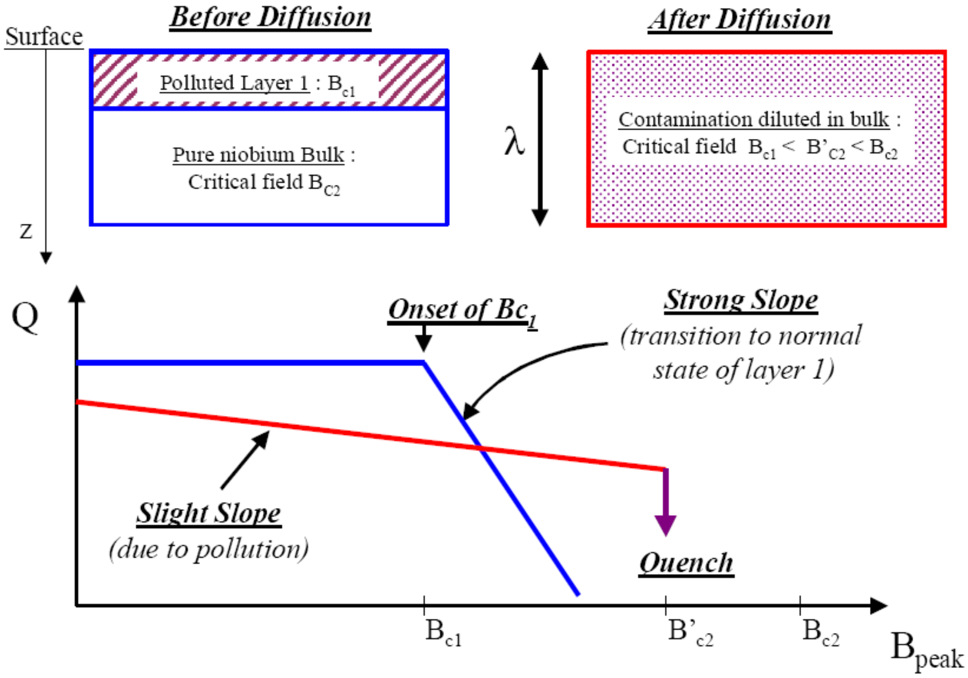

Figure 4.9: Schematic of oxygen pollution model. Before mild baking the high field Q-slope exists due to the oxygen polluted layer. After mild baking oxygen is dissolved via diffusion, so the high field Q-slope disappear.

erties that are worse than those of pure niobium. Mild baking of a cavity at 100°C for 48 hours, a typical baking procedure, dilutes the oxygen pollution layer, so that there is no bad superconductor layer, which quenches at low magnetic field. Indeed, for the oxygen diffusion coefficient in niobium it follows that oxygen diffuses several tens of nanometers under such conditions.

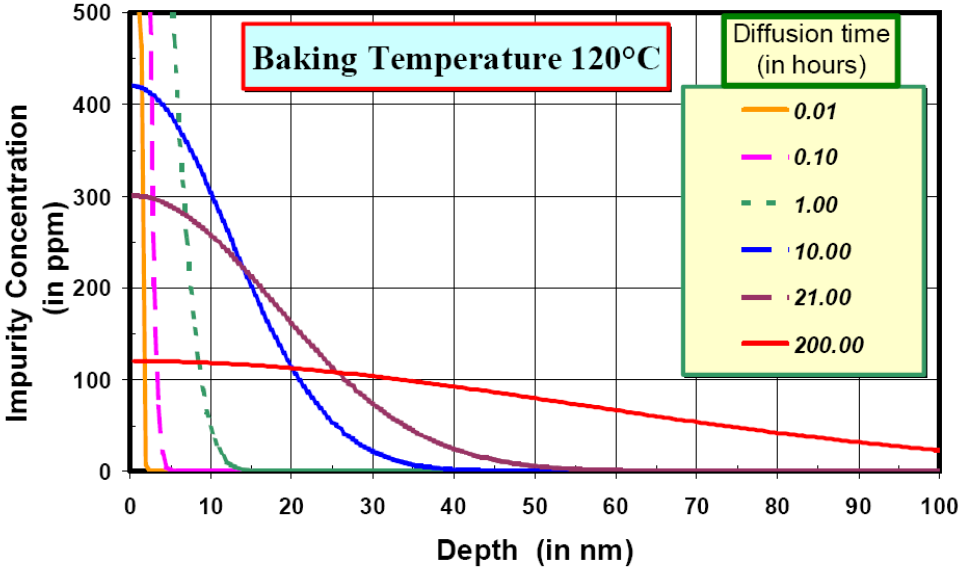

Figure 4.10: Oxygen diffusion profiles calculated in [39].

This model was realized to be incomplete, because it could not incorporate the results after baking at higher temperatures, i.e. 150-180°C for 48 hours, in which the high field Q-slope remains unchanged or even becomes stronger. In order to accommodate these results, the oxygen pollution model was improved by G. Ciovati [42]. He introduced a temperature-dependent destruction of the oxide layer during mild baking; the idea supported by surface studies. Indeed, there is difference in XPS spectra of as-received and mild baked samples. This difference suggests a reduction of niobium pentoxide to lower oxides. The oxygen, released during pentoxide destruction, was suggested to move into niobium, enriching niobium with oxygen. Thus Ciovati suggested that the mild baking

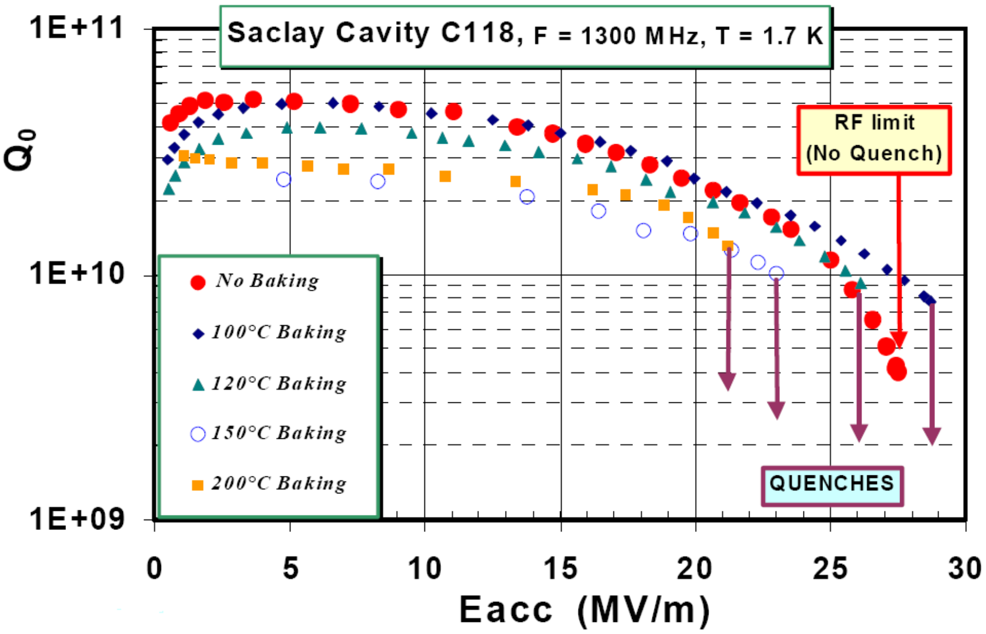

Figure 4.11: High field results for cavities baked at different temperatures [39].

effect can be split into two counteracting processes, one is diffusion of oxygen from the pollution layer into bulk, the other one is diffusion of oxygen from oxide into the pollution layer.

He suggested that the following equation describes the process:

$$\frac{\partial c(x,t)}{\partial t} = D(T)\frac{\partial^2 c(x,t)}{\partial x^2} + u_0 k(T) e^{-k(T)t}\delta(x) \tag{4.12}$$

Where $k(T) = Ae^{-E_a/RT}$ is a oxide total reduction rate, from $Nb_2 0_5$ to NbO, with $A = 310^9$ 1/s and $E_a = 135$ KJ/mol, as inferred from surface studies, $D(T) = 0.0138e^{-111530/RT}$ cm^2/s is diffusion rate, c(x,t) is concentration of oxygen as a function of time and depth. Boundary conditions were zero concentration at infinity and no particle flux across the zero. The initial condition was $c(x,0) = c_0\delta(x)$, where c_0 was 10 at. percent. The solution for different baking condition yielded that oxygen concentration will have minimum for mild baking at 140 °C for 48 hours and will be higher for baking at higher and lower temperatures,

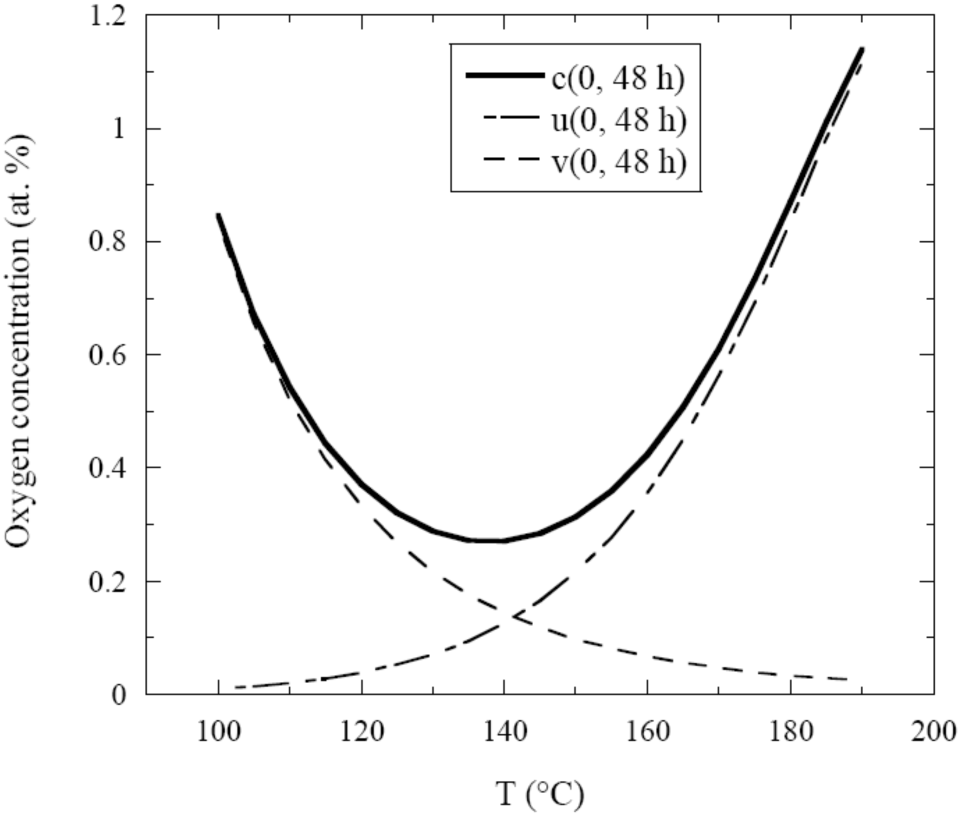

Figure 4.12: Diffusion calculation based on the modified oxygen pollution model proposed by G. Ciovati.

Fig. 4.12, which is in qualitative agreement with RF data.

CHAPTER 5

GENERAL THERMOMETRY RESULTS ON THE HIGH FIELD Q-SLOPE

5.1 Distribution of losses

As we mentioned in chapter 3, thermometry is an extremely powerful tool to distinguish a variety of phenomena in superconducting cavities:*multipacting*,*field emission*,*hydrogen disease* etc. via the heating patterns. Also, close examination of the response as a function of increasing field helps to separate and to classify various types of anomalous losses. Below we give examples of thermometry results for typical cavity phenomena. The configuration of the electromagnetic field in the cavity is such that near the equator at a certain field level an electron extracted from niobium by electric field may return to the same point. In the impact more electrons are generated. This resonance process is called *multipacting* and appears on the temperature map as a large hot spot on the equator, Fig. 5.1, when the impacting electrons cause thermal breakdown.

Particle contaminants or protrusions on the surface can enhance the local electric field, facilitating emission of electrons. This is called *field emission*. These electrons are then accelerated by the electric field. Finally they hit the surface transferring their energy to the lattice. This is field emission heating. Because all forces acting on the electrons are coplanar to the axis of symmetry of cavity, the phenomenon presents itself as a strip of heating on the surface, typically 1-2 thermometers wide, Fig. 5.2.

At low temperatures hydrogen that is present in the niobium bonds to niobium, forming niobium hydride. This phenomenon is called the hydrogen Q-disease. The first indication of hydrogen disease on the temperature map is a

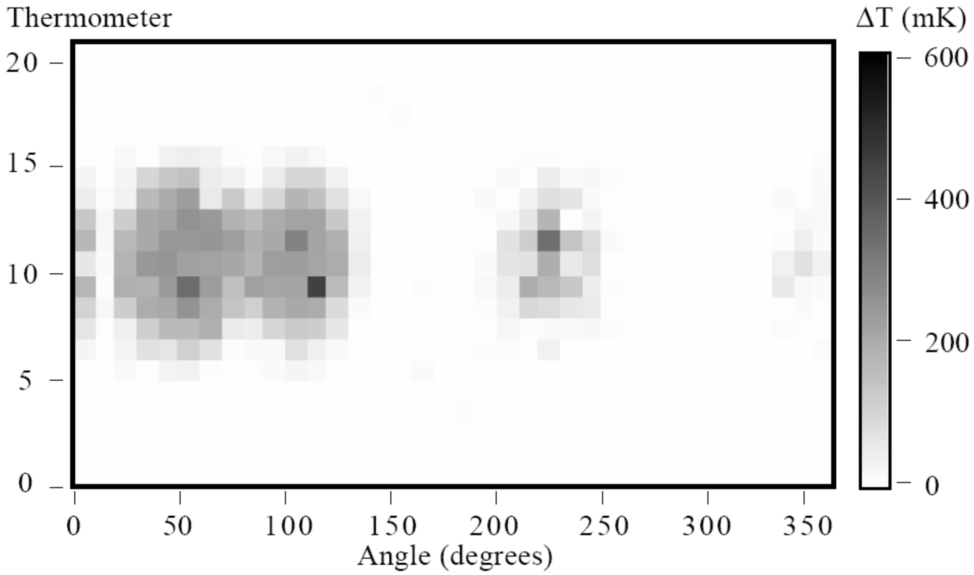

Figure 5.1: Examples of temperature map dominated by multipacting. LE1-17 at B_{peak}=79 mT. Picture taken from [25].

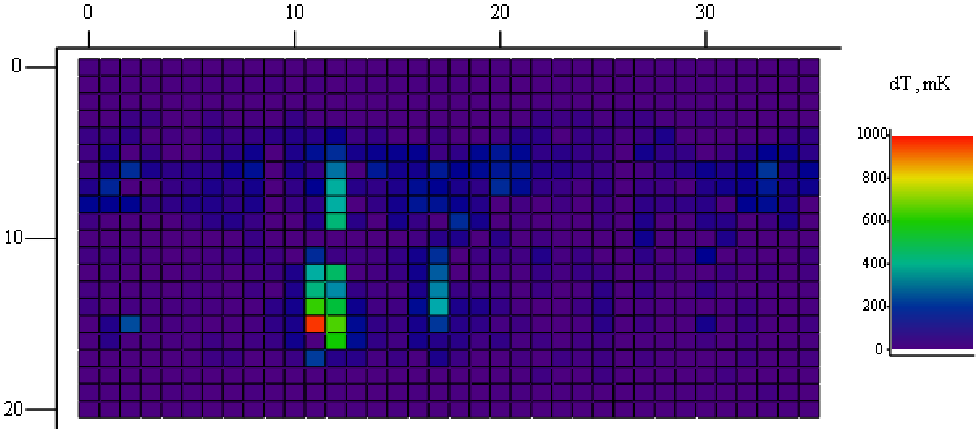

Figure 5.2: Example of temperature map dominated by field emission. LE1-35 at B_{peak}=157 mT.

band of heating on the equator(it also can be an indication of the bad weld in a new cavity), Fig. 5.3.

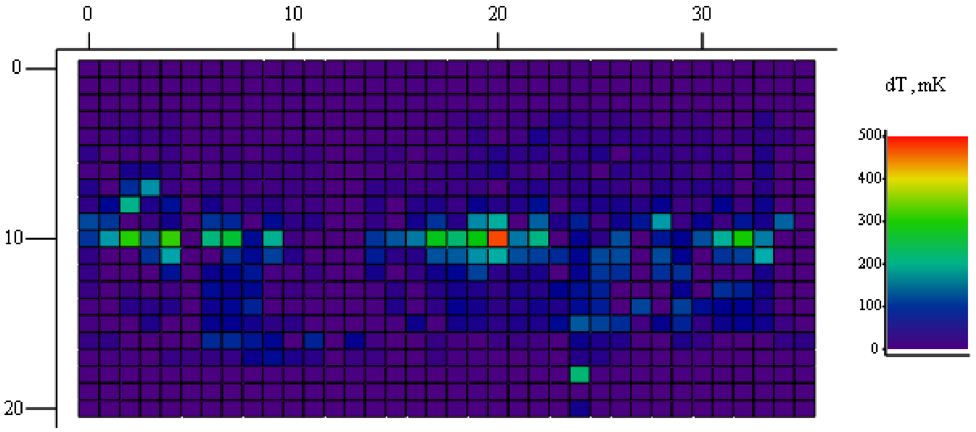

Figure 5.3: Example of temperature map dominated by hydrogen Q-disease. LE1-30 at B_{peak}=91 mT.

Finally, a normal-conducting inclusion or more usually a surface irregularity, e.g. ”pit”, produces a hot area typically with the diameter of 1-2 thermometers. This phenomenon is called a defect, Fig. 5.4.

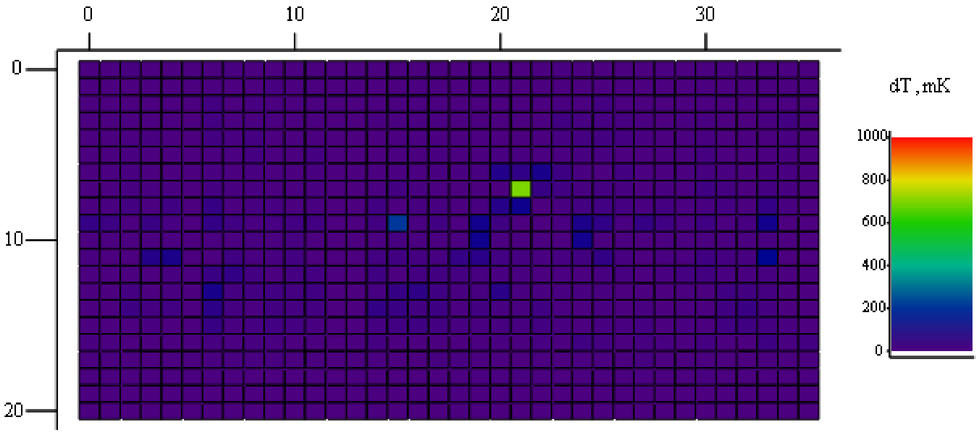

Figure 5.4: Example of temperature map dominated by defect. LE1-37 at B_{peak}=98 mT.

As we see, when a certain loss mechanism takes place a thermometry system is an essential tool in recognizing the problem. Each loss mechanisms has a certain pattern on the temperature map and is easily recognized.

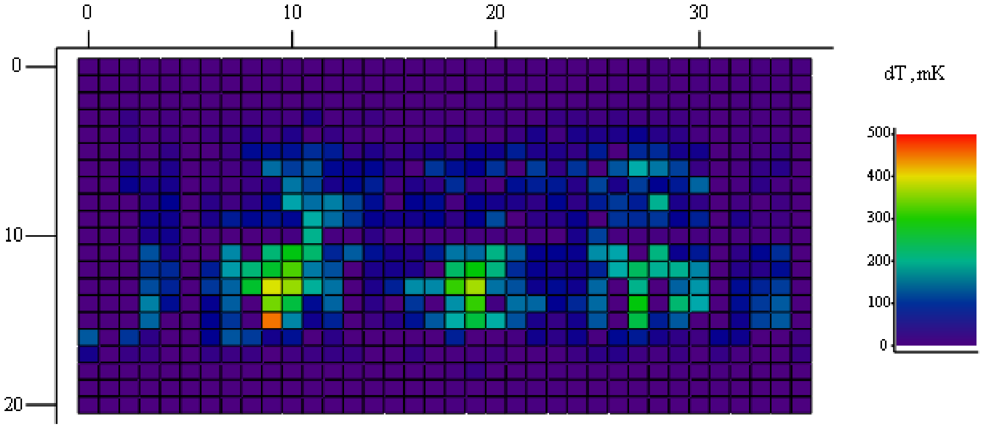

Figure 5.5: A typical distribution of losses(temperature map) in the high-field-Q-slope regime

The high field Q-slope also has its own pattern on the temperature map. The high field Q-slope appears as several hot areas(hot-spots) in the high-magnetic-field region, Fig. 5.5. Unlike other loss-mechanisms the high field Q-slope is not a single hot area, but several hot areas appear simultaneously on the temperature map in the high-magnetic-field region. Sometimes it is not clear from the excitation curve, whether the cavity is limited by the high field Q-slope or some other phenomena. The non-local feature of the high field Q-slope helps to distinguish high-field-Q-slope-dominated cavities from cavities dominated by other effects. This non-local feature holds true after mild baking as well, Fig. 5.6 and Fig. 5.7.

5.2 Typical reading of a temperature sensor

Each temperature sensor on the cavity surface measures a mean dissipated power in the region of about 1x1 cm^2. In the medium-field-Q-slope regime

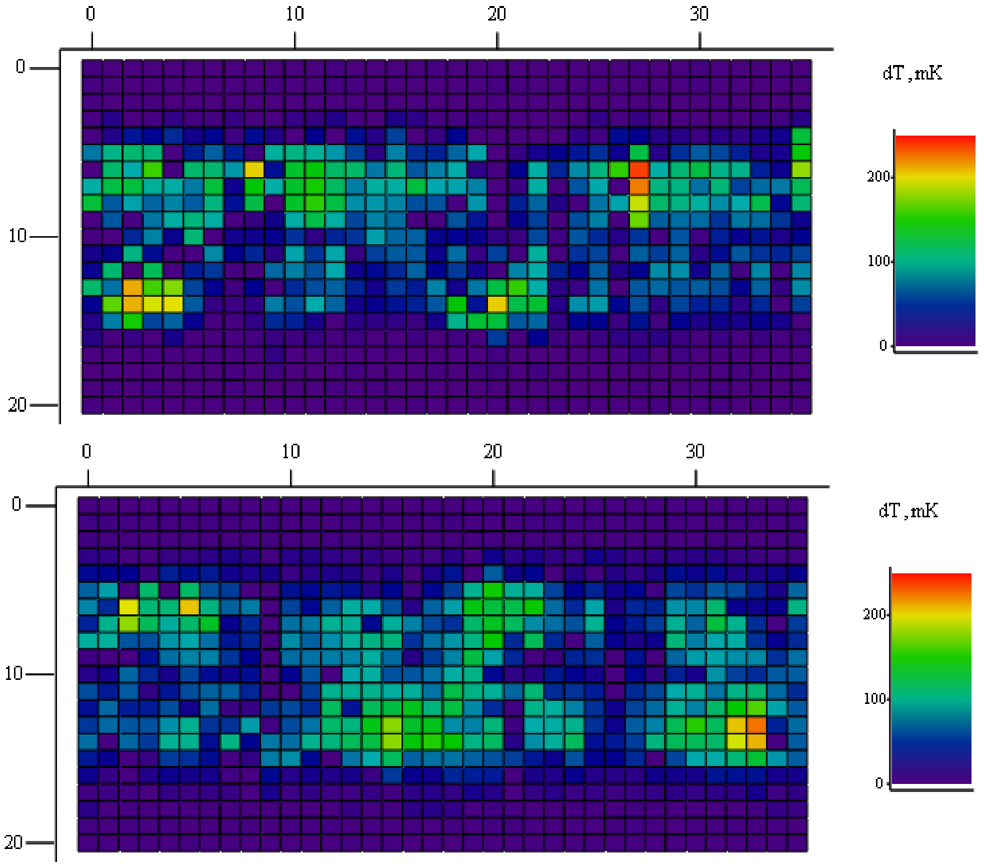

Figure 5.6: Temperature maps for tests after BCP on 03/11/03[top] and 06/27/03[bottom] at B_{peak} = 117 mT.

the temperature grows approximately quadratically with field as expected from Ohm's law. Some deviation from the quadratic law is expected because of two factors: thermal feedback and the intrinsic efficiency of the temperature sensors. But once the onset of the high field Q-slope is reached the readings of each thermometer in the high-magnetic-field region follow a highly non-quadratic law, Fig. 5.8[circles], i.e. exponential temperature rise with different exponents in different regions. Slopes of *log dT vs log E* range from 10 to 40. However, such high slopes are observed only for thermometers in the high-magnetic-field regions. In the low-magnetic-field regions, i.e. high-electric-field regions, no high field Q-slope appears up to the highest field, Fig. 5.8[squares]. One conclusion

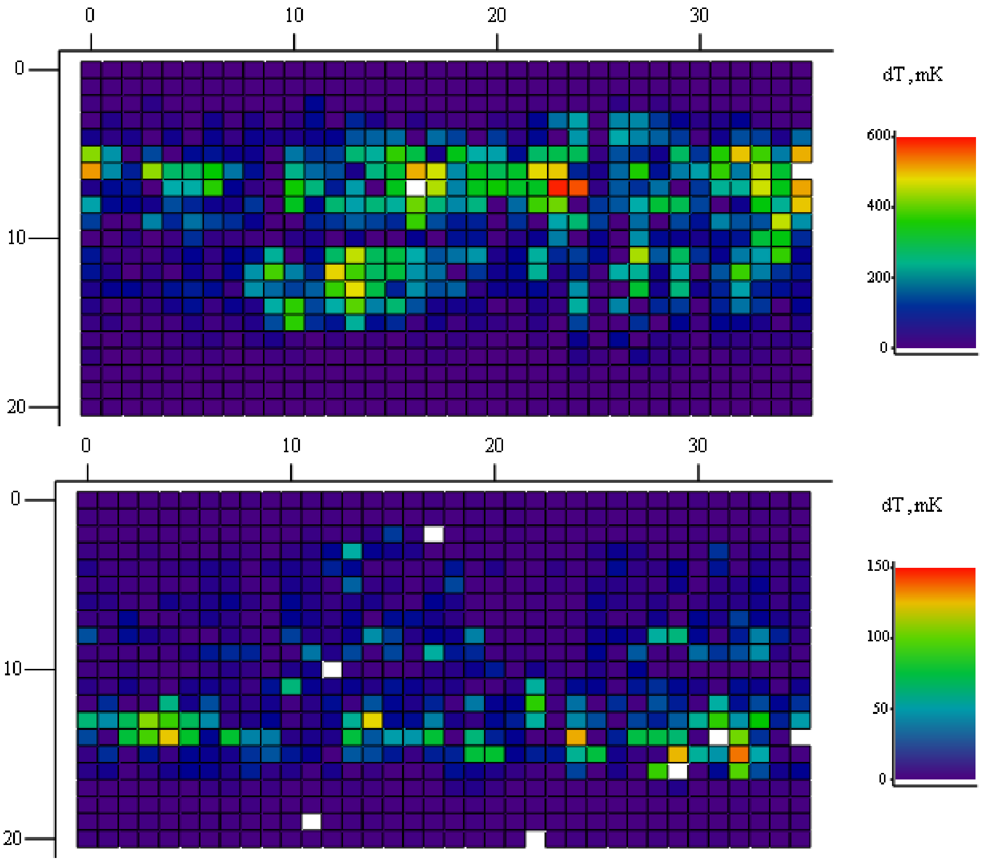

Figure 5.7: Temperature maps for tests after baking.[top] Temperature map at B_{peak} = 145 mT, test on 09/23/03 after mild baking at 125-138°C for 48 hours.[bottom] Temperature map at B_{peak} = 130 mT, test on 12/05/03 after 106-110°C for 48 hours.

that follows immediately is that, since the bath temperature is the same at every point on the surface, the global heating of the bath is not responsible for the high field Q-slope.

It is important to note that for niobium surfaces after chemical treatment high-field slopes are observed for all thermometers in the high-magnetic-field region. The only instances, when we don't see the high field Q-slope, is when it is masked by other phenomenon, e.g. a defect. In such cases readings of thermometer in the high-magnetic-field region may show "quadratic" behavior up to the highest field. At medium fields these readings are an order of magnitude

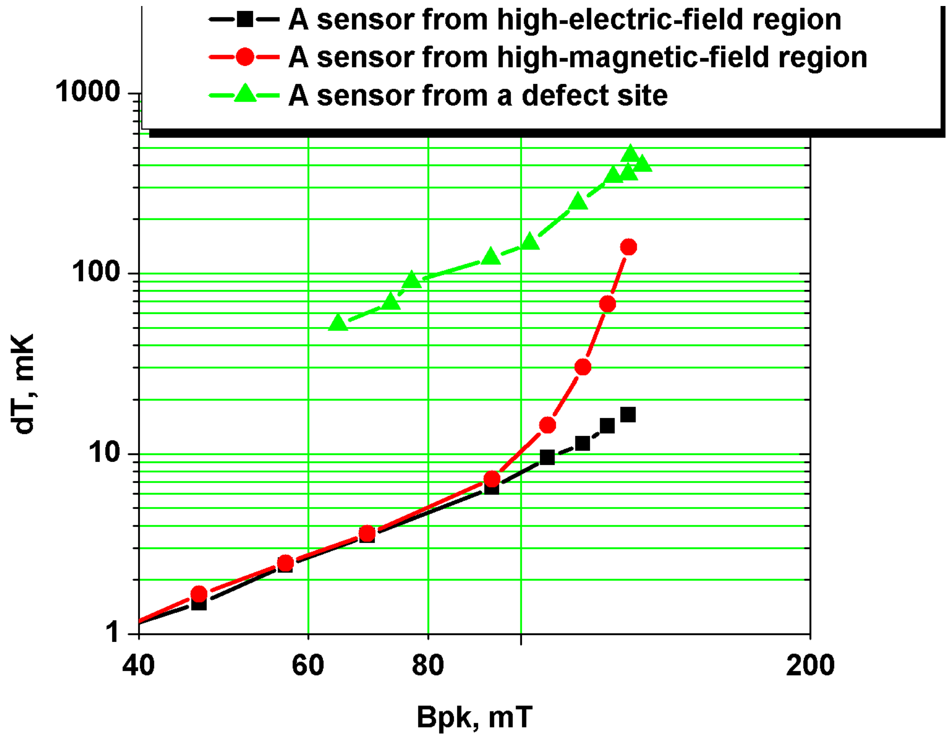

Figure 5.8: A typical reading of a temperature sensor in the defect site[triangles]. Compare with a typical reading of sensors in the high-magnetic- and high-electric-field regions.

higher as compared to readings from other thermometers. Such behavior is typical of a defect, which subsequently may cause a thermal breakdown at higher fields, Fig. 5.8[triangles].

5.3 Field dependence of high field losses

An important question in quantification of the high field Q-slope is whether the field dependence of thermometer's readings follows an exponential or a power law. One way to answer this question is to take a numerical derivative of the data in order to see whether the derivative grows with field or whether it saturates at a certain level. For most thermometers' readings we studied, this approach suggests that the field dependence is exponential, Fig. 5.9, but there are exceptions.

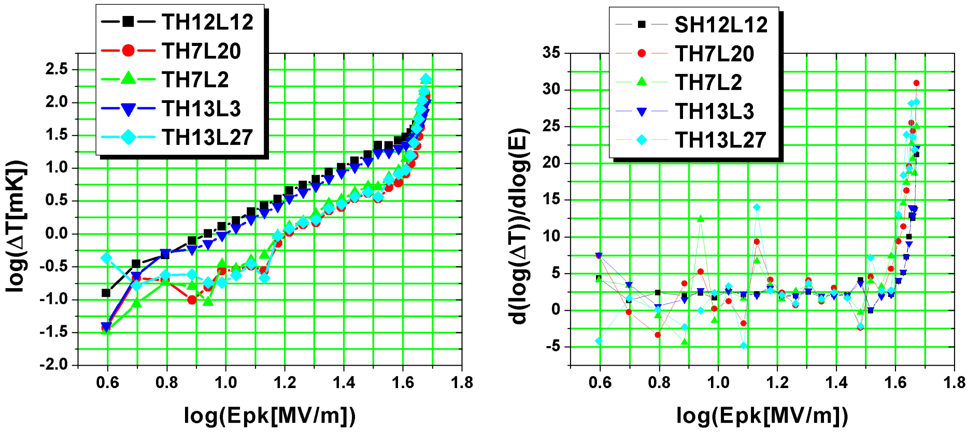

Figure 5.9: Exponential dependence of thermometer's readings.

A different approach is to compare the data from the high field Q-slope with the data from the region, which we know to have an exponential dependence on field. Readings of a thermometer from a field emission site are from such regions. We used the data from [25](Fig.5.6), and replotted the the data for activated field emission site in log-log scale in Fig. 5.10[right]. On the left side in Fig. 5.10 we plotted the data from the thermometer in the high-field-Q-slope region. The behaviors, except for difference in field levels, are the same. Thus even though on the log-log scale the readings from high-field-Q-slope regions appear as power laws, the underlying mechanism has exponential dependence.

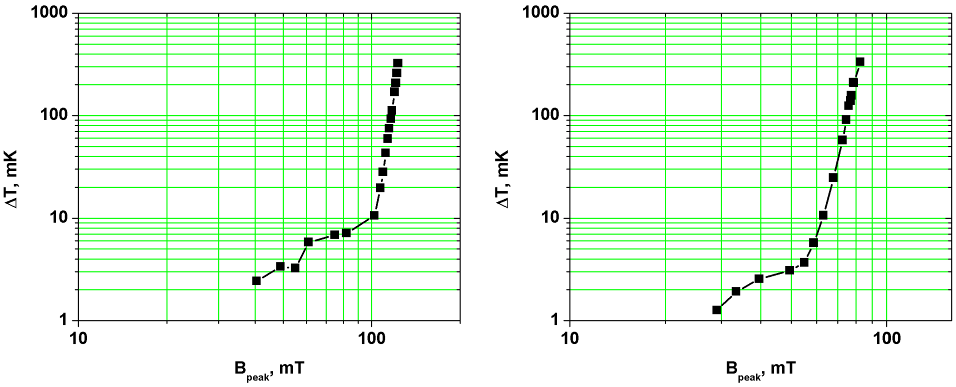

Figure 5.10: Comparison of readings of thermometer from field-emission site[right] to readings of thermometer from high-field-Q-slope region[left].

5.4 Electric vs. magnetic field

The onset field of the high field Q-slope for 1.5 GHz cavities after chemistry is about 100 mT. After the onset the dissipation follows a highly non-quadratic law, Fig. 5.8[circles]. Normally at high fields, slopes in thermometers' readings of *log(dT) vs log(E)* vary from 10 to 40 depending on the location of the thermometer. Several important observations can be made from the data. Firstly, there is no abnormal heating in the low-magnetic(high-electric) surface field regions. In these regions the heating depends quadratically on applied field even after the high field Q-slope has began in the high-magnetic-field regions. On the contrary the interface tunnel exchange model predicts strong dependence of resistance on electric field. But up to the highest field,E_{peak} = 64 MV/m we have not been able to measure any abnormal increase in resistance. Our results show no exponential increase in heating contrary to the prediction from ITE model, Fig. 5.8[squares].

Due to symmetry of the TM_{010} mode all thermometers with the same vertical coordinate(in the same row) on the temperature map see the same electric

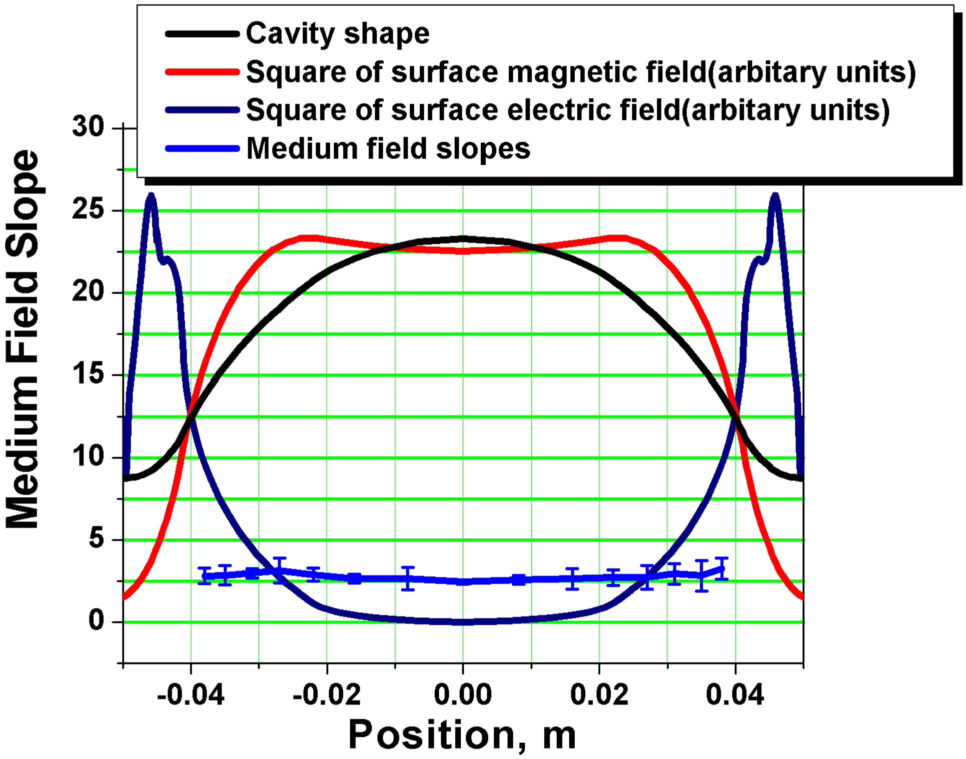

Figure 5.11: Typical distribution of the mean medium-field-slope as function of longitudinal position. Note that the strength of the slope is spatially uniform.

and magnetic fields. We calculated the mean of the medium-field and high-field slope over all thermometers with the same vertical coordinate, and then plot the mean and standard deviation as function of vertical coordinate. One sees that in the medium-field regime no spatial dependence is present; slopes are distributed uniformly with some random variation, Fig. 5.11. On the other hand a plot of the mean of high-field slopes shows a correlation between the longitudinal position of the thermometer and the strength of the high field Q-slope, Fig. 5.12. For comparison, the amplitudes of surface electric field and surface magnetic field are also presented in the plot. There is an anti-correlation between the high field slope and strength of electric field, which again demonstrates that there is no anomalous losses at high electric field regions. On the other hand there is a

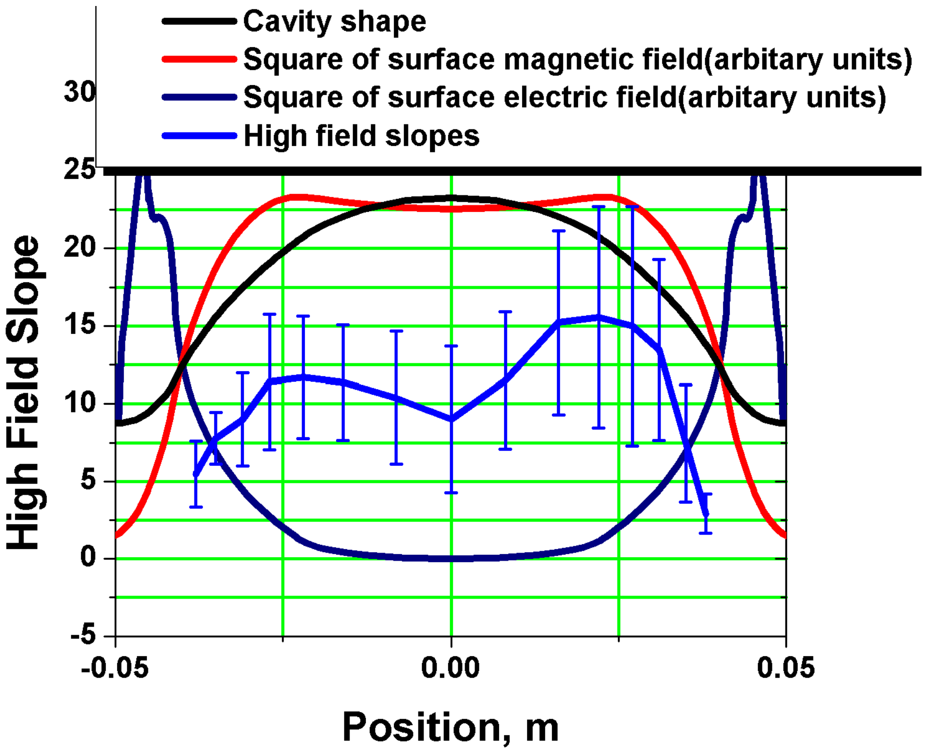

Figure 5.12: Typical distribution of the mean high-field slopes as function of longitudinal position. Note correlation with magnetic field.

correlation between the strength of magnetic field and high field losses.

CHAPTER 6

GENERAL RF RESULTS ON THE HIGH FIELD Q-SLOPE AND THE MILD BAKING EFFECT

6.1 Introduction

Superconducting cavities are limited to about 120 mT after chemical treatment. Our experiments show that several tests of the same cavity after BCP result in the high field Q-slope with the same limitation field. We have also compared five cavities made of different RRR niobium, different wall thickness, different grain size and chemically treated by BCP and EP. All cavities were limited at about 120 mT by the high field Q-slope. In all cavities the high field Q-slope started at about 100 mT.

The high field Q-slope after chemical treatment can be reduced by heat treatment at about 100 °C for 48 hours, so-called mild baking. We have carried out a number of baking experiments with niobium cavities treated by BCP and EP. Our results contradict the modified oxygen pollution model, presented in Chapter 4. Also we found that mild baking increases the limiting field in cavities treated by BCP, but the effect is not reproducible; the same mild baking of the cavity treated in same way gives different improvements in performance.

6.2 Reproducibility of the high field Q-slope

The study of the high field Q-slope starts from establishing the baseline for the effect. After any series of treatments and tests the performance of niobium cavity is restored to the baseline by chemical etching. The performance after chemical etching is reproducible for cavities we tested, i.e. 1.5 GHz elliptical shape(LE) cavities. Unlike field emission that may start at almost any field, and is defined by the properties of the emitter, the high field Q-slope starts at a well-defined field for cavities after chemical treatment. In all cavities after chemical etching it started at about peak surface magnetic fields of 100 mT. When the peak surface magnetic field reached 120 mT, the quality factor dropped by a factor of 10, at which point our measurements were usually limited by available power, Fig. 6.1.

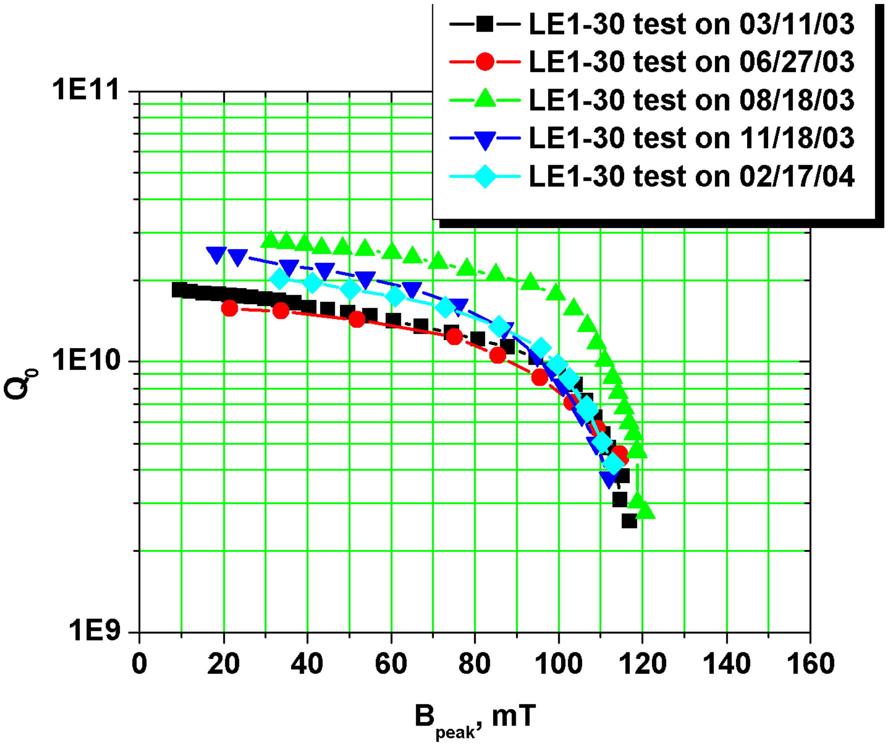

Figure 6.1: Performance of LE1-30 after chemistry in different test .

This reproducibility of the high field Q-slope is a feature of all niobium cavities, which we studied. In five different cavities, which have different material parameters, such as RRR, wall thickness, grain size and chemical treatment, the anomalous losses started at the same field level after chemical treatment. There was not a single instance that peak surface magnetic field of 120 mT was reached without high field Q-slope. Moreover one of these cavities was electropolished with vertical-electropolishing setup. Still the onset of the high field Q-slope was the same for all cavities, Fig. 6.2.

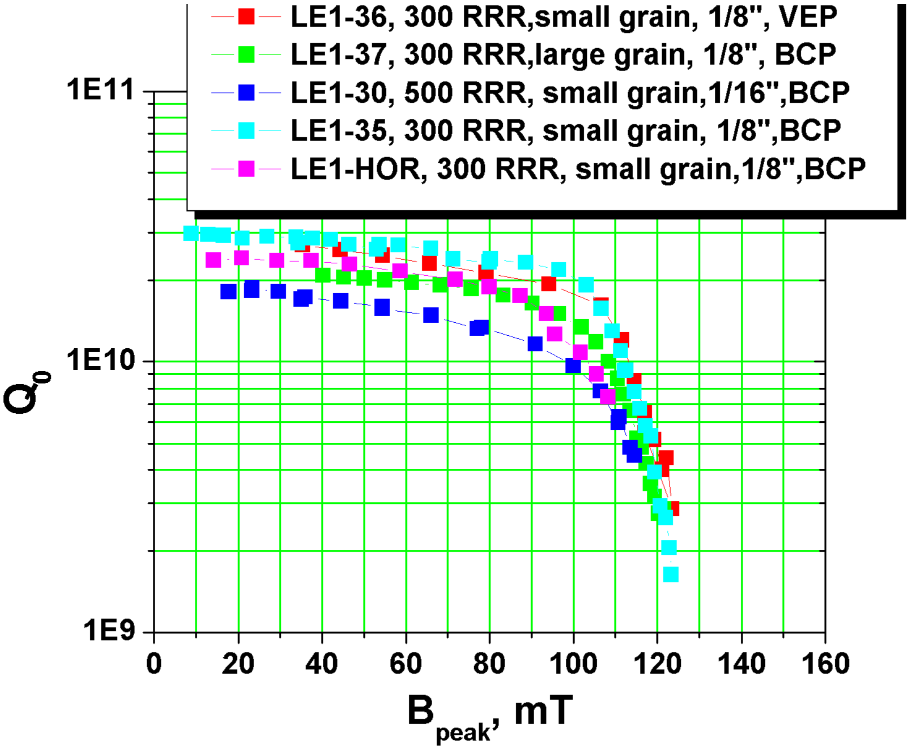

Figure 6.2: Performance of five different cavities after chemistry.

6.3 Dependence on the bath temperature

The independence of the high field Q-slope on the different material parameters shows that the thermal feedback effect is not the cause of the high field Q-slope. If the high field Q-slope is caused by thermal feedback effect, discussed in chapter 4, one expects that the high field Q-slope will vary with bath temperature. The numerical simulations done by J. Vines et al. show that indeed the high field Q-slope becomes stronger with higher bath temperature, Fig. 6.3.

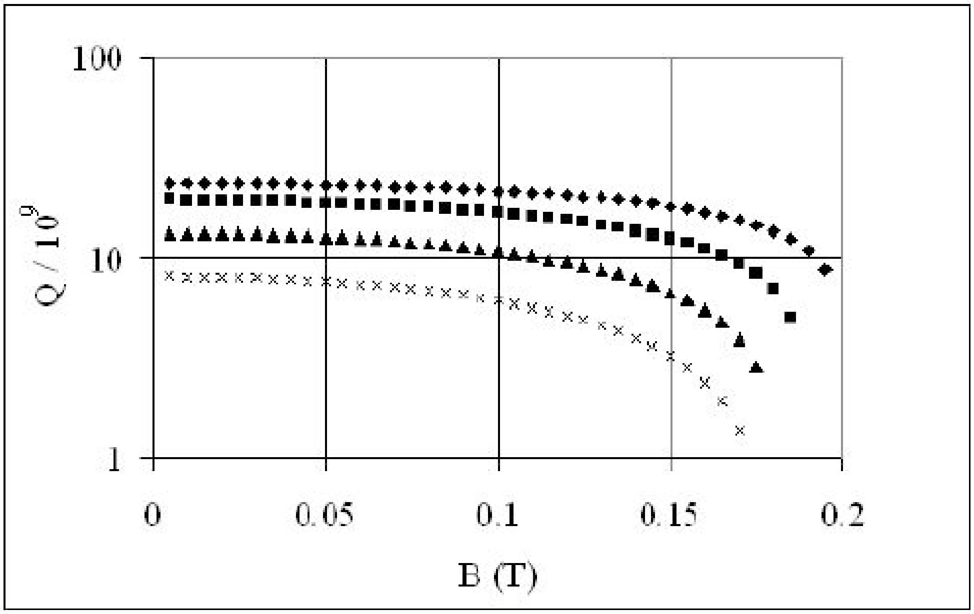

Figure 6.3: Numerical simulations of the high field Q-slope in the framework of the thermal feedback model: variation of quality factor with magnetic field for bath temperatures T_b=1.4 °K(rhomb),1.6 °K(square),1.8 °K(triangle) and 2.0 °K(cross).

In order to see whether the high field Q-slope depends on bath temperature we have done measurements of the high field Q-slope as function of temperature. The LE1-30 cavity was processed with BCP, and then typical preparation steps were followed. In the first test the cavity had a typical high field Q-slope. The excitation curve is presented in Fig. 6.1[squares]. Next the cavity was baked at 100 °C for 48 hours. In the test after mild baking the onset of the high field Q-slope moved from about 100 mT to about 140 mT. After measuring the quality factor as a function of field at helium bath temperature of 1.5 °K, we measured it also at 1.8 °K, 1.95 °K and 2.1 °K to study effect of the bath temperature on the high field Q-slope, Fig. 6.4. At higher bath temperatures the medium-field

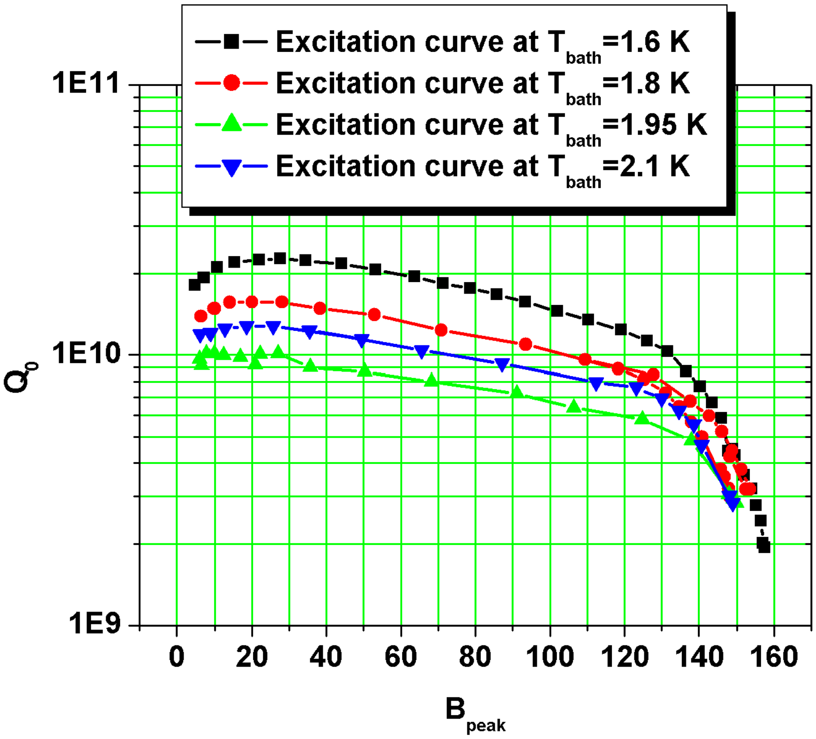

Figure 6.4: Quality factor as a function of field was measured for the four different bath temperatures. At low field due to the exponential dependence of dissipation of temperature the quality factor decrease as the temperature increase. In the high-field-Q-slope regime all curves merge into one.

quality factor decreased, as it is expected from the BCS expression for the RF resistance of superconductor. Surprisingly, there was no major change in the high-field-Q-slope: four curves merged into one as the high field Q-slope took place. Since the onset field of the high field Q-slope does not depend on the temperature, we suggest that thermal feedback effect is not responsible for the high field Q-slope. Similar results were reported by L. Lilje [43].

6.4 Dependence on baking temperature

A systematic research on the change of BCS parameters of superconducting niobium after mild baking was carried out by G. Ciovati [44]. The experiments were carried out on 1.5 GHz CEBAF-shaped post-purified cavity. Prior to each mild baking the cavity was chemically treated. The experiments confirmed the decrease in the BCS resistance after mild baking. Fig. 6.5 shows the temperature dependence of decrease on the baking temperature.

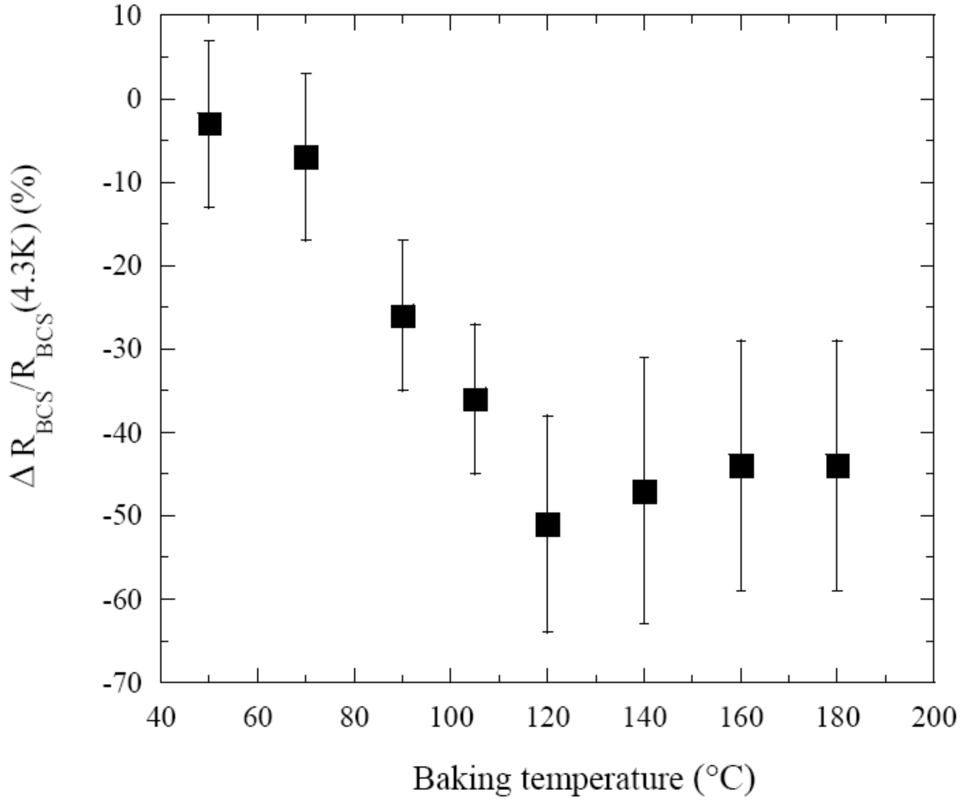

Figure 6.5: Results from [44]. Plots present the improvement in BCS resistance and the quality factor before[squares] and after[triangles] mild temperature heat treatment.

We also did experiments with different baking conditions to study the effect of baking temperature on the high field Q-slope, but we focused on the improvement in the onset of the high field Q-slope. The reproducibility of the high field Q-slope was shown before, so we are presenting only one test result before baking in Fig. 6.6[circles]. Other curves present the test results after mild baking under different baking condition.

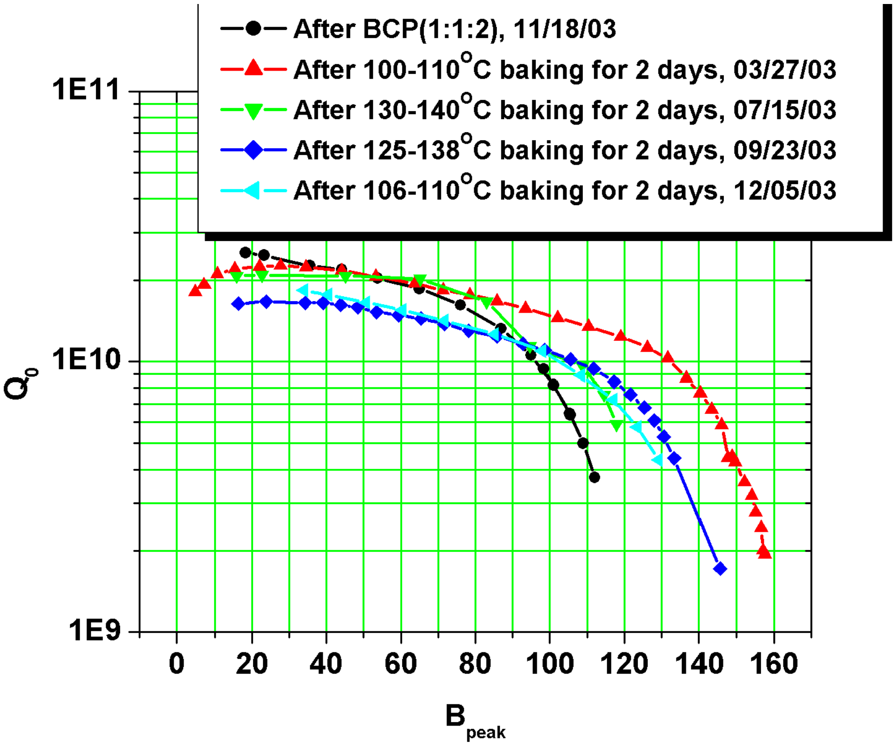

Figure 6.6: Results for LE1-30 after mild baking at different temperatures. One 100°C baking steps out of other baking experiments.

The performance improved in all tests following mild baking. The least improvement was observed after mild baking at 140°C, though except for one 105°C baking the performances are very similar and show little dependence on baking condition. This result is consistent with Ciovati results, which show that improvement in BCS resistance saturates at about 40-50 percent for baking temperatures above 100 °C, Fig. 6.5. In one instance in our experiments the cavity reached a significantly higher field after mild baking at 105 °C. The cause for this outstanding result is not clear. The only notable difference in the cavity preparation was that the cavity was standing in the clean room for three years prior to testing, whereas in other cases the cavity was typically tested in less than one week after chemistry.

6.5 Successive mild baking

According to the modified oxygen diffusion model, presented in chapter 4, baking at temperatures above optimum temperature is not beneficial to cavity performance, because it creates more oxygen by destroying oxide. On the basis of the model we speculated that the excess of oxygen, which was created by destruction of oxide, can be reduced by another mild baking at low temperature. We performed such a sequence of experiments twice. In the first case the cavity LE1-30 was baked at 130 °C for 48 hours after chemistry. After mild baking the high field Q-slope started at B_{peak} = 120 mT, Fig. 6.7[circles]. Next the cavity was baked at 100°C for 48 hours. Surprisingly, the performance degraded instead of improving and the onset of the high field Q-slope again was B_{peak} = 120 mT, Fig. 6.7[triangles]. Next the cavity was baked at 90 °C for 48 hours. The high field Q-slope stayed intact after mild baking, Fig. 6.7.

Later we performed a similar set of experiments after the hydrogen degassing at 800 °C. First the cavity was tested after chemical etching with BCP. Next the cavity was baked at 150°C for 48 hours. After the high field Q-slope did not improve, but rather remained the same. Next the cavity was baked at 100°C for 48 hours and then at 120°C for 48 hours. There was no change in the high field Q-slope, Fig. 6.8.

These results contradict the modified oxygen pollution model. Within this model one expects the high-field performance to improve in 130 °C $\longrightarrow$ 100 °C

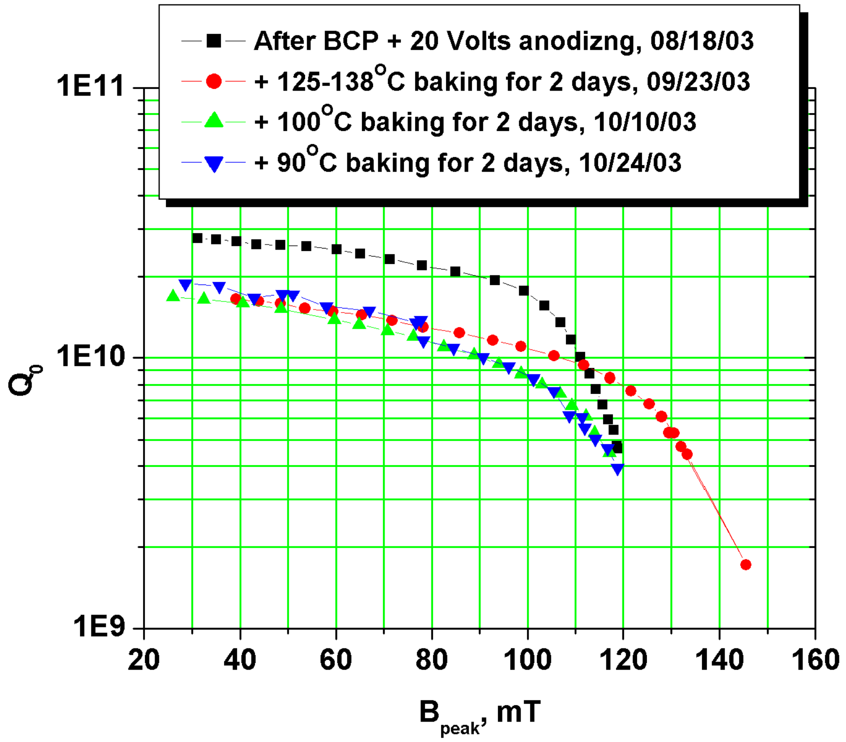

Figure 6.7: Results of LE1-30 for successive mild baking at different temperatures. Note that after second successive baking the performance was the same as it was after chemistry.

successive baking sequence, because oxide destruction has, virtually, zero rate at 100 °C and the only process that happens is diffusion of oxygen in the bulk. Thus one expects that in 130 °C $\longrightarrow$ 100 °C successive baking sequence the surface oxygen concentration increase after 130 °C, but it drops after 100 °C. Since the model suggests that losses at high field are proportional to oxygen concentration at the surface, the performance can only improve. But in the first set of experiments the high-field performance after 100 °C mild baking was worse than that after previous 130 °C baking, Fig. 6.7. A similar situation is observed in second set of experiments, where an improvement in the performance was expected after successive mild baking, but was not observed. These results contradict the modified oxygen pollution model and suggest that modified oxygen

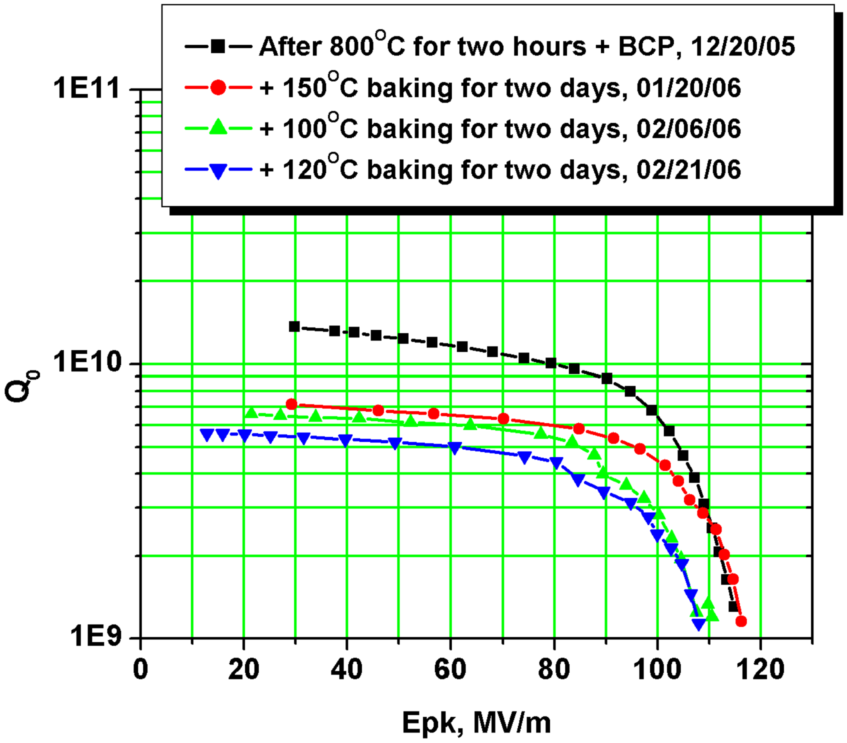

Figure 6.8: Results of LE1-30 for successive mild baking at different temperatures. Note the high field Q-slope is the same in all experiments.

pollution model is not the correct model for the high field Q-slope.

CHAPTER 7

CHANGE IN THE HIGH FIELD Q-SLOPE BY BAKING AND ANODIZING

7.1 Introduction

Numerous experiments have shown that cavities reach higher quality factor at higher fields after mild baking. During the mild baking treatment the properties of niobium are altered beneficially. The beneficial modification occurs either in the entire niobium wall, i.e. it is a bulk improvement,or only near the surface. A quantification of the length scale for this effect is essential for choosing the appropriate tool to perform material studies related to the high-field-Q-slope problem, and for selecting correct models for the mild baking effect. The studies discussed here attempt to determine the depth of the baking benefit.

Previous experiments, in which cavity's surface was etched for a few microns after the mild baking, suggest that the mild baking effect is not a bulk effect, but rather a surface one. In these experiments the Q-slope improvement was lost after 1 minute of BCP(1:1:2). Since the typical removal rate is 1-3 μm per minute for a standard BCP(1:1:2), the conclusion is that the depth of the baking effect is less than 1 μm. In another experiment a cavity, treated by mild baking, was rinsed in HF. This treatment dissolves niobium oxide with a subsequent growth of a new oxide during water rinsing. But the cavity's performance did not degrade; the high field Q-slope did not return. This experiment suggests that the mild baking effect extends deeper than the first 1-3 nanometer of the surface.

To measure the depth of the mild baking benefit, a cavity was progressively anodized at increasing voltage. Anodizing converts a certain thickness of niobium into a dielectric niobium oxide, thereby consuming niobium in the layer that was altered by the mild baking. Since niobium oxide, formed by anodizing, is a low-loss dielectric, the superconducting currents are pushed deeper into the metallic niobium, probing superconducting properties of deeper layers of niobium. Eventually the entire niobium layer that was improved by the mild baking is consumed by anodizing and the voltage at which the anodizing was conducted defines the thickness of the niobium layer.

This method was successfully applied by Peter Kneisel at TJNAF [45], to determine the depth of the reduced mean free path layer, which is responsible for the reduced BCS resistance due to mild baking. Kneisel carried out step-by-step anodizing on a cavity that was baked at 145^0C for 45 hours. In the experiment the BCS surface resistance of the cavity was improved by the mild baking. The cavity had to be anodized for 150 Volts in order to remove the effect of the mild baking on BCS resistance completely. Anodizing for 150 Volts creates a niobium oxide of about 300 nanometer thick. Thereby Kneisel's experiments suggest that mild baking at 145^0C for 45 hours modifies the BCS resistance of a layer about 100 nanometer thick. However the high field Q-slope was not an objective of these experiments. We carried out a similar experiment with progressive anodizing to determine the depth of the mild baking benefit layer. The results and the discussion of such experiments is presented below.

Because the response of the BCP and EP cavities to mild baking is quite different, we carry out the anodizing experiments on cavities polished by both BCP and EP. Thermometry was used to study the behavior of the cavity losses in more detail than it is possible with just RF power measurements. Because of the thermometry we could anodize each half cell at different voltage to reduce the number of tests needed to probe the depth. In the table 7.1 the summary of cavities' parameters is presented.

Table 7.1: The summary of cavities' parameters

	$Cavity No.1$	$Cavity No.2$
Frequency	1500 GHz	1500 GHz
Shape	Elliptical MARK-III	Elliptical MARK-III
RRR	500	300
Grain size	1 mm	1 mm
Thickness	1.5 mm	3 mm
Initial Treatment	BCP(1:1:2)	Vertical EP

7.2 Anodizing BCP cavity

The following experiments were carried out with the cavity No.1:

- Test No.1. The cavity's performance was measured after chemical polishing by BCP(1:1:2). The baseline for the high field Q-slope was established.
- The cavity was baked at $100°$C ″in situ″ for 48 hours.
- Test No.2. The high field Q-slope was reduced.
- The cavity was anodized for 5 volts.
- Test No.3. The high field Q-slope remained reduced.
- The top-half of the cavity was anodized for 60 volts, the bottom-half of the cavity was anodized for 30 volts.
- Test No.4.The high field Q-slope was the same as in the baseline test.
- The cavity was baked at $100°$C ″in situ″ for 48 hours.
- Test No.5. The high field Q-slope was reduced.

In the test No.1.,Fig. 7.1 (squares), the excitation curve has an onset of the high field Q-slope at about H_{peak}=90 mT, which is typical. After the onset of the high field Q-slope the quality factor degraded by a factor of two over 25 mT and at the highest field point, at about H_{peak}=115 mT, the measurement was limited by available power. The temperature maps, taken in the high-field-Q-slope region, show several broad hot spots in the high magnetic field region, which is also typical for the high field Q-slope, Fig. 7.2. In this test the baseline for the experiments was established. Next the cavity was baked at 100°C for 48 hours. After the mild baking the excitation curve shows an onset of the high field Q-slope at about H_{peak}=110 mT, which is about 20% higher than before the mild baking. Past the onset the quality factor degraded by a factor of two in the next 30 mT and there, at about H_{peak}=140 mT, the measurement was limited by available power, Fig. 7.1(circles). Temperature maps again showed a general reduction of heating, although some broad areas of heating remain on the top half-cell, Fig. 7.2. The bottom half-cell was not limited by high field Q-slope after baking: thermometers on the bottom half-cell show only quadratic heating up to the highest field. This assymetry is attributed to a deficiency of the baking setup with heat tapes, which resulted in a non-uniform baking. Next the cavity was anodized for 5 volts, which has a negligible effect on the cavity's performance, Fig. 7.1(upward triangles). 5 Volts anodizing increases the thickness of the oxide layer from the natural oxide thickness of 5 nm to 10 nm, converting about 2 nm of niobium to niobium oxide. The high field Q-slope does not return.

For the next step it was proposed to take advantage of the thermometry system by anodizing the half-cells of the cavity at different voltages and then calculate the contribution of each half-cells to total losses from thermometry data. Since the rf penetration depth is about 50 nm, we attempted to take bigger steps

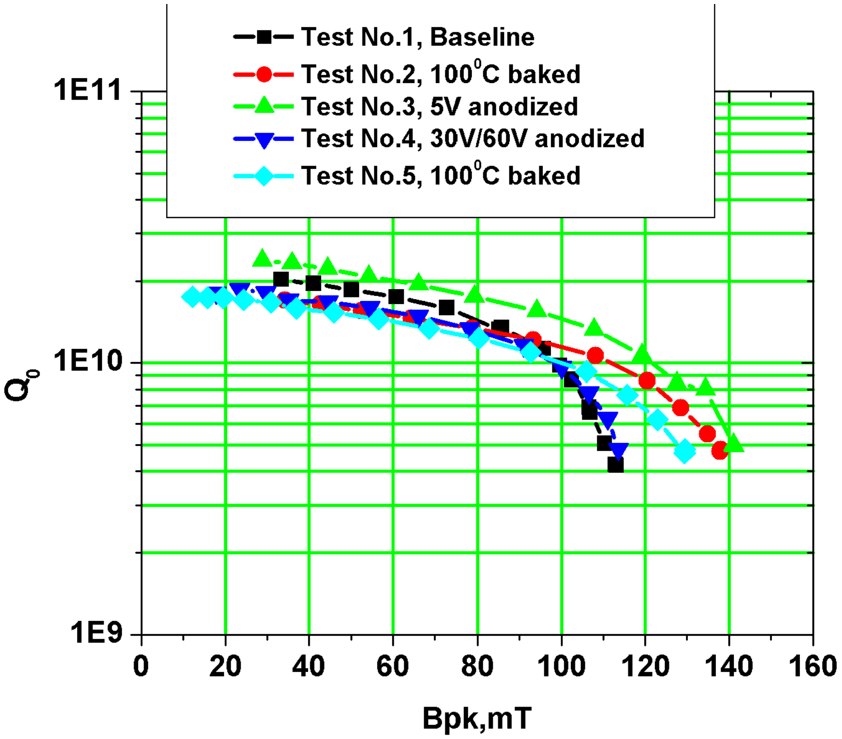

Figure 7.1: Quality factor vs. peak magnetic field. [squares]The baseline: the cavity's performance after chemical treatment before mild baking shows a typical high field Q-slope;[circles]The mild baking improvement: the cavity's performance was improved by 100°C for 48 hours baking;[upward triangles]The 5 Volts anodizing: the cavity's performance was not altered by 5 Volts anodizing;[downward triangles]The 30/60 Volts anodizing: the baseline was restored by 30/60 Volts anodizing;[rhomb]Another mild baking: the cavity's performance was improved by another mild baking

into the metal layer. The cavity's top and bottom half-cells were anodized for 60 and 30 Volts respectively. After the anodizing, the cavity's excitation curve coincided with that before the mild baking, Fig. 7.1(downward triangles). The high field Q-slope returned. The temperature maps in the high-field-Q-slope region show broad hot spots on both the top and bottom half-cell, Fig. 7.3. From the thermometry data the contribution of the top and bottom half-cell was calculated, Fig. 7.4. The results show that both half-cells contribute equally to the

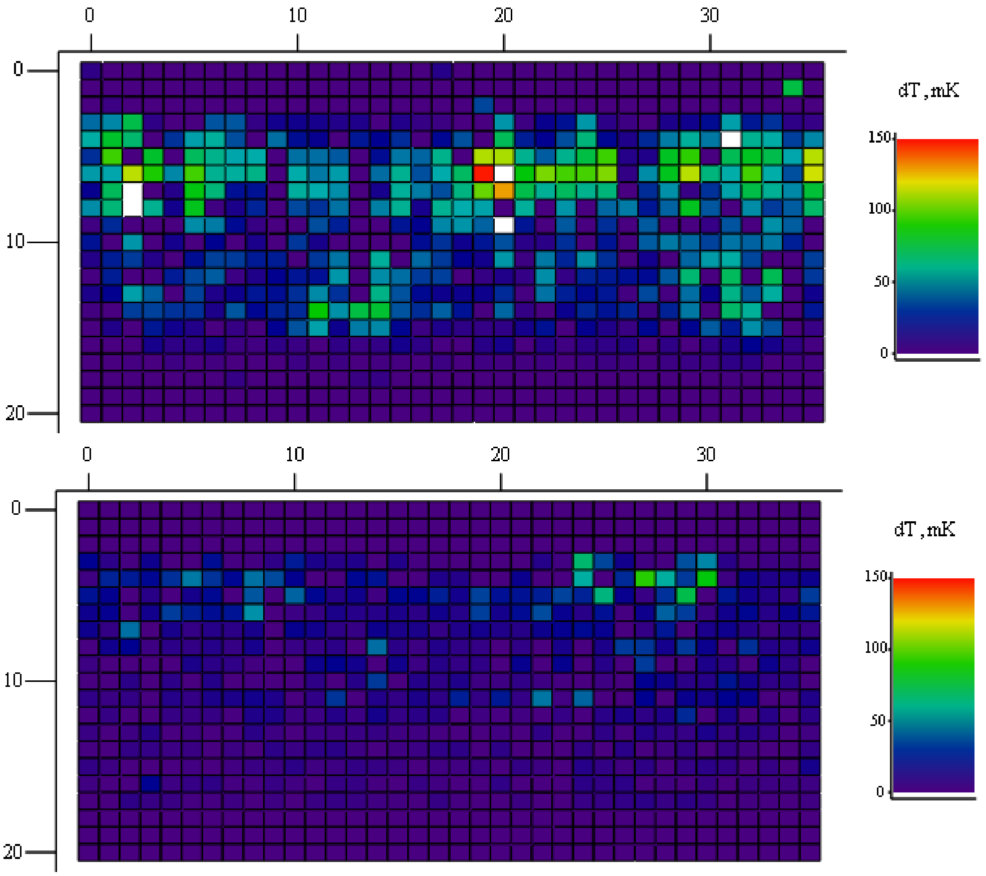

Figure 7.2: Top temperature map, taken at Hpk=110 mT in the test preceding the mild baking's treatment, shows several hot-spots in the high magnetic field's region; bottom temperature map, taken at Hpk=120 mT in the test after the mild baking, show that the cavity is not limited by the high field Q-slope after mild baking.

high-field-Q-slope degradation of the quality factor. Thus after both 30 Volts and 60 Volts anodizing the surface layer that was improved by the mild baking was converted to oxide. Therefore the niobium layer that was improved by the mild baking at 100°C for 48 hours was consumed by 30 Volts anodizing. Since the density of amorphous niobium pentoxide is 4.47 g/cm3, the atomic mass of two atoms of niobium and five atoms of oxygen is 4.42*10^{-22} g, the density of niobium is 8.58 g/cm3 and the atomic mass of two niobium atoms is 2*1.54*10^{-22} g, the volume per an atom of niobium in niobium pentoxide is 2.74

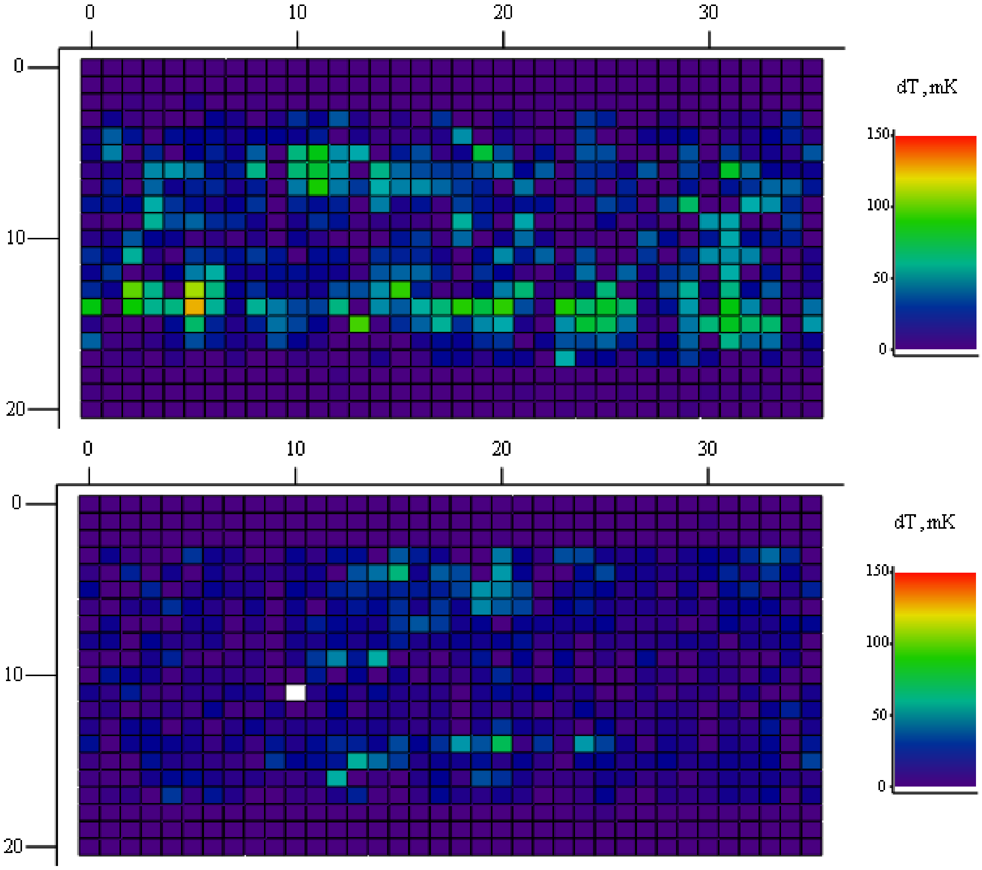

Figure 7.3: Top temperature map: temperature map, taken at B_{peak}=115 mT in the test after 30/60 Volts anodizing, shows that both the top and bottom cavity's half-cell are limited by high field Q-slope at the same field level as for the baseline; bottom temperature map: temperature map, taken at B_{peak}=116 mT in the test after second mild baking, shows the absence of the high field Q-slope.

times more than that in bulk niobium. The oxide grew only in one dimension, so the thickness of the niobium layer consumed by the anodizing, in order to make 60 nm thick niobium oxide at 30 Volts, is about 22 nm.

Next a new mild baking was performed to show that despite presence of a thick oxide layer the metallic niobium can still be improved by the mild baking. Indeed the excitation curve after another mild baking shows a higher onset of high field Q-slope at about H_{peak}=110 mT. The measurement was limited at

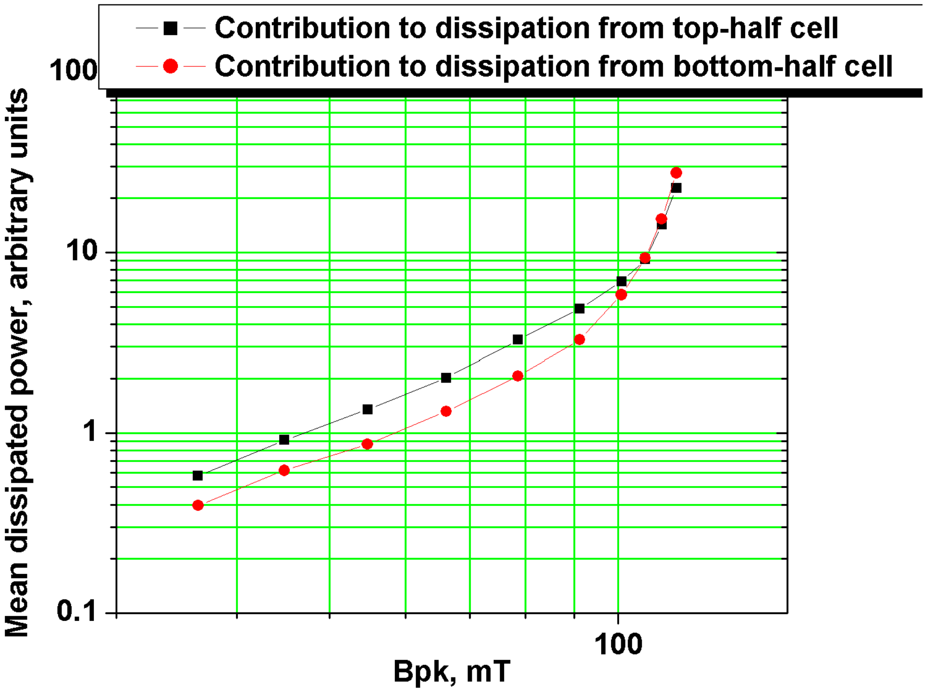

Figure 7.4: In the test after 30/60 Volts anodizing a relative contribution to the total dissipation from top and bottom half-cell was calculated. The calculation shows that both half-cells contribute equally to the high field Q-slope.

H_{peak}=130 mT and $Q_\circ=5\cdot10^{10}$ by the available power. This excitation curve is noticeably better than the baseline. Thereby the oxide layer that was grown in place of the niobium improved by a mild baking does not prohibit a future improvement by another mild baking.

7.3 Anodizing EP cavity

A similar series of experiments was carried out with the cavity No.2., which was vertically electropolished. We skipped the measurement before baking, because the high field Q-slope after EP is well known to be similar to that after

Table 7.2: Summary of the anodizing experiments for the chemically polished cavity

	Tbath, K	R_{surf}, nOhm	γ	Limitation
BCP	1.5	11.4±0.2	3.24±0.27	HFS
100^0C Baked	1.7	14.0±0.1	2.34±0.06	HFS
5V anodized	1.5	10.0±0.1	2.97±0.10	HFS
30V/60V anodized	1.5	13.0±0.3	3.14±0.28	HFS
100^0C baked	1.5	14.4±0.1	2.77±0.08	HFS

BCP. As a baseline for EP we used a result from the previous series of experiments with BCP cavity. The following experiments were carried out with the cavity No.2:

•The cavity was baked at $100°$C "in situ" for 48 hours.

•Test No.1. There was no high field Q-slope.

•The cavity was anodized for 10 volts.

•Test No.2. A high field Q-slope appeared.

•The cavity was anodized for 20 volts.

•Test No.3. The high field Q-slope was aggravated.

•The cavity was baked at $100°$C "in situ" for 48 hours.

•Test No.4. The high field Q-slope was removed.

In Fig. 7.5 we present the excitation curve for this series of experiments. After the mild baking the cavity reached 160 mT, Fig. 7.5(circles). The was no high field Q-slope. Field emission was the limitation for this test. The temperature map at B_{peak}=160 mT shows localized losses with a pattern characteristic for a field emission, Fig. 7.6. Note that the EP baked cavity still reached a higher field

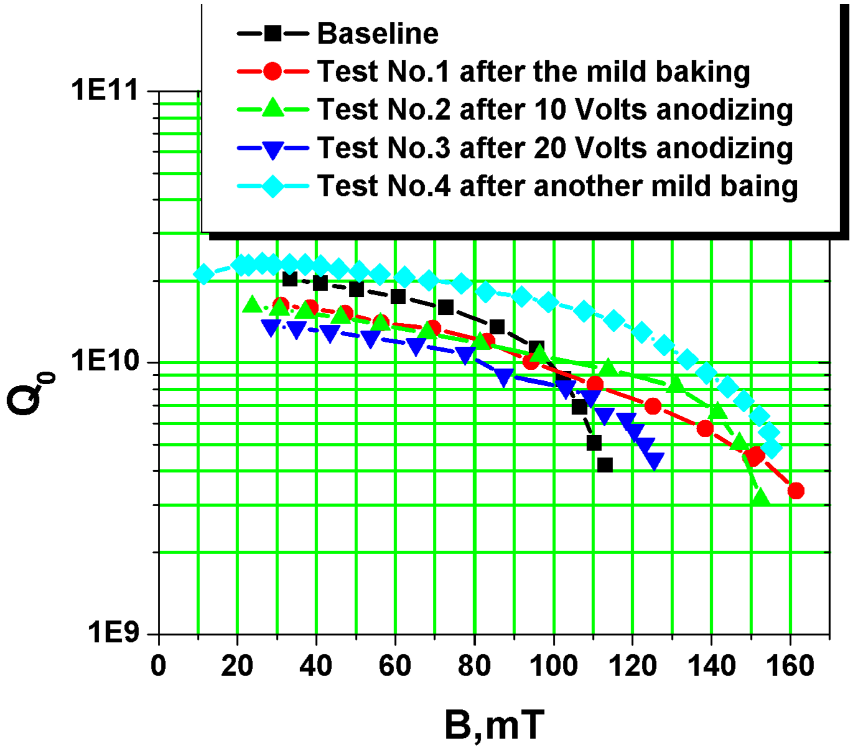

Figure 7.5: Quality factor vs. peak magnetic field. [squares]The baseline: the cavity's performance after chemical treatment before mild baking show a typical high field Q-slope; [circles]The mild baking improvement: the cavity's performance was improved by 100°C for 48 hours baking; [upward triangles]The 10 Volts anodizing: the cavity's performance was not limited by the high field Q-slope; [downward triangles]The 20 Volts anodizing: the cavity's performance was limited by high field Q-slope at field level close to the baseline's; [rhomb]Another mild baking: the cavity's performance was improved by another mild baking.

than the BCP baked cavity, Fig. 7.1. After 10 Volts anodizing the high field Q-slope reappeared. It started at B_{peak}=135 mT, Fig. 7.5(upward triangles). The quality factor degraded by a factor of 3 over next 10 mT. At this point the measurement was limited by the high field Q-slope. After 20 Volts anodizing the high field Q-slope started at 110 mT, Fig. 7.5(downward triangles). The quality factor degraded by a factor of 2 over next 10 mT. X-rays radiation was measured in this experiment, but thermometry data suggests that the measurement was

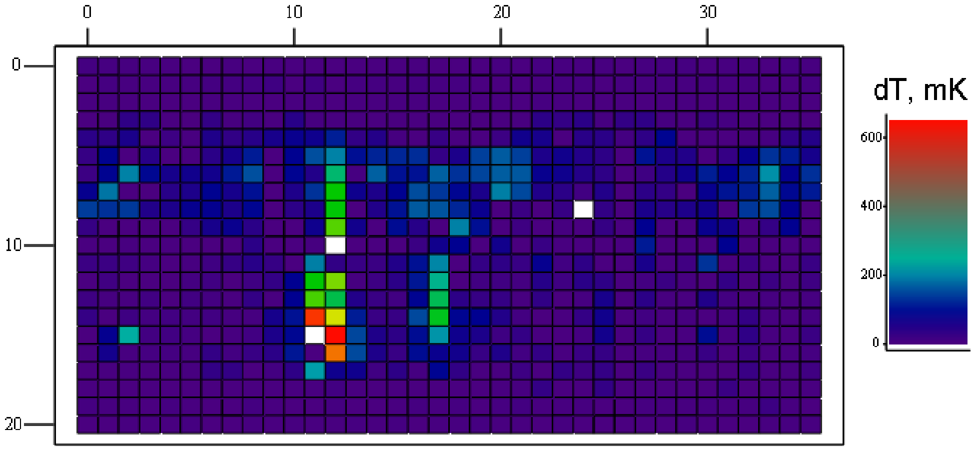

Figure 7.6: Temperature maps for the test after mild baking at B_{peak}=160 mT. The temperature map shows the field emission site, which contribute the most to overall surface losses. Note the absence of the high field Q-slope.

Table 7.3: Summary of the anodizing experiments for the vertically electropolished cavity

	Tbath, K	Rs, nOhm	γ	Limitation
100^0C Baked	1.6	14.2±0.4	3.49±0.31	FE
10V anodized	1.6	15.4±0.1	2.42±0.04	HFS
20V anodized	1.6	17.4±0.4	2.84±0.28	HFS
100^0C baked	1.6	10.4±0.1	2.05±0.09	FE

limited by the high field Q-slope. Three temperature maps at about B_{peak}=130 mT show the absence of the high field Q-slope for the test after mild baking and after 10 Volts anodizing, but the return after 20 Volts anodizing, Fig. 7.7. After another mild baking no high field Q-slope was present, Fig. 7.5(rhombs). The cavity was limited by field emission. The temperature maps in Fig. 7.7 show that the cavity before anodizing at 20 volts the cavity has no high field Q-slope

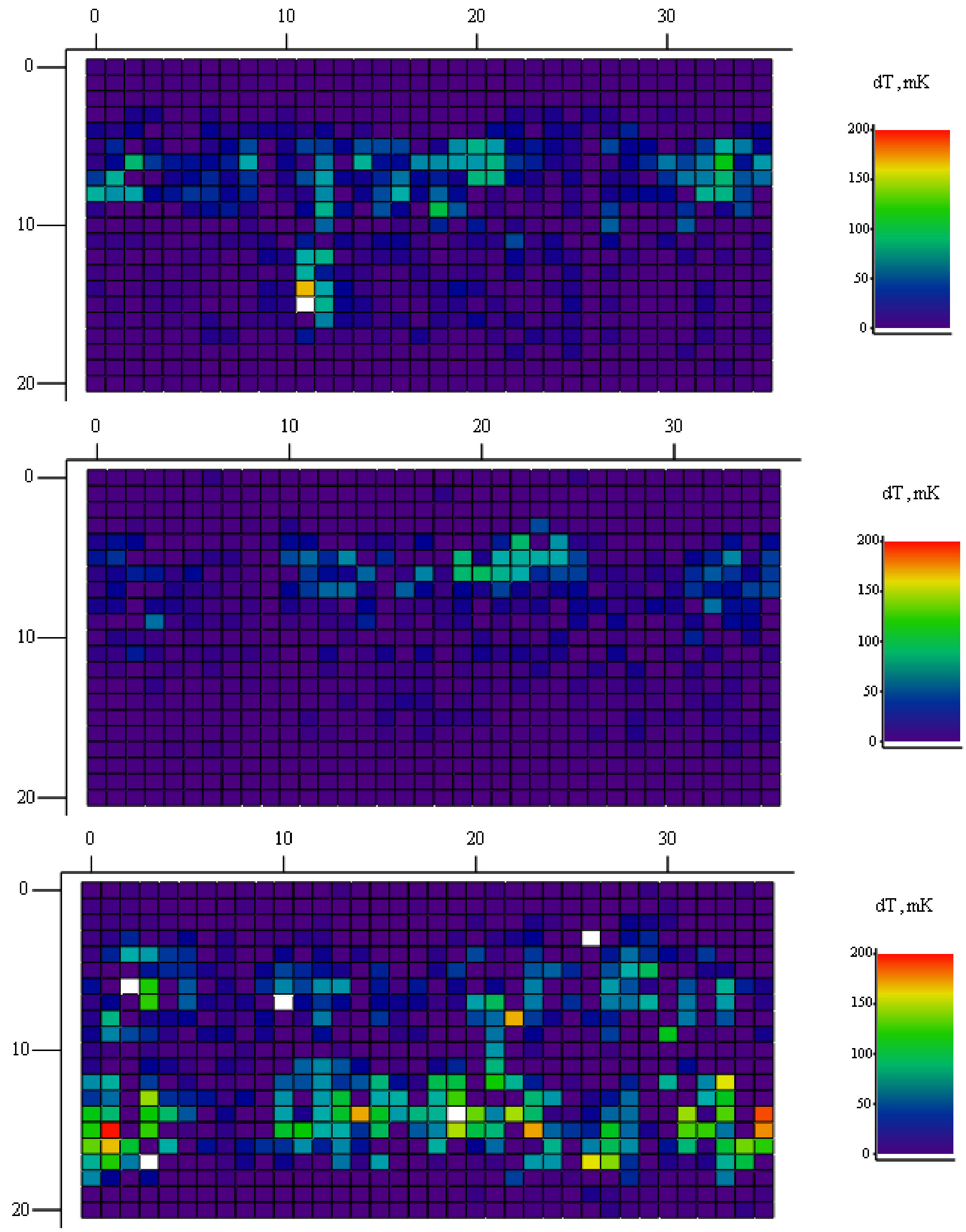

Figure 7.7: Three temperature maps: top temperature map was taken in the test after mild baking at B_{peak}=138 mT, center temperature map was taken in the test after 10 Volts anodizing at B_{peak}=131 mT, bottom temperature map was taken in the test after 20 Volts anodizing at B_{peak}=127 mT. Note the absence of distributed losses in top and center temperature map compared to bottom temperature map.

at H = 120 mT. But after 20 Volts anodizing the cavity lost beneficial baking effect and is limited by high field Q-slope at H = 120 mT. These experiments show that a cavity should be anodized for 20 Volts in order to remove beneficial effect of heat treatment, which is equivalent to removal of 15 nm of metallic niobium. After 20 Volts the quality factor was still slightly higher than for a typical high field Q-slope, but the improvement was marginal, so the conclusion is that 20 Volts anodizing almost consumed the layer benefited by the mild baking. Possibly 20 Volts anodizing has not consumed completely the layer of niobium which was improved by heat treatment at 100^0C for 48 hours. Therefore the thickness of the niobium layer benefited by the mild baking at 100°C for 48 hours is between 15 and 22 nm(from the BCP cavity experiments).

7.4 Discussion

Recently similar series of experiments were carried out by G. Ciovati et al. for two different baking conditions [46]. One baking condition was baking at 120 °C for 20 hours, the second baking condition was 120 °C for 12 hours. In the paper they report that the cavity has to be anodized for 40 volts in both cases in order to restore the high field Q-slope, Fig. 7.8. The difference in results for different baking condition can be understood within oxygen pollution model or modified oxygen pollution model. We plotted oxygen profile calculated from modified oxygen pollution model for different baking conditions, Fig. 7.9. In the legend to the picture we also denote voltage(and niobium thickness converted to oxide), to which niobium was anodized in order to remove baking benefit, for given baking conditions. Thus we see that diffusion of oxygen explains anodizing experiments very well and we have direct correlation between diffusion

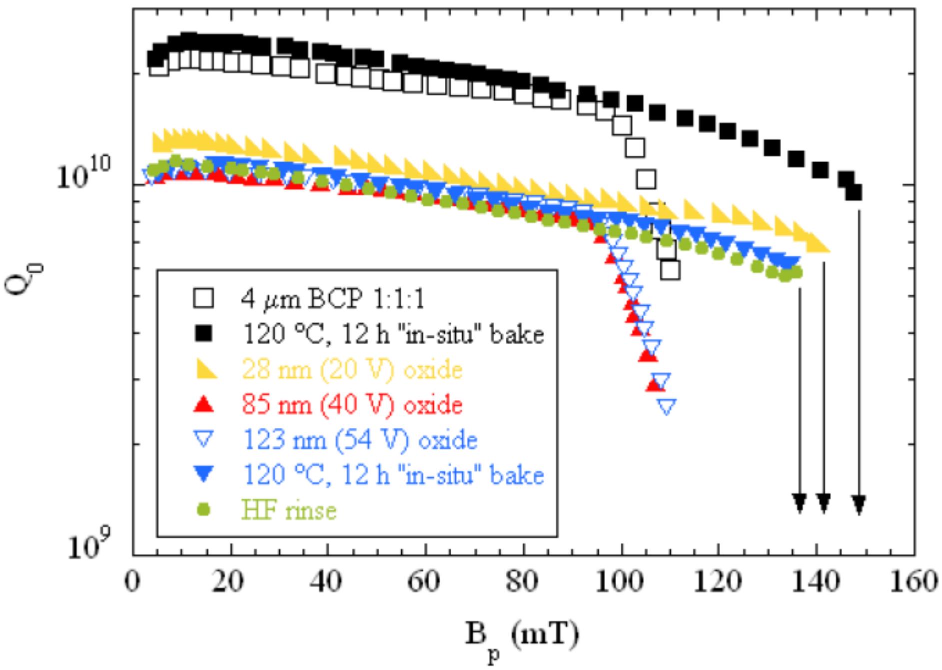

Figure 7.8: Anodizing experiments carried out by G. Ciovati et al.

length $\sqrt{D(T) \cdot t}$, where $D(T)$ is diffusion coefficient of oxygen in niobium and t is time of mild baking, and voltage needed to consume baking modified niobium. The dependence of the thickness of the baking-benefited layer was also suggested by recent experiments by Bernard Visentin [47].

Despite this correlation it is still not clear how anodizing experiments can be explained within oxygen pollution model or modified oxygen pollution model. If we assume that anodizing does not change oxygen content in the bulk niobium, then it is not clear why high field Q-slope re-appears after anodizing, since no pollution layer is produced by anodizing. If we assume that anodizing does change oxygen content in the bulk niobium, then it is not clear why anodizing for low voltages does not cause the high field Q-slope in niobium cavities.

These contradictions are resolved, if we assume, that the oxygen pollution

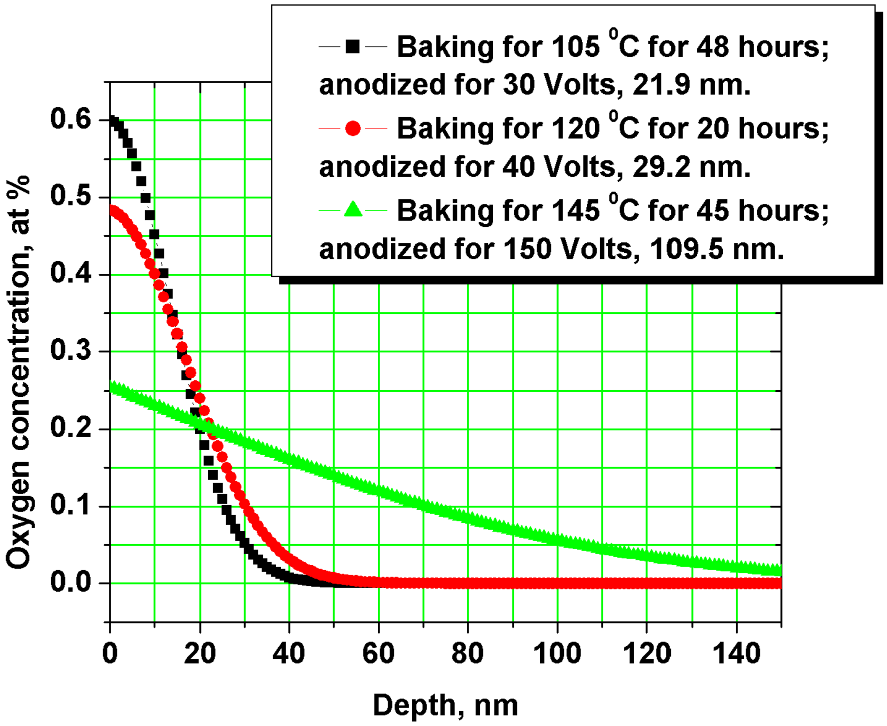

Figure 7.9: Calculation of oxygen profile with modified oxygen pollution model for different baking conditions. In the legends the voltage, to which niobium was anodized in order to remove baking benefit, is presented next to the baking condition.

layer, existence of which was only confirmed for samples treated at 1000 °C in vacuum [48], does not exist at the oxide-niobium interface after chemical treatment. Instead, there is a uniform distribution of oxygen, which, however, is not an equilibrium distribution due to the surface tension on the oxide-niobium interface. We speculate that in the equilibrium there is a decrease in the concentration of oxygen at the surface. Mild baking at 100 °C reduces the amount of oxygen at the niobium surface. Whereas mild baking at 150 °C causes a destruction of oxide [49] and disrupts the oxide-niobium interface. We speculate that for such a disrupted oxide-niobium interface the mild baking is not effective anymore.

7.5 Oxide-purifier model

We also want to point out that for other impurities there could be a concentration gradient between the bulk concentration of impurities and the concentration of the impurities in the niobium pentoxide, which grows to the thickness of 3-5 nm, stretching the lattice by a factor of three. Other impurities usually are out of consideration because of their low diffusion rates at the temperatures of interest [50]. However, firstly, other data for carbon suggest diffusion lengths at the temperatures of interest comparable to the penetration depth of niobium [51]; secondly, the diffusion rates near the surface may be higher than the bulk ones.

To illustrate what was said above, we considered a simple model problem: we assumed an initial step-function in the impurity concentration between the niobium pentoxide and the bulk niobium; we assumed the same constant diffusion coefficients both for the oxide and for the bulk niobium; and we assumed that impurities can freely move through the niobium-niobium oxide interface. For this model problem the diffusion equation is:

$$\frac{\partial C(x,t)}{\partial t} = D_0(T)\frac{\partial^2 C(x,t)}{\partial^2 x}$$

$$C(x,0)|_{0<x<\delta} = C_0; C(x,0)|_{\delta<x} = C_1;$$

$$C(x,0)|_{x=\delta} = \frac{C_0 + C_1}{2};$$

$$C(x,t)|_{x=+\infty} = C_1; \frac{\partial C(x,t)}{\partial x}|_{x=0} = 0;$$

Where C(x,t) is concentration of interest in arbitrary units, $D_0(T)=1.5\cdot 10^{-6} \cdot exp(\frac{-13600}{T})m^2s^{-1}$, where T is temperature in Kelvin, is diffusion coefficient from [51], δ is oxide thickness, C_1 is concentration of impurities in the bulk and C_0 is concentration of impurities in the oxide. The solution to the model problem is:

$$C(x,t) = C_1 + \frac{C_0 - C_1}{\sqrt{\pi}} \int_{\frac{x-\delta}{2\sqrt{D_0(T)t}}}^{\frac{x+\delta}{2\sqrt{D_0(T)t}}} exp(-z^2)dz$$

Now we assume that the concentration of impurities in the niobium pentoxide is 2.74 times less in the bulk niobium and consider a redistribution of impurities under different baking conditions. The solution of the model problem shows that baking at $100°$C for 48 hours lowers the concentration of the impurity in the first 30 nm of bulk niobium in this model, Fig. 7.10. Anodizing for 30 Volts

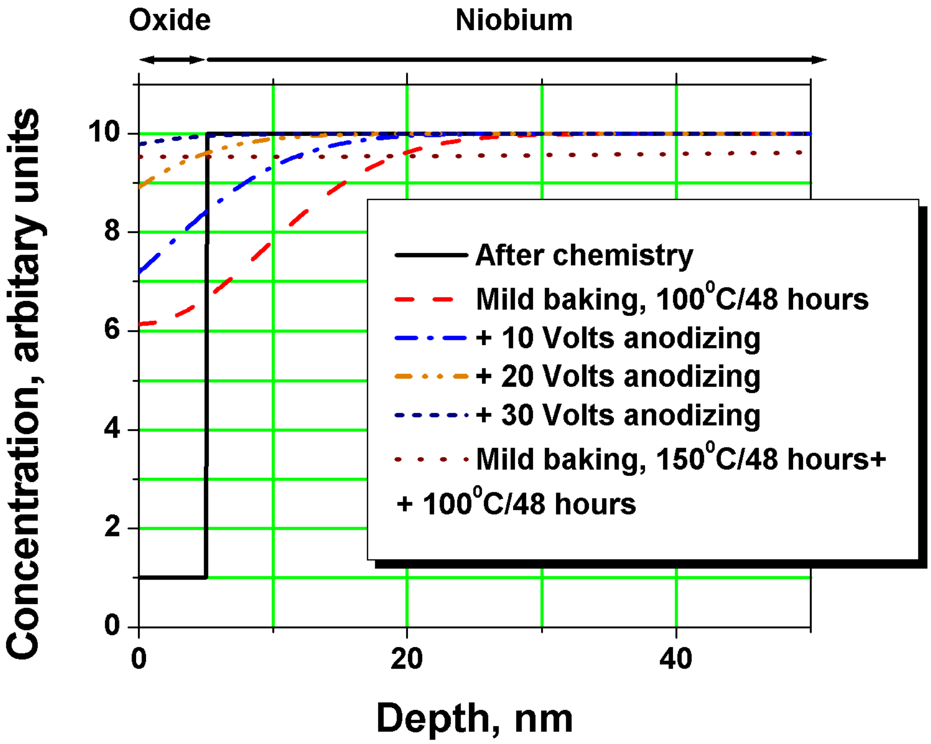

Figure 7.10: "Oxide-purifier" model. Initial distribution is the step-function[solid]. Mild baking at 100 ^{circ}C for 48 hours reduces the concentration of impurities in the penetration depth[dashed]. Anodizing for 30 Volts consumes the layer of niobium with the reduced concentration[dash-dot]. Subsequent mild baking at 100 °C for 48 hours after mild baking at 150 °C for 48 hours does not have any effect on the concentration profile.

consumes the niobium with the reduced concentration of impurity, bringing the concentration back to what it was before the mild baking. Mild baking at $150°$C for 48 hours has a minor effect on the impurity concentration in first 50 nm of bulk niobium. After 150 °C for 48 hours additional mild baking at 100 °C for 48 hours has no effect on the concentration. If we now connect the concentration of impurities in the penetration depth with the strength of the high field Q-slope, we have an agreement with experimental data for the mild baking effect.

CHAPTER 8

RESULTS WITH THE LARGE GRAIN CAVITY

8.1 Introduction

Grain boundaries have been long suspected as one of the possible causes for the high-field-Q-slope degradation. One of the mechanisms suggested was that the oxide formed in the grain boundaries creates a Josephson junction, which has a low critical current, and thus grain boundaries cause additional losses by going normal-conducting at fields lower than critical field of niobium [52].

Grain boundaries are also a key point in the magnetic field enhancement model. Due to the field enhancement on the sharp corner grain boundaries become normal-conducting at fields lower than the critical field by field enhancement factor, thus causing additional losses at fields lower than the theoretical maximum.

Recently magneto-optical studies have been done on niobium samples [53]. Magneto-optical imaging is based on the Faraday effect, which is a rotation of the polarization plane of light in magnetic field. The setup developed by A.A. Polyanskii was based on a polar magneto-optical Kerr effect, which is referred to instead of Faraday effect when the measured light is reflected, not transmitted. The setup allows to measure the magnetic field on the surface of niobium samples with the resolution of about 1 mT. The spatial resolution is about 5 μm. Their experiments have shown that, when the grain boundary is perpendicular to the surface of the sample, DC magnetic flux penetrates at the grain boundary at fields 20x lower than H_{c1} of niobium, Fig. 8.1. The results from this experiment renewed discussion about penetration of the RF magnetic flux into niobium at fields above lower critical field, thus again causing additional dissipation and possibly the high field Q-slope.

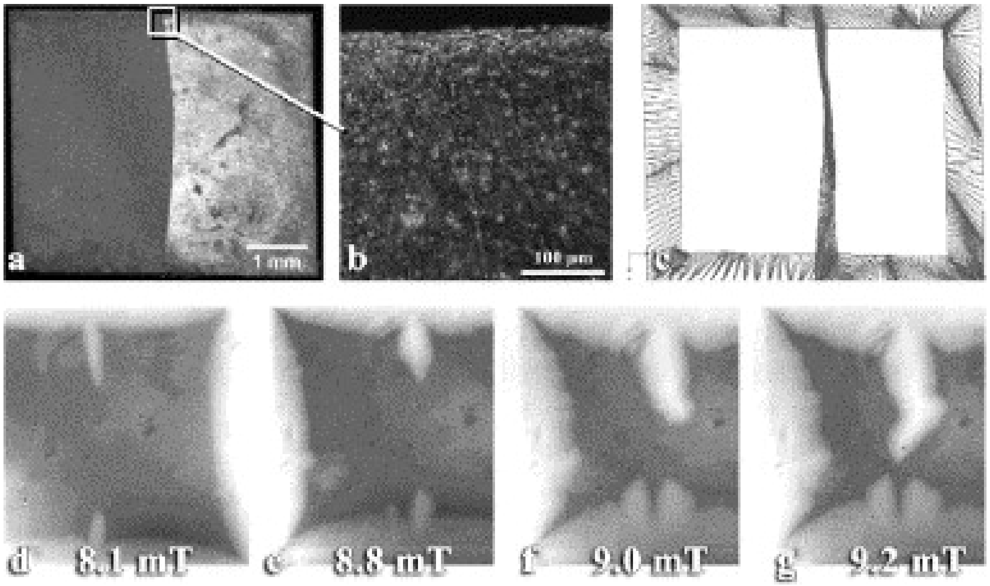

Figure 8.1: Magneto-optics images of niobium sample show a premature flux penetration at the grain boundary at fields much lower than H_{c1} of niobium.

To answer the question, whether grain boundaries contribute to losses in the high-field-Q-slope regime, a program aimed on creating a single-grain cavity was launched at TJNAF. After it was shown that the elongation of the single-grain material is better than that of the small-grain material [54], a single-grain cavity was manufactured and tested. Surprisingly, the performance of the single-grain cavity resembles the typical performance of small-grain cavities, Fig. 8.2: both the high field Q-slope and the mild baking effect are present, even though there are no grain boundaries.

Following TJNAF, it was decided to test a large-grain cavity at Cornell in order to study the contribution of the grain boundaries to the losses at high fields with our thermometry system. The large-grain cavity was made an elliptical shape 1.5 GHz cavity with 3 mm wall thickness. The cavity was made of 300

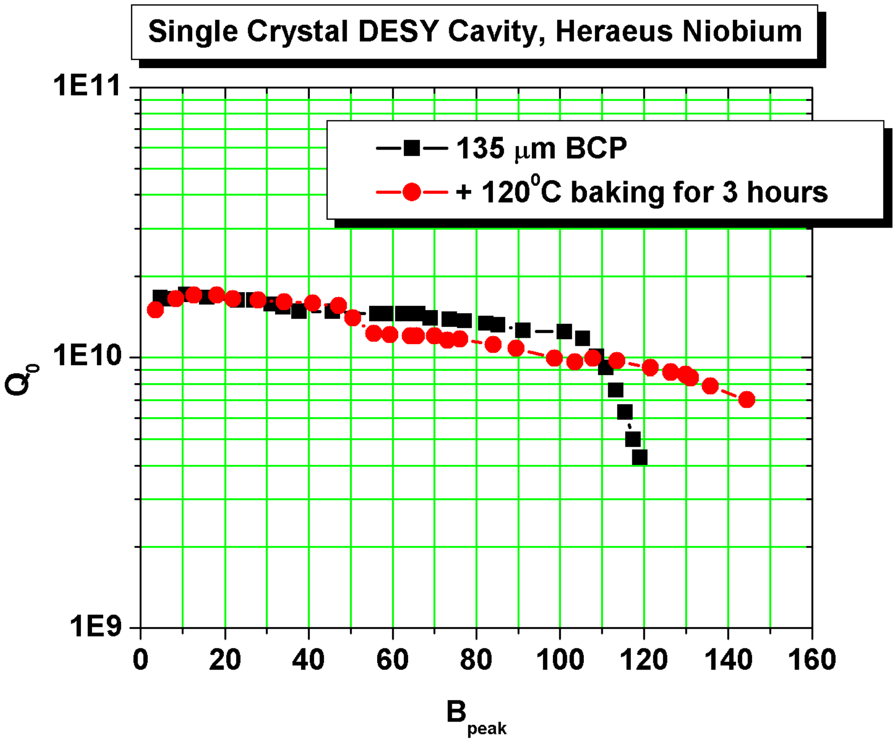

Figure 8.2: RF results from the single-grain cavity [54]. The high field Q-slope of the single-grain cavity starts at $B_{peak} \approx 100$ mT[squares], which is also typical for a small-grain cavity. After mild baking the high field Q-slope was removed[circles].

RRR material purchased from OTIC, China. In the first test the cavity was limited by the thermal breakdown at $B_{peak} \approx 100$ mT. Since the high field Q-slope typically starts at about $B_{peak} \approx 100$ mT, it was not possible to study it in this experiment. In order to get into the high-field-Q-slope regime, the cavity was removed from the test stand for inspection and further treatment. During inspection of the inner surface of the cavity a pit was found at the spot prompted by the thermometry system at the quench location. In order to smoothen the edges of the pit, the cavity was treated for about 150 μm with BCP(1:1:2). After the chemical etching the cavity was assembled on the test stand and tested. During the test the initial bath temperature was 1.5°K, but it increased with field in the cavity and was around 1.7°K at highest fields. Below the subsequent sequence of experiments is summarized:

- The cavity was tested. The cavity is limited by the high field Q-slope.
- The cavity was baked at 100^0C for 48 hrs.
- The cavity was tested. The high field Q-slope was removed. The cavity was limited by the thermal breakdown.
- The cavity was heat treated at 800^0C for 3 hrs in vacuum furnace to remove hydrogen.
- The cavity was etched for 150 μm in BCP(1:1:2).
- The cavity was tested at the helium bath temperature of $1.5°$K. There was a high field Q-slope.

8.2 Results

In the first test the low-field quality factor of the cavity was about $2{\cdot}10^{10}$, Fig. 8.3[squares]. At B_{peak} $\approx$ 100 mT the high field Q-slope started. The measurement was limited by available power($\approx$ 30 W) at B_{peak} = 121 mT and $Q_\circ$=$3{\cdot}10^9$. The temperature maps before the onset of the high field Q-slope show that the heating is not localized to the grain boundaries in the medium-field-Q-slope regime, Fig. 8.5[top]. In the high-field-Q-slope regime the temperature maps show that hot regions are not necessarily located on or near the grain boundaries, Fig. 8.4[top]. This temperature map has several hot-spots in the high-magnetic-field region, which is typical for the high field Q-slope. The individual readings of thermometers also show the high field Q-slope at high fields in both hot- and cold-spots, Fig. 8.6. Two regions however show quadratic losses up to the highest field. Possibly due to a defect in these regions the contribution

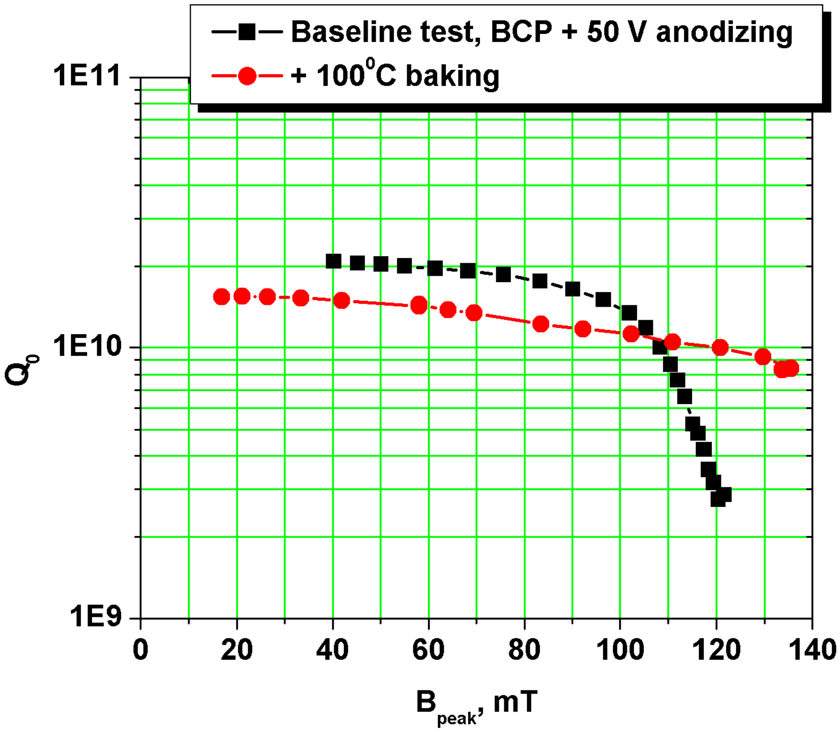

Figure 8.3: Quality factor as a function of field before and after 100°C baking. In the test before 100°C baking the cavity was limited by high field Q-slope[squares]; in the test after 100°C baking no high field Q-slope was observed, the limitation was thermal breakdown due to a defect[circles].

from the high-field-Q-slope losses is not discernible there.

An interesting point is that one of the regions which show quadratic losses up to the highest field was very close to the high-field-Q-slope hot-spot(one thermometer away), nevertheless, the quadratic region was not affected by the adjacent high field Q-slope and losses stayed quadratic up to the highest field. In the cold regions however, which are often 5 or more thermometers away from the hot high-field-Q-slope regions, the high field Q-slope is still observed. Thereby the high field Q-slope in cold regions, cold-spots, is not caused by hot-spots. Cold-spots have high field Q-slope independently.

In Fig. 8.7 the result for the large-grain cavity[squares] is compared to the re-

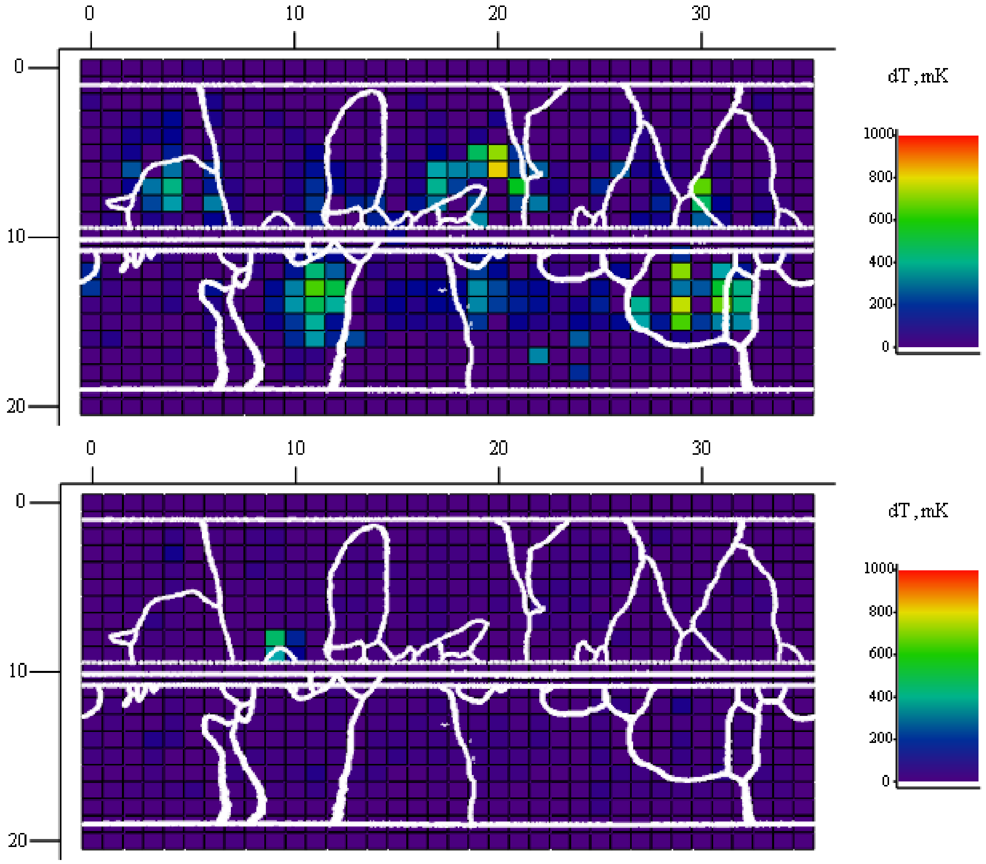

Figure 8.4: Temperature maps before baking at B_{peak} = 121 mT[top] and after 100°C baking at B_{peak} = 124 mT[bottom]. The temperature map before baking shows several hot spot in the high-magnetic-field region, which is typical for the high field Q-slope. Note that in the high-field-Q-slope regime the heating is not localized at grain boundaries. The temperature map after 100°C baking show no high field Q-slope regions. The temperature map after mild baking has only one hot-spot(near column 9, row 8-9), which showed quadratic losses up to the thermal breakdown.

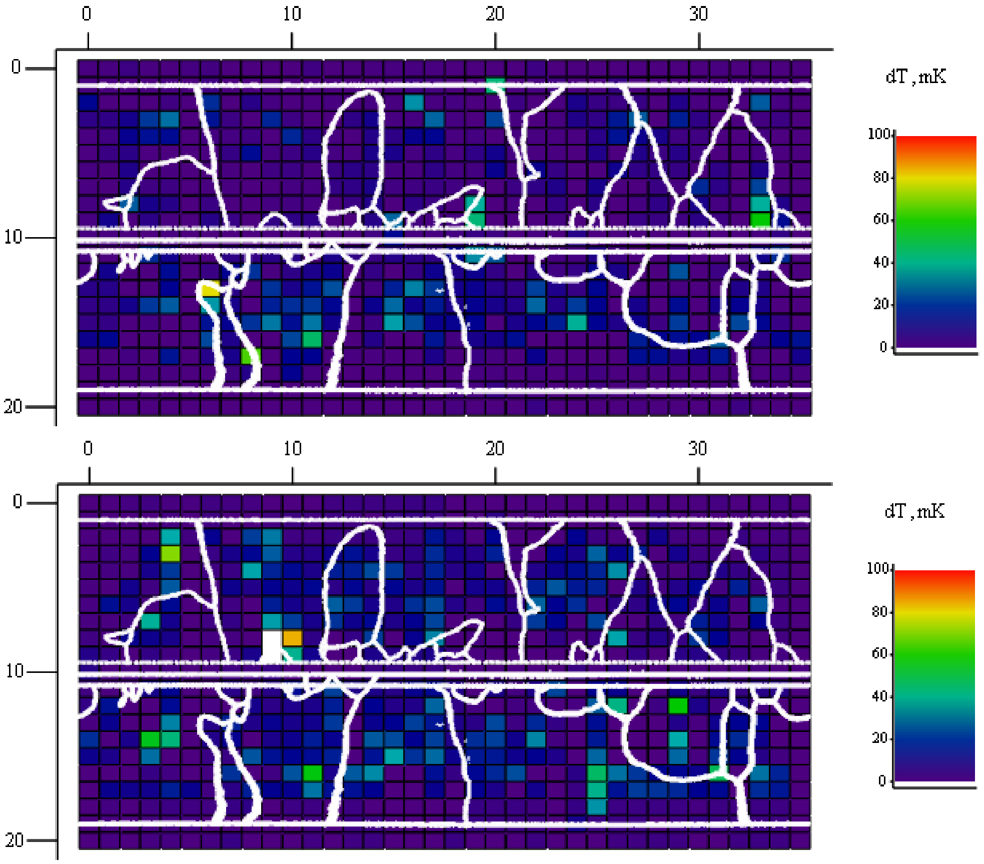

Figure 8.5: Temperature maps for the test before baking at B_{peak} = 100 mT[top] and for the test after 100°C baking at B_{peak} = 102 mT[bottom]. The temperature maps are similar before and after 100°C baking in the medium-field-Q-slope regime. Note that in the medium-field-Q-slope regime the heating is not related to the grain boundaries in both tests.

sults for a small-grain cavity[circles] after both cavities received similar treatment. Both cavities have the same onset of the high field Q-slope and the strength of the high field Q-slope.

Fig. 8.8 shows that before the onset of the high field Q-slope the hot spots are more localized in case of the large-grain cavity. It appears true in the high-field-Q-slope regime as well, the half-width of hot-spots is smaller in the case of the large-grain cavity than it is for the small-grain one, Fig. 8.9.

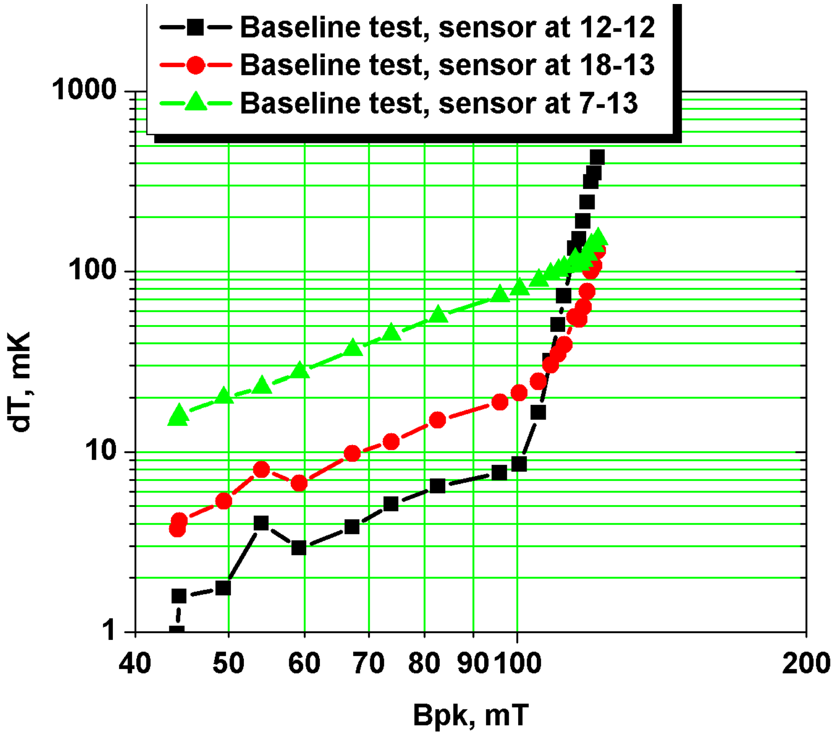

Figure 8.6: Readings of thermometers as a function of field. ”Sensor at C-R” denotes spot at column C, row R in Fig. 8.4[top]. Note that thermometers in both hot[squares] and cold[circles] regions show the high field Q-slope. Two regions(defects), about 5 thermometers each, show quadratic losses up to the highest field[triangles]. The high-field-Q-slope contribution to losses is not seen in these regions probably due to high quadratic losses, which are present at low field as well. It is interesting to note that both these regions are on the grain boundaries, though it is not clear whether the defect is located on the grain boundary itself or near it.

After the cavity was baked at 100°C for 48 hours, the low-field quality factor was lower than before baking - $Q_\circ \approx 1.5 \cdot 10^{10}$, Fig. 8.3. The cavity was not limited by the high field Q-slope, but by the thermal breakdown at B_{peak} = 134 mT with $Q_\circ = 8 \cdot 10^9$. The temperature map showed that losses were dominated by a single hot-spot where losses were quadratic up to the highest field, Fig.8.5[bottom]. Eventually this hot-spot caused the thermal breakdown. Af-

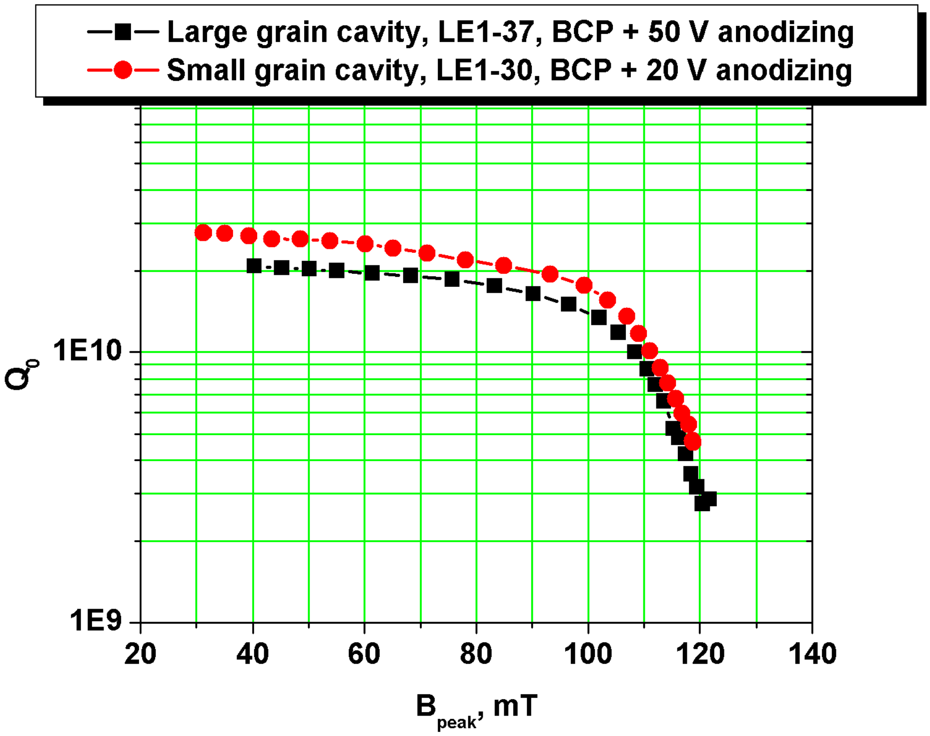

Figure 8.7: Results for the large-grain cavity[squares] and small-grain cavity[circles] show that both small- and large-grain cavities have the same high field Q-slope after similar treatment.

ter disassembling a pit-like irregularity was found on the inside surface of the cavity in the place where the hot spot was according to the temperature map. Fig.8.5[bottom] shows that aside from the appearance of the defect the heating in the medium-field-Q-slope regime is not affected by mild baking. However Fig.8.4 shows a striking difference before and after mild baking in the high-field-Q-slope regime. Temperature map after mild baking at B_{peak} = 134 mT was rescaled so that losses other than that at the defect sight can be seen, Fig.8.10. Even at the highest field reached after mild baking, B_{peak} = 134 mT, there is no preferential heating at the grain boundaries. These results confirm that the grain boundary heating is not the dominant cause of the high field Q-slope.

After the cavity was baked, it was re-treated with BCP(1:1:2) in order to see

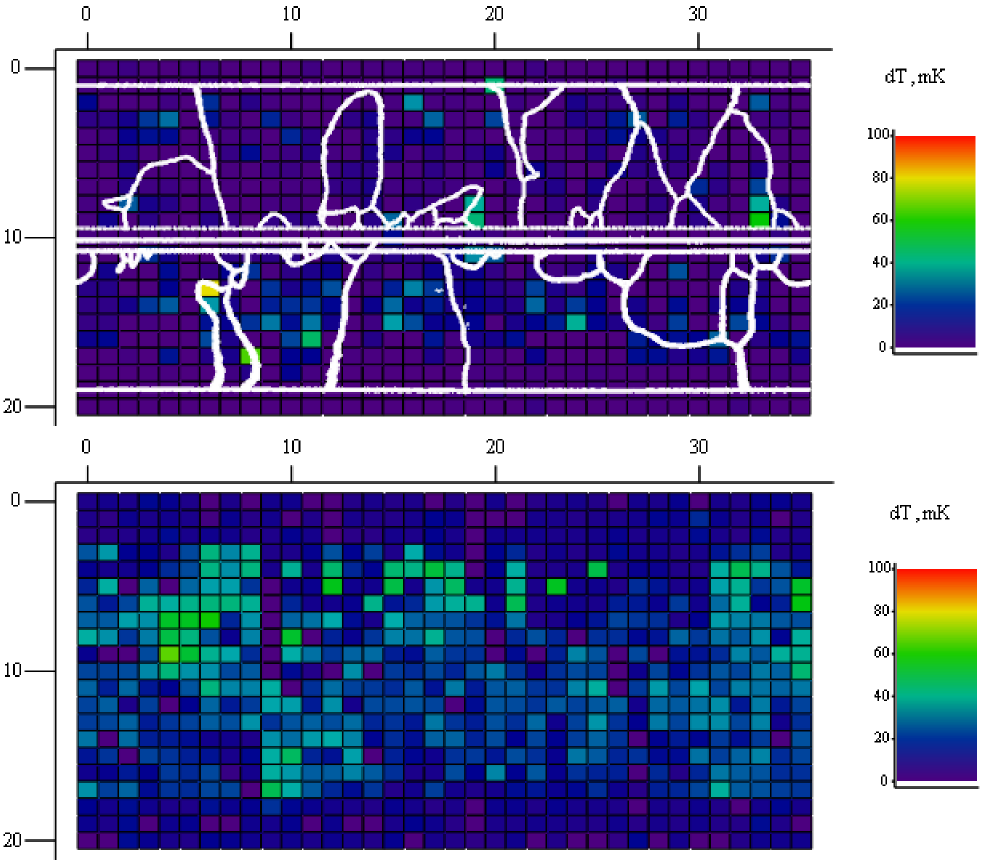

Figure 8.8: Temperature map for the large-grain cavity at B_{peak} = 100 mT[top] and a small-grain cavity at B_{peak} = 100 mT[bottom] after similar treatment. The heating in the case of large-grain cavity is more localized compared to that of a small-grain one.

whether the heating will stay with the same grains in the high-field-Q-slope regime or move to different grains. Incidentally during the chemical etching the temperature of solution got above 15 °C. This error resulted in the hydrogen Q-disease, which showed up as a strong medium field Q-slope. In order to remove hydrogen the cavity was treated in the vacuum furnace for 3 hours at 800°C. After annealing the cavity was etched with BCP(1:1:2) for $\approx$ 150 μm. Following chemical etching the cavity underwent typical preparation steps for the RF test with thermometry. In Fig. 8.11 the results after annealing and subsequent BCP are presented. For comparison the previous result with the same

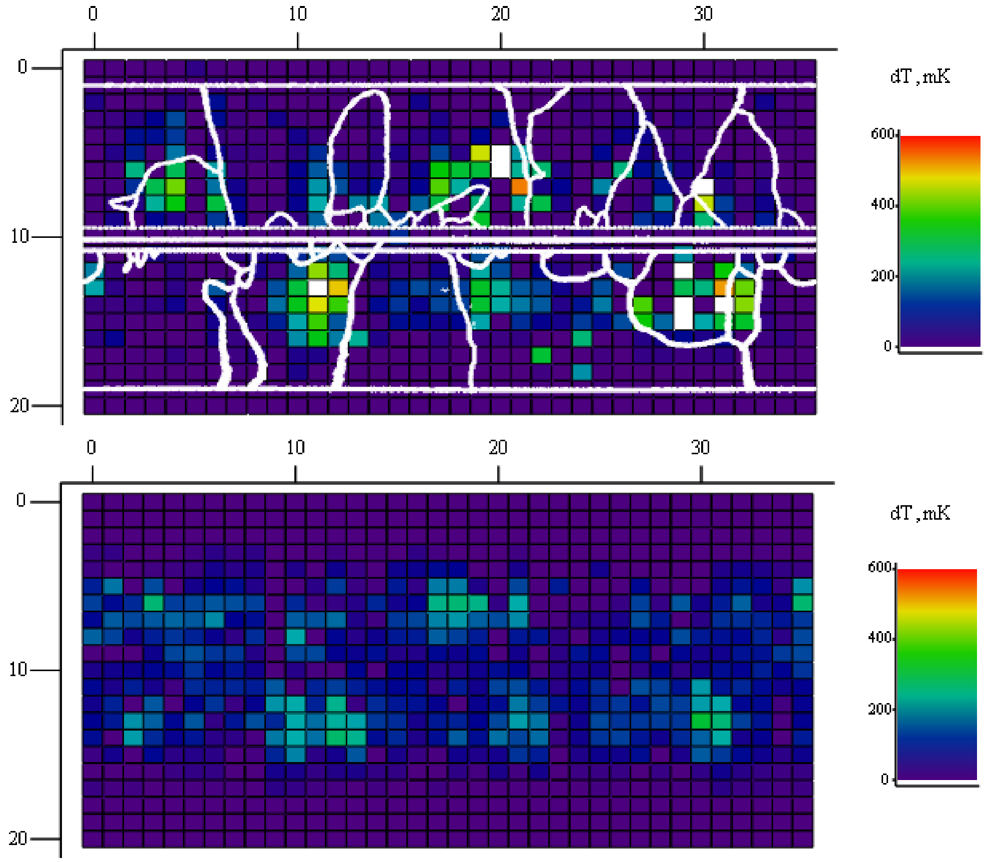

Figure 8.9: Temperature map for the large-grain cavity at B_{peak} = 121 mT[top] and a small-grain cavity at B_{peak} = 118 mT[bottom] after similar treatment. The heating in the case of large-grain cavity appear to be more localized compared to that of a small-grain in the high-field-Q-slope regime.

cavity after fresh chemistry is also shown. Cavity being annealed has higher low-field quality factor, above $7 \cdot 10^{10}$ at $T_{heliumbath} \approx 1.5$°K. At $B_{peak} \approx 100$ mT the high field Q-slope started. The quality factor dropped to below $Q_{peak} = 2{\cdot}10^{9}$ at B_{peak}= 130 mT.

The temperature maps in the experiment have a few hot-spots in the high-field-Q-slope regime. Surprisingly the hot-spots after re-treatment seemed to stay where they were in the first test, Fig. 8.12. The only new hot-spots were one on the bottom half-cell at column 24, row 18, and another on the top half-

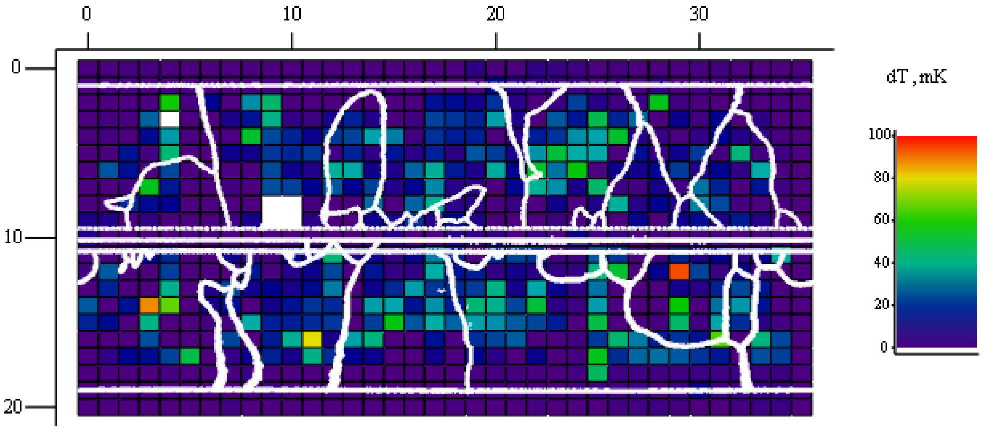

Figure 8.10: Temperature map with overlaid grain boundaries after 100°C baking at B_{peak} = 134 mT shows that losses in the medium-field-Q-slope region are not distributed preferentially along grain boundaries. A four-thermometer hot-spot at column 10, row 9 dominated losses at medium fields and eventually caused the thermal breakdown at $B_{peak} \approx 134$ mT.

cell at column 9, row 9, of which the former is near the iris and therefore is irrelevant to the high-field-Q-slope. Also a few of the hot spots from the first test did not appear.

Another interesting topic is to compare the spatial extent of hot spots in the high-field-Q-slope-dominated region with the heating pattern from a defect-dominated region. Calculations [55] suggest that for a known thermal conductivity, Kapitza resistance [56], and a wall thickness of niobium cavity the width of heat spread on the outer surface from a point-like defect on the inner surface is about 1 cm. The distance between thermometers is also about 1 cm. And so for a point-like defect, i.e. less than 100 μm in diameter, one would expect to see a hot spot with 1-2 thermometers spread. This is what was found in the test after 100°C baking, when the cavity was limited by the thermal breakdown. On the other hand the spatial distribution of a hot spot in the high-field-Q-slope regime is more than 1-2 thermometers: in Fig. 8.14 spatial distributions for a

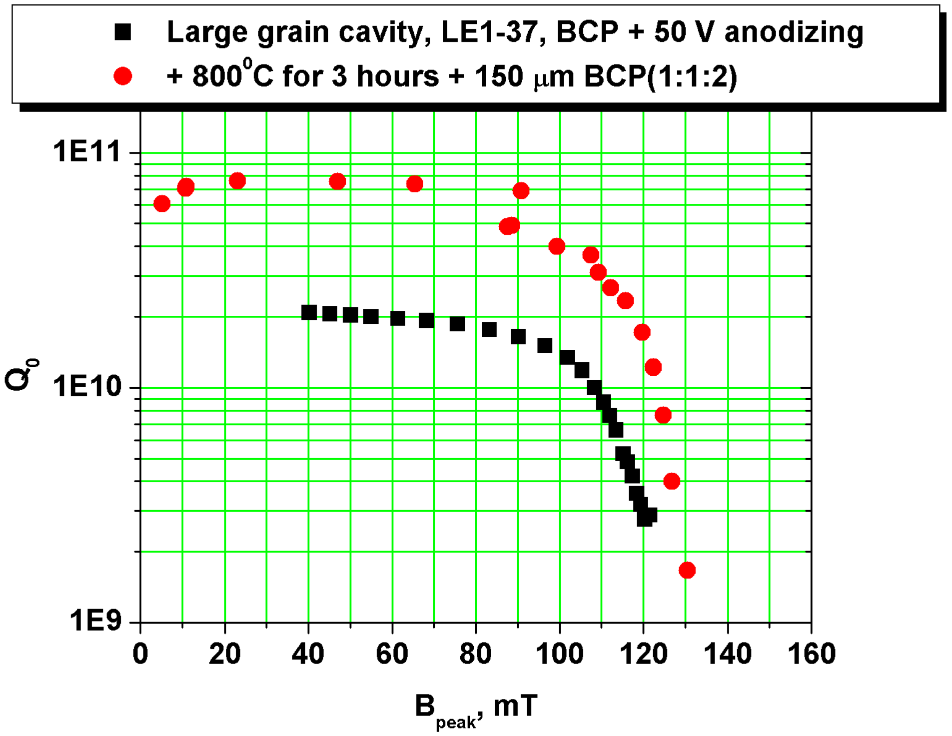

Figure 8.11: Q vs. B_{peak} curves for the first experiment with the large-grain cavity, in which the high field Q-slope was measured[squares], and for another experiment, after mild baking, annealing at 800°C for 3 hours and more chemical etching, in which there also was the high field Q-slope. Note that, although the highest reached field is higher in the second experiment, high-field-Q-slope onsets and slopes are comparable in both tests.

high-field-Q-slope hot-spot and a defect hot-spot of the large-grain cavity are compared. For the high-field-Q-slope hot-spot the distribution is wider. Therefore hot-spots that appear due to the high field Q-slope are not caused by the growth of a single point-like defect, which contradicts the hot-spot model.

The evolution of the defect's spatial distribution, Fig. 8.16, to the evolution of the hot spot in the high-field-Q-slope region, Fig. 8.15, was also compared. While a defect site dominates at all fields, the high-field-Q-slope region shows a different behavior: the hot-spot is centered at one place at low fields, but as

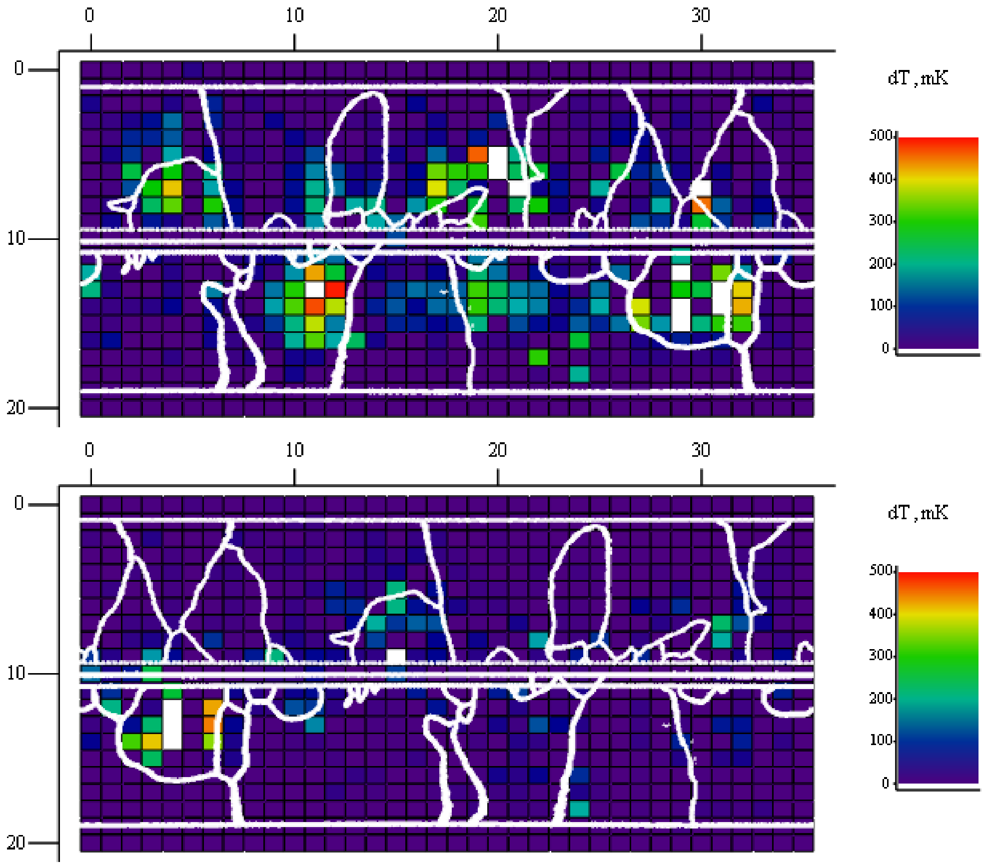

Figure 8.12: Temperature maps acquired in the high-field-Q-slope regime.Temperature map at B_{peak} = 121 mT with overlaid grain boundaries for the first test after fresh chemistry[top];Temperature map at B_{peak} = 123 mT with the overlaid grain boundaries for another test after annealing and additional chemistry[bottom]. Note that many of the grains that were hot in the first experiments were hot in the second as well, e.g. the region on the bottom half-cell located near column No.30 on the top temperature map and the region on the bottom half-cell located near column No.4 on the bottom temperature map.

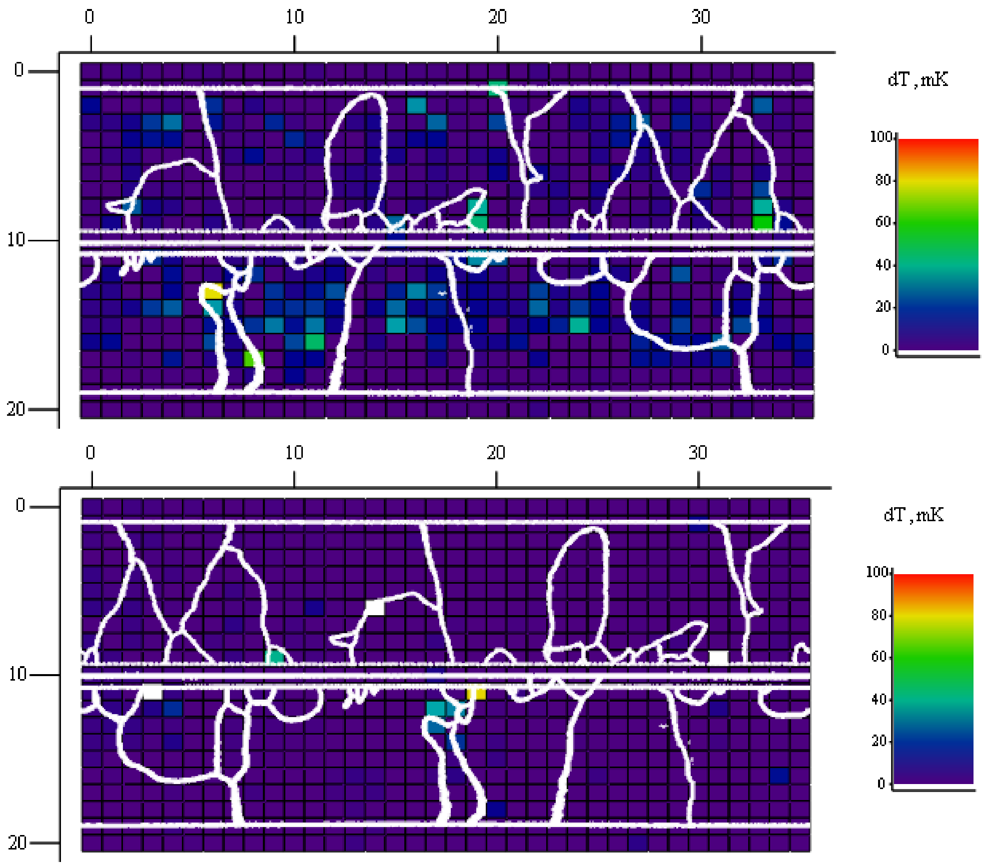

Figure 8.13: Temperature maps acquired in the medium-field-Q-slope region.Temperature map at B_{peak} = 100 mT with overlaid grain boundaries for the first test after fresh chemistry[top];Temperature map at B_{peak} = 96 mT with the overlaid grain boundaries for the another test after annealing and additional chemistry[bottom].

the field increases the center of the hot-spot moves to where magnetic field is higher on the cavity's surface. It clearly shows that the high field Q-slope is a magnetic effect and it strongly depends on the magnetic field.

Finally the sensitivity of thermometry system to the grain-boundary heating is to be discussed. The temperature maps show that heating in the high-field-Q-slope regime is located both near and away from the grain boundaries. Thus grain boundaries as the only cause of the high field Q-slope can be eliminated.

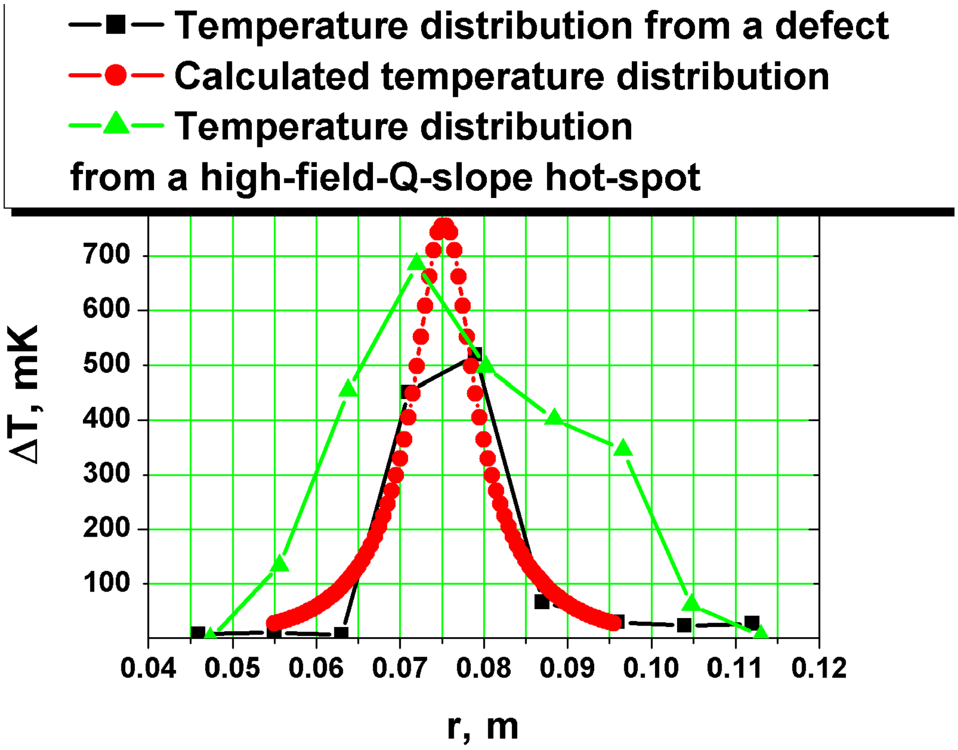

Figure 8.14: Spatial distribution of hot-spots. While the calculation[circles] and the data[squares] for a defect hot-spot agree, the high-field-Q-slope hot-spot has wider spatial distribution. A single point-like defect is eliminated as the source of the high-field-Q-slope hot-spot.

On the other hand, the question of heating in the grain boundary is more complex, as we shall show the heating in the grain boundaries might be orders of magnitude higher than in the intragrain niobium despite the thermometry results.

Readings of a single thermometer are proportional to the power dissipated on the area of about 1 cm^2. The area covered by a grain boundary is of the order of 1 cm x 10 nm. Hence for the grain boundary to dissipate as much as the rest of the grain probed by the thermometer the density of dissipated power in the grain boundary has to be 10^6 higher than that in the intragrain niobium. It implies that the resistance of the grain boundary must be 10^6 higher in order to

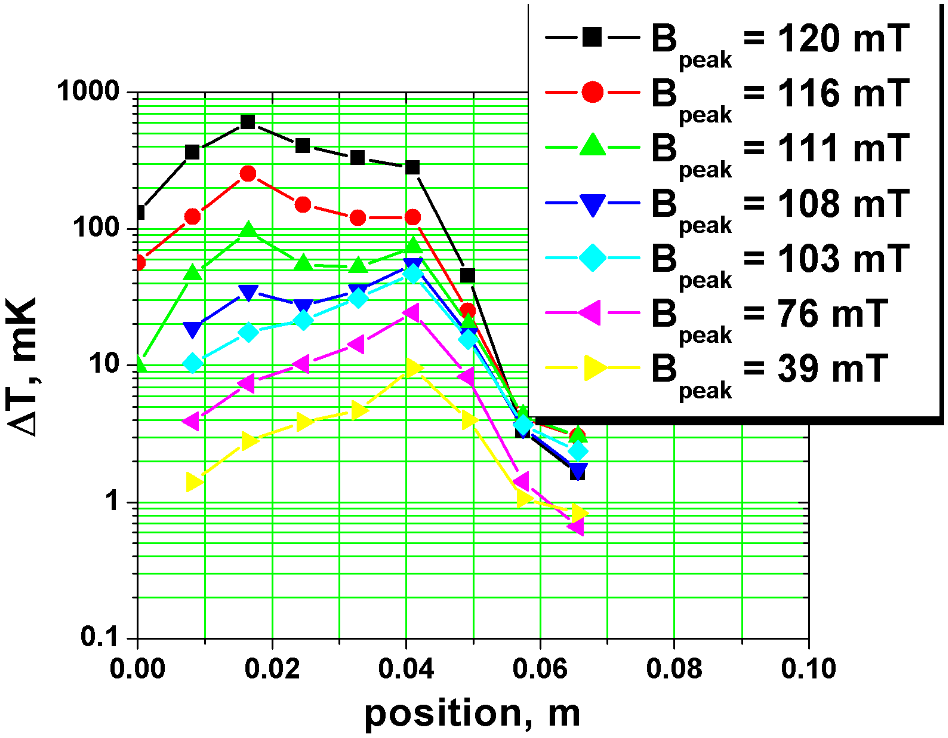

Figure 8.15: Spatial distribution as function of field for high-field-Q-slope region.

contribute to the dissipation as much as the rest of the grain probed by the thermometer. The conclusion is that, although the high field Q-slope is not caused by grain boundaries, the upper limit of the grain boundary's resistance, as set by the resolution of the thermometry system, is about 10^5 that of superconducting niobium.

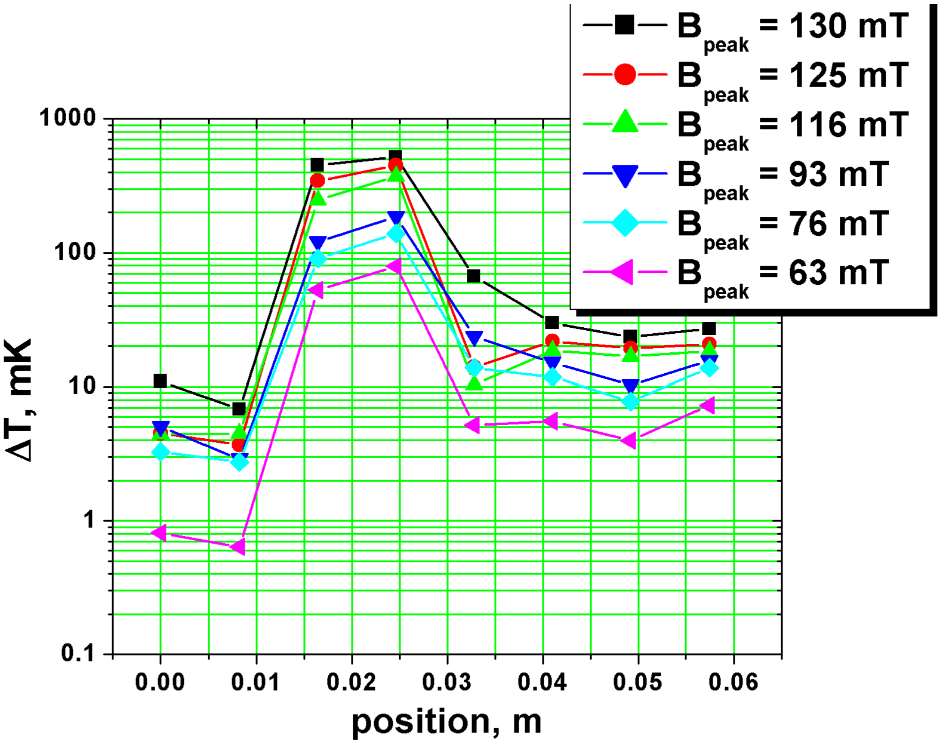

Figure 8.16: Spatial distribution as function of field for defect region.

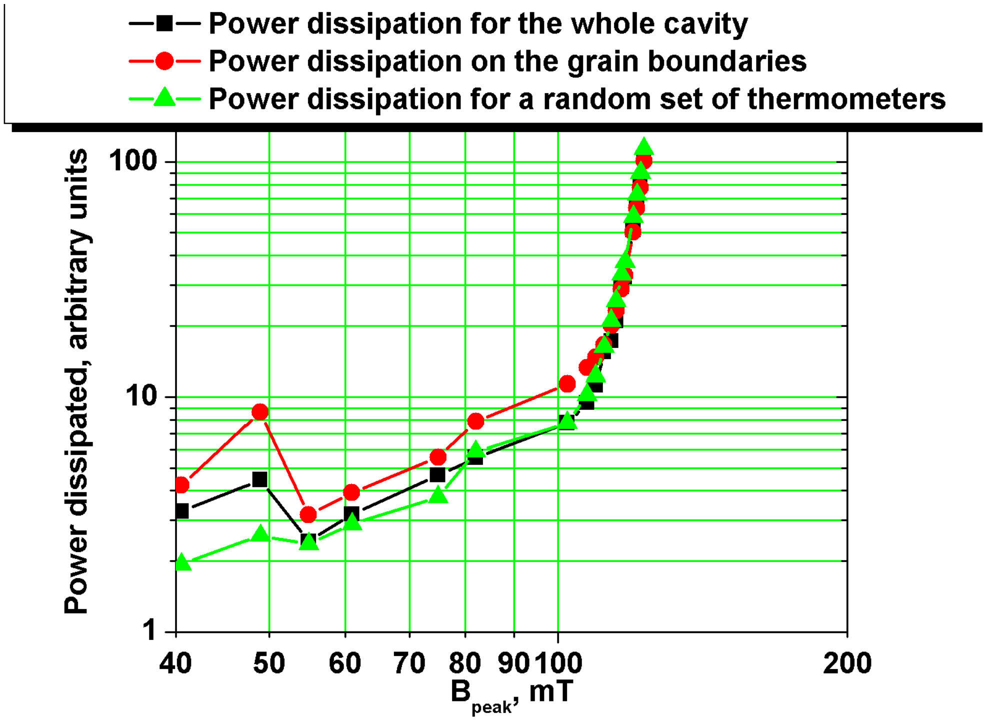

Figure 8.17: Comparison of the power dissipation on the grain boundaries to that in the intragrain niobium for the test in which high field Q-slope was observed.Power dissipated in the cavity surface as calculated from the thermometry data[squares];power dissipated on the grain boundaries as calculated from the thermometry data of the thermometers located on grain boundaries[circles];power dissipated as calculated from the thermometry data of a random set of thermometers[triangles]. Note that in the high-field-Q-slope region all three curves coincide. In the medium-field-Q-slope region the thermometry data of the thermometers located on grain boundaries shows more dissipation possibly due to two high-loss regions, which were located near or on the grain boundaries, see Fig. 8.6.

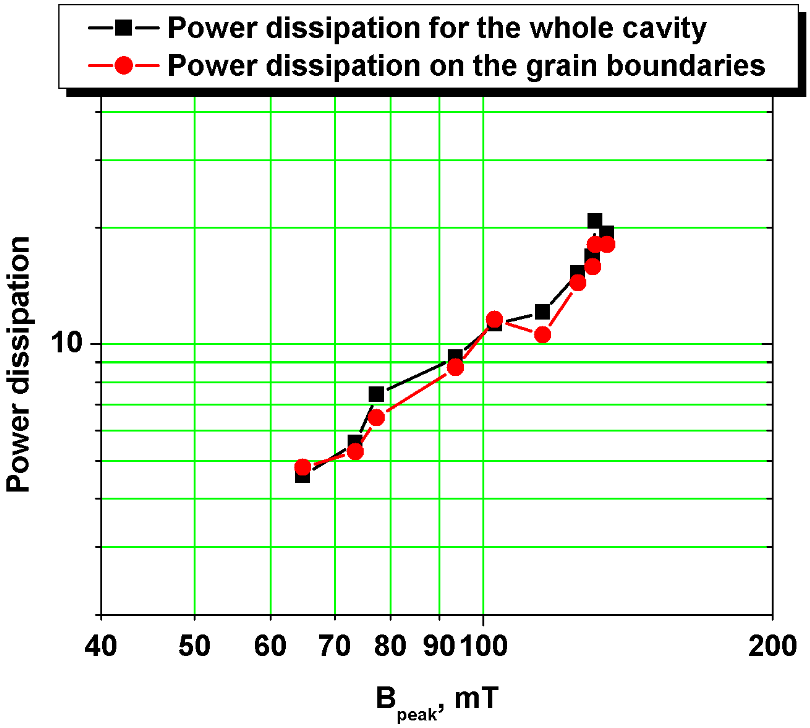

Figure 8.18: Comparison of the power dissipation on the grain boundaries to that in the intragrain niobium for the test after mild baking effect is removed by additional etching(HFQ-slope is present).Power dissipated in the cavity surface as calculated from the thermometry data[squares];power dissipated on the grain boundaries as calculated from the thermometry data of the thermometers located on grain boundaries[circles]; Note that no enhanced losses for grain-boundary regions compared to intragrain regions in both medium-field-Q-slope and high-field-Q-slope regimes.

Nevertheless, by the same speculations the quenching of the grain boundaries suggested by magnetic-field-enhancement model is rejected. In the magnetic-field-enhancement model it is suggested that during the high field Q-slope the width of the grain boundaries that goes normal-conducting is about 1 μm. Since the resistance of niobium is five orders of magnitude higher in the normal-conducting state than it is in the superconducting state at T$_{heliumbath}$=1.5°C, a quenched grain boundaries produce an order of magnitude more heating. Neither in the readings of any thermometer on the grain boundary a reproducible jump of such kind was observed in the experiment, nor the average power dissipated on all grain boundaries, as measure by thermometry, is higher than the average for the whole cavity surface, Fig. 8.17,Fig. 8.18. Thus we claim that for the large-grain cavity that we tested no quenching at the grain boundaries of the kind predicted by magnetic-field-enhancement model was observed up to B = 134 mT.

CHAPTER 9

HIGH TEMPERATURE BAKING

In this last chapter we describe a series of a new class of on-going experiments, which serve to check the prevailing models, but which also open up a host of new questions for the future. At one time the ever-existing oxide was suspected to play a role in RF performance of niobium cavities including the high field Q-slope. For some time oxide was also suspected to be a source of residual resistance in niobium. In the early 1990's F. Palmer carried out experiments on 8400 MHz niobium oxide-free cavities, in order to study effect of niobium oxide on a low field surface resistance of niobium cavities [57]. We decided to try the oxide-free approach to study the high field Q-slope. In order to remove oxide, Palmer sealed cavities while they were under UHV and heated them to 1100^0C in vacuum. The preliminary surface studies [58] have shown that niobium oxide is completely destroyed by such heat treatment and the resulting oxygen diffuses from the surface into the bulk niobium. Palmer's experiments have shown that natural oxide contributes no more than 1.5 nOhm to residual resistance at 8.6 GHz in RF cavities. Palmer continued his experiments and did some studies on niobium suboxide and oxygen contribution to losses. In his experiments he baked oxidized niobium cavities at 325°C to destroy some of the oxide and diffuse the excess of oxygen into niobium. The results of the experiments was reduction of the BCS resistance by as much as 20 percent due to the reduction of the mean free path, but an increase in the residual resistance by 40 nOhm. He also measured the critical temperature after 325°C baking and found out that the critical temperature was reduced by 5 percent after the baking. As conclusion Palmer attributed these changes to oxygen-enriched niobium. He excluded the role of the niobium oxide, because he failed to find a correlation between the results from cavities and XPS data provided by R. Kirby. The excitation curve was not measured in those experiments, because the main subject was BCS and residual resistance of niobium cavities.

The interest in the high field Q-slope and in the baking effect triggered similar surface studies on niobium samples before and after heat treatment at different temperatures. X-ray photoelectron spectroscopy is one of the best tools at the moment to study the first few nanometers of material. Studies, performed at SLAC by R. Kirby, have shown that niobium oxide can be destroyed within 30 minutes at temperatures as low as 400 °C, Fig. 9.1 He also studied whether oxide will reform on the sample surface during cool down because of, for example, diffusion of oxygen to the surface or exposure to residual gases in the vacuum chamber. His results show that the niobium surface can be left in vac-

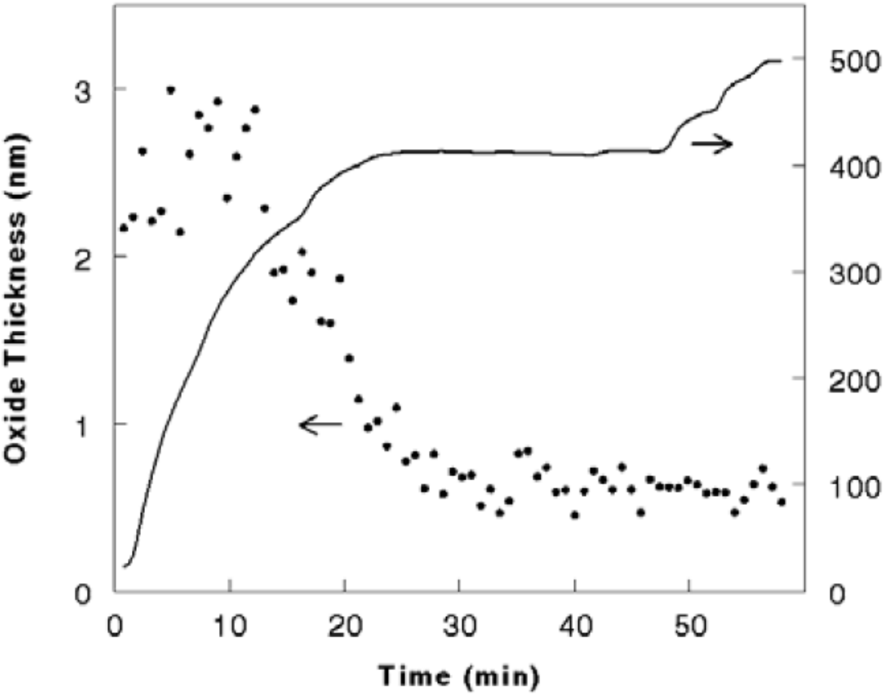

Figure 9.1: Oxygen to niobium ration as inferred from XPS results for heated niobium sample.

uum chamber overnight, and niobium will not re-oxidize, Fig. 9.2. Other studies

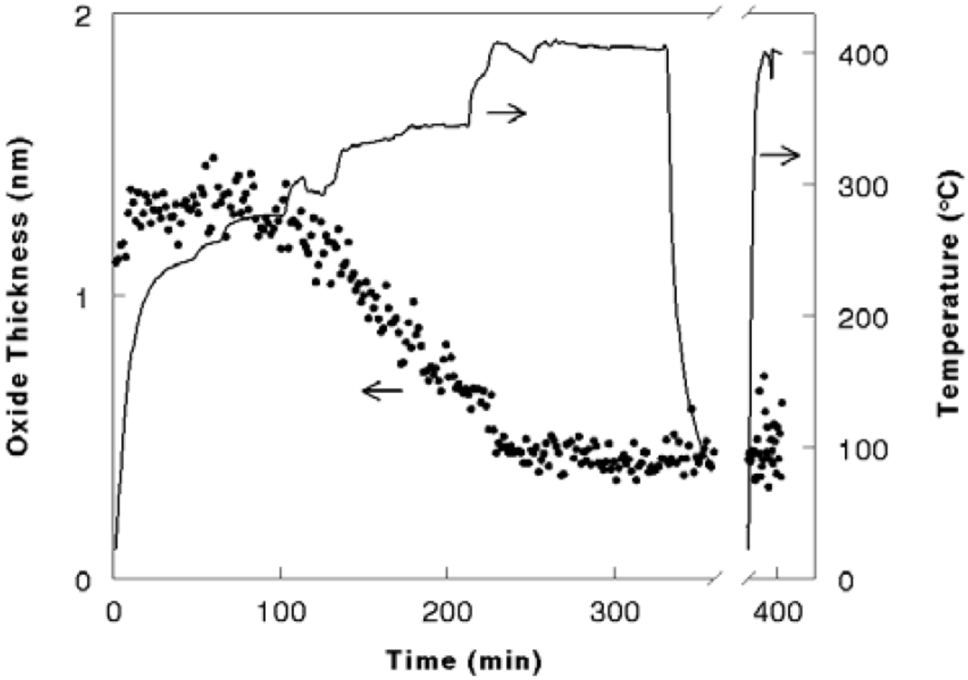

Figure 9.2: XPS results for the sample left in vacuum chamber overnight.

suggested that temperatures around 250^0C [59] are enough to remove Nb_20_5 and NbO_2, but not NbO.

The Q-slope phenomena renovate the interest in niobium oxides and the niobium-oxide interface. Baking at 400 °C not only destroys most of the oxide, but should also dilute any excess of oxygen present below the oxide, with the possible exception of NbO clusters. This is an important test of the oxygen pollution models discussed in Chapter 4. We decided to study the effect of niobium oxide removal on high field performance of niobium cavity using our 1.5 GHz RF setup with thermometry.

The cavity, which was used in these experiments, was a 1.5 GHz elliptical cavity, made of 300 RRR niobium sheet of 3 mm thickness with 1 mm grain size. The half-cells, shaped by deep drawing, were post-purified at 1300^0C for 2

Table 9.1: The summary of cavity's parameters

	$Cavity No.1$
Frequency	1500 GHz
Shape	Elliptical MARK-III
RRR	500
Grain size	1 mm
Thickness	3 mm
Initial Treatment	Vertical EP + 10 sec BCP(1:1:2)

hours to raise RRR and then at 1200^0C for 4 hours. The half-cells were vertically electropolished [29] before welding. After welding, the cavity was vertically electropolished for about 100 μm. After electropolishing the cavity was chemically treated with BCP ($HF:HNO_3:H_3PO_4$ - 1:1:2) for 10 sec (flash BCP). The temperature of the solution was kept below 15^0C. After the chemical treatment the cavity was rinsed with ultra pure water and transferred to the clean room of class 100. In the clean room the cavity was rinsed for two hours with high purity water under 1000 psi pressure. Then the cavity was assembled on the 1500 MHz test stand in the clean room. Each test was carried out at the bath temperature of 1.5^0K at low fields and increased to 1.7^0K at high fields.

The cavity's parameters are summarized in the table. 9.1.

The 400 °C setup is briefly presented in Chapter 3 and reviewed here. For the baking a steel box was put around the cavity and pressurized with argon, preheated to 250°C, to avoid oxidation of the outer surface of the cavity during the heat treatment. The inside of the cavity was kept under UHV. The heating elements were two 1.5 kW band heaters placed on copper rings, which were shaped to follow the profile of the cavity. Copper foils were used to improve the temperature distribution. Only the cell itself was heat treated, the rest of the vacuum system was kept at a room temperature by water-cooling clamps on beam pipes. The pressure during the heat treatment was $4.5 \cdot 10^{-7}$ Torr. The main constituents were water($2 \cdot 10^{-7}$ Torr) and CO($3 \cdot 10^{-8}$ Torr) as was indicated by residual gas analyzer. The oxygen partial pressure was $8 \cdot 10^{-11}$ Torr. The mean delay between heat treatment and RF cryogenic test was two days. In Fig. 9.3 the schematic drawing of the 400 °C baking setup is presented.

For air exposure Zero Grade Air from Airgas was used. After air exposures the cavity was pumped down to 10^{-7} Torr.

The sequence of all tests is presented below:

- The cavity was tested after chemistry.
- The cavity was heated to above 400 °C for at least one hour.
- The cavity was tested at 1.5 °K.
- The cavity was exposed to $\approx$ 150 Torr·sec of dry air.
- The cavity was tested at 1.5 °K.
- The cavity was heated to above 400 °C for at least one hour.
- The cavity was tested at 1.5 °K.
- The cavity was exposed to $\approx$ 150 Torr·sec of dry air.
- The cavity was tested at 1.5 °K.
- The cavity was exposed to $\approx 10^7$ Torr·sec of dry air(1 atm for 12 hours).
- The cavity was tested at 1.5 °K.
- The cavity was heated to above 400 °C for at least one hour.
- The cavity was tested at 1.5 °K.
- The cavity was exposed to $\approx$ 300 Torr·sec of dry air.

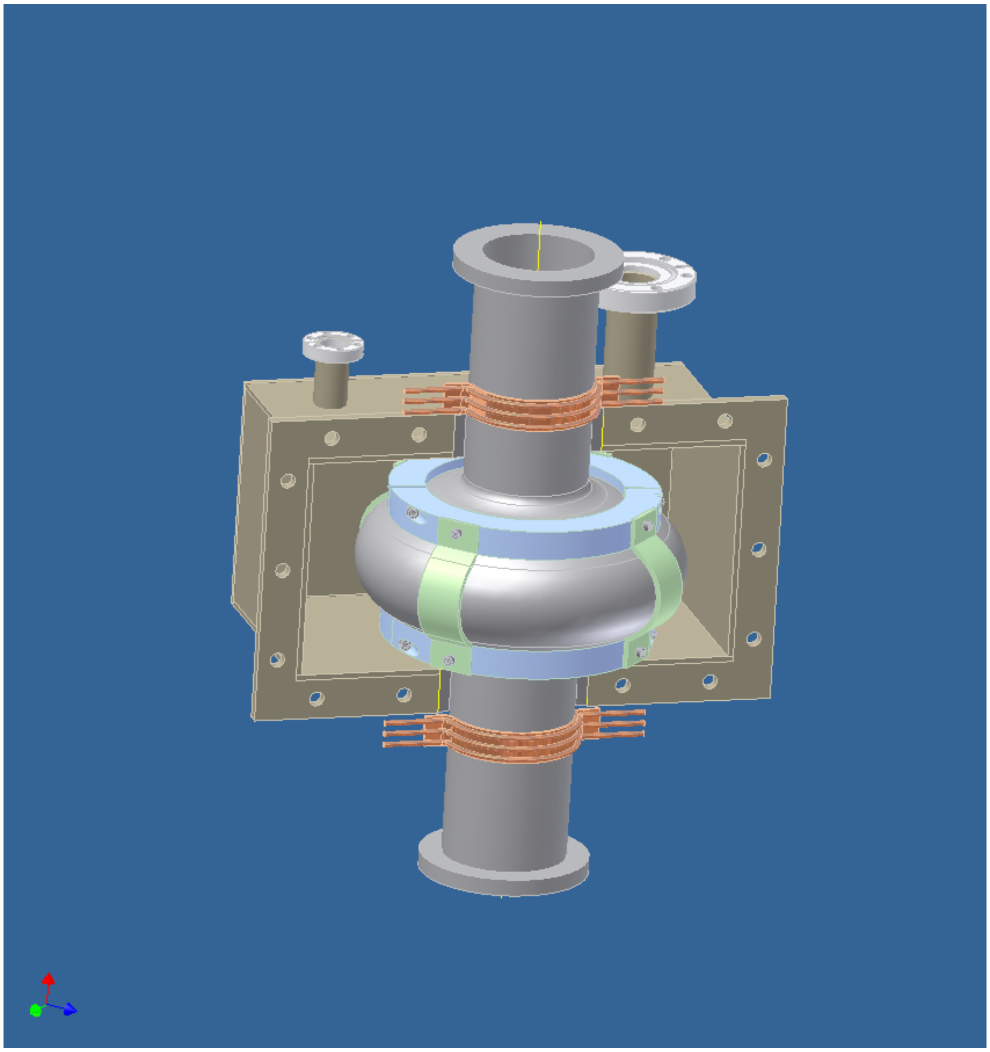

Figure 9.3: Sketch of the setup for high temperature baking of one-cell 1.5 GHz cavity

- The cavity was tested at 1.5 °K.
- The cavity was exposed to $\approx 10^7$ Torr·sec of dry air(1 atm for 24 hours).
- The cavity was tested at 1.5 °K.

9.1 Results

In order to compare the performance of a nearly-oxide-free, thin-oxide and standard-oxide niobium cavities, it was necessary to establish a baseline for the high field performance. Thus the first step was to test after chemistry. After the cavity was chemically treated, assembled in the clean room, the thermometry system was assembled and the cavity was tested in the cryostat. The low-field quality factor of the cavity was about $3{\cdot}10^{10}$, Fig. 9.4[squares]. Above B_{peak} = 110 mT the typical high field Q-slope was observed. At B_{peak} = 123 mT we were limited by available RF power(30 W), the quality factor was about $3{\cdot}10^{9}$. The temperature map taken above 110 mT shows three hottest regions on the bottom half-cell, Fig. 9.5. All temperature sensors, both in these hot regions and in other high-magnetic-field regions equally showed a non-quadratic increase in heating with power laws as high as B^{20} above 100 mT, Fig. 9.7[squares]. No x-rays were present during the test. Thus in this test the baseline for high-field-Q-slope studies was established. We did not carry out any mild baking so as to preserve the high field Q-slope.

Having established the baseline for the study of the high field Q-slope, we proceeded to 400°C baking. The cavity was taken out of the cryostat, the baking setup was attached to the cavity and the cavity was heated to 400°C for two hours under UHV condition. Then the baking setup was removed, the thermometry system was put onto the cavity, the cavity was lowered into the cryostat and tested. The excitation curve for this test is presented in Fig. 9.4[circles]. The excitation curve for this experiment differs little from the baseline test. The high field Q-drop did not change much. The highest B_{peak}, which was reached, was 117 mT in this test, where the cavity was limited by a thermal breakdown.

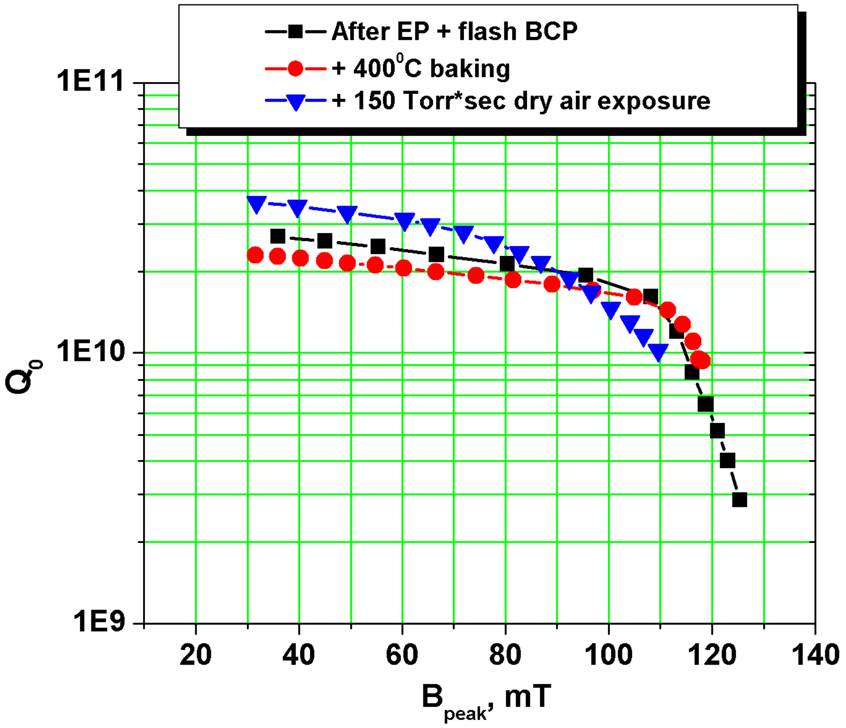

Figure 9.4: Quality factor versus peak magnetic field for the first three tests: after chemical treatment the excitation curve has typical medium- and high-field Q-slopes; the cavity was then baked at 400°C; the cavity was exposed to ≈ 150 Torr·sec of dry air.

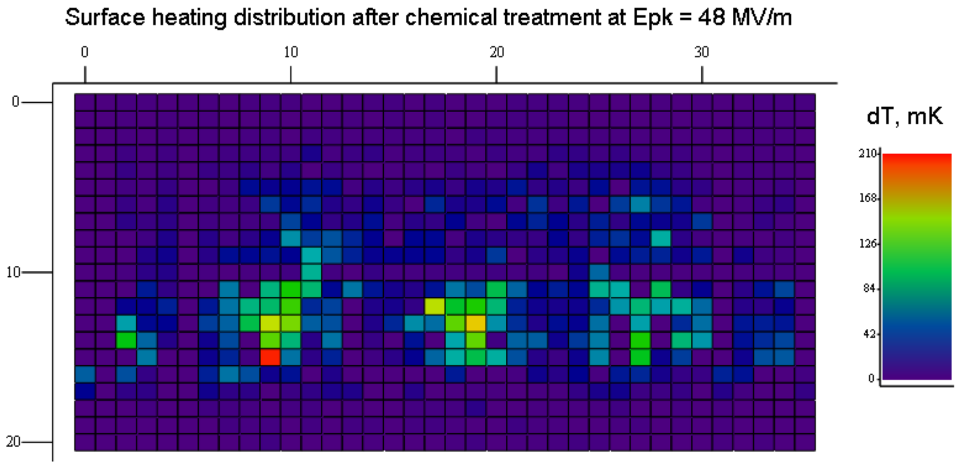

Figure 9.5: Temperature map at B_{peak}=117 mT after the chemistry show three broad hot-spots.

The temperature maps in the high-field-Q-slope region shows four similar but stronger broad hot regions, Fig. 9.6, and the analysis of the reading of individual thermometers shows that three of these regions were also hot at low fields, because they have higher surface resistance after baking, Fig. 9.8[circles]. The resistance in these regions was an order of magnitude higher than in other regions. Except for the thermometers in these three hot regions, which cover about 15 percent of the cavity surface, all other thermometers show readings typical for the high field Q-slope, Fig. 9.7[circles]. So we concluded that the most of cavity surface still exhibited the high field Q-slope after the 400°C baking.

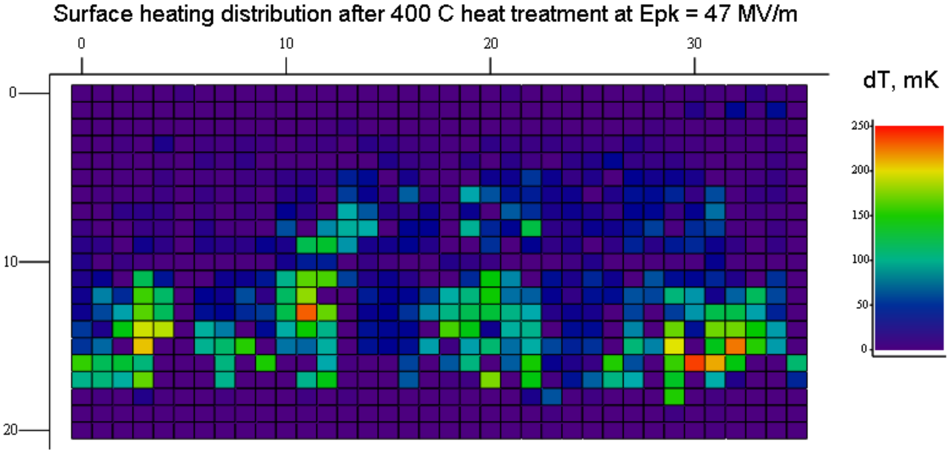

Figure 9.6: Temperature map at B_{peak}=117 mT after the cavity was baked at 400°C.

9.2 Complementary air exposure studies

Since 400°C baking dissolved most of the oxide, we decided to study the effect of oxide re-growth by a controllable exposure to dry air. Typically a delay between the 400°C baking and RF test was two days, therefore the niobium

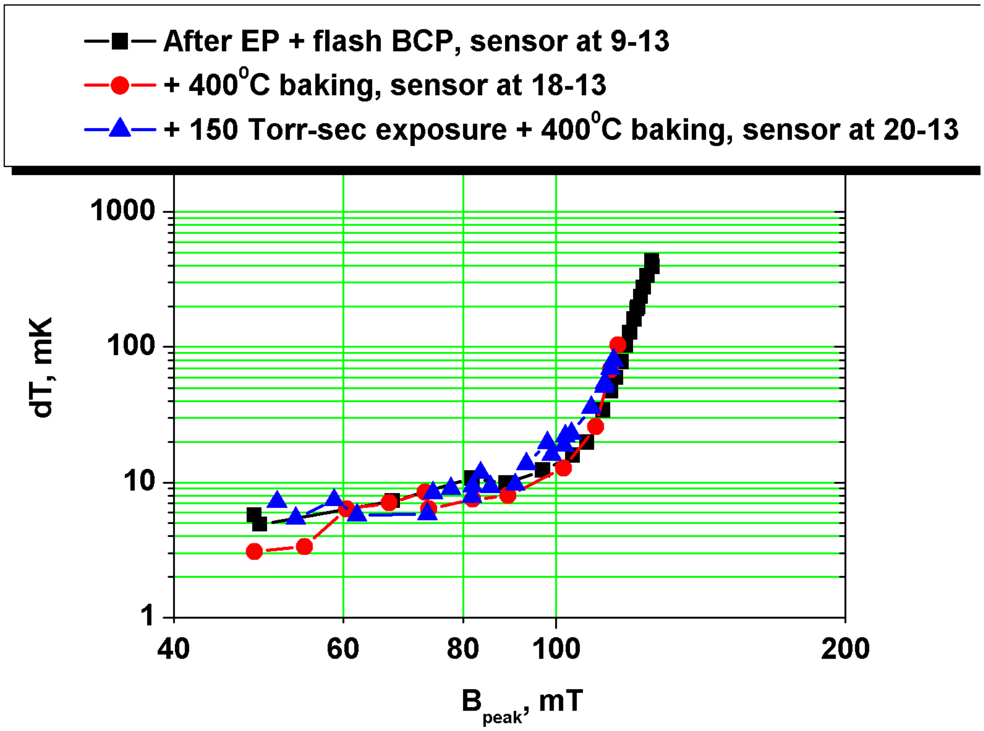

Figure 9.7: Thermometry data from the regions that showed high field Q-slope: after chemistry, after first 400°C baking, after second 400°C baking.

surface is inevitably exposed to about .1 Torr-sec of water vapors, which put the lower limit on the exposure. The upper limit is set by exposure to one atmosphere of air. First it was decided to expose the cavity to about 100 Torr-sec. The cavity was warmed up and then, while still inside the cryostat, was pressurized to 2.4 Torr for a minute. After exposure it was evacuated and an RF test was performed. In this test the low-field quality factor was slightly higher, Fig. 9.4[triangles], but the cavity exhibited a strong medium-field Q-slope. The cavity was limited by a thermal breakdown at B_{peak} = 114 mT. The field at which the cavity was limited in this test is lower than that at which the high field Q-slope typically starts. The temperature map shows that, following the short exposure, a new hot region appeared on the top half-cell, Fig. 9.10. This hot

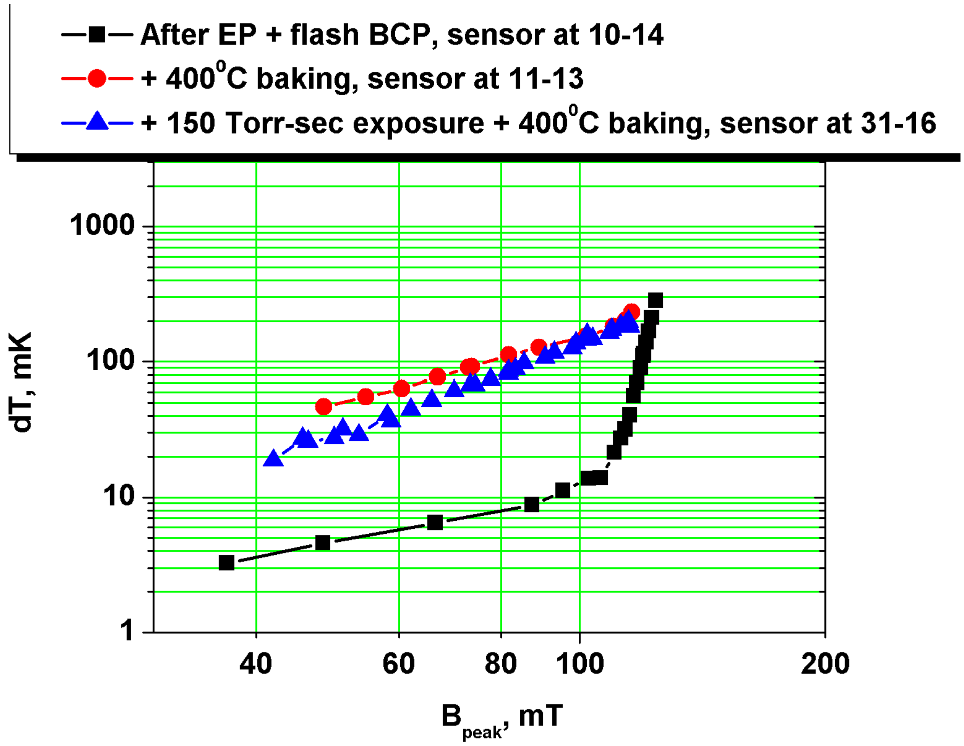

Figure 9.8: Thermometry data from the regions that showed high surface resistance: after chemistry, after first 400°C baking, after second 400°C baking.

spot was a major source of losses. The readings of the thermometers from this region show non-quadratic increase with field, Fig. 9.11[circles]. The three regions with a high surface resistance from the previous test still exhibited high losses, but these high-surface-loss regions slightly improved after the short exposure, Fig. 9.9[circles].

9.3 Second set of experiments

In order to confirm results of the first 400°C baking and air exposure, the experiments were repeated. Since 400°C baking removes most of the oxides from

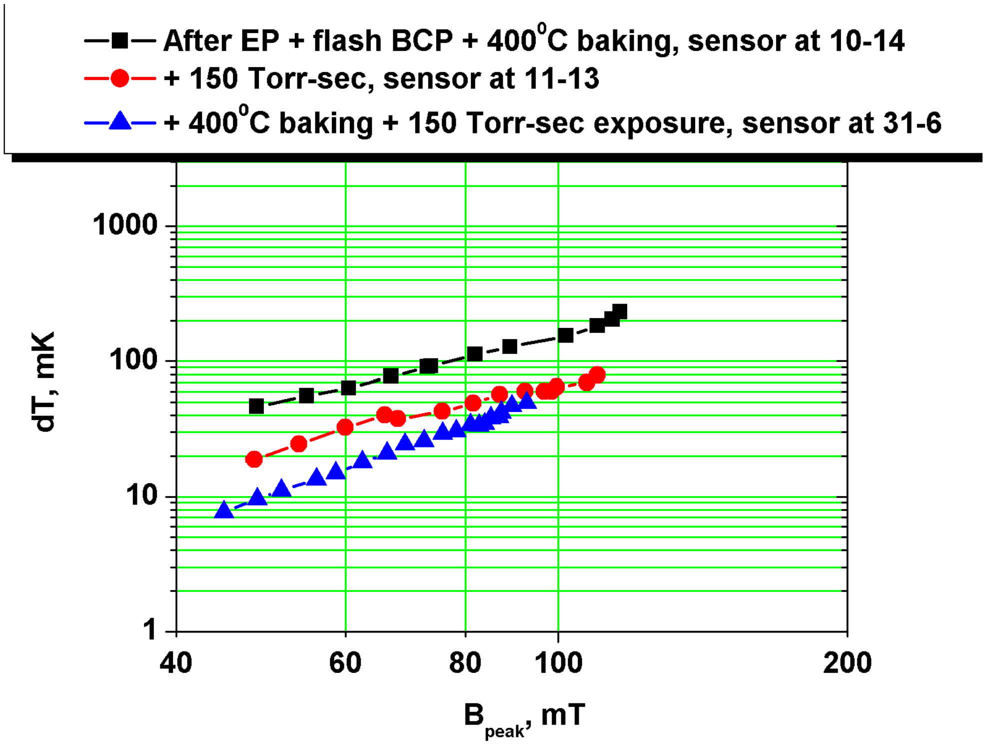

Figure 9.9: Thermometry data from the regions with high surface resistance after 400°C baking, that shows improvement of this regions by short exposure: following the first 400°C baking[squares], after first 150 Torr·sec air exposure[circles], finally, second 150 Torr·sec air exposure[triangles].

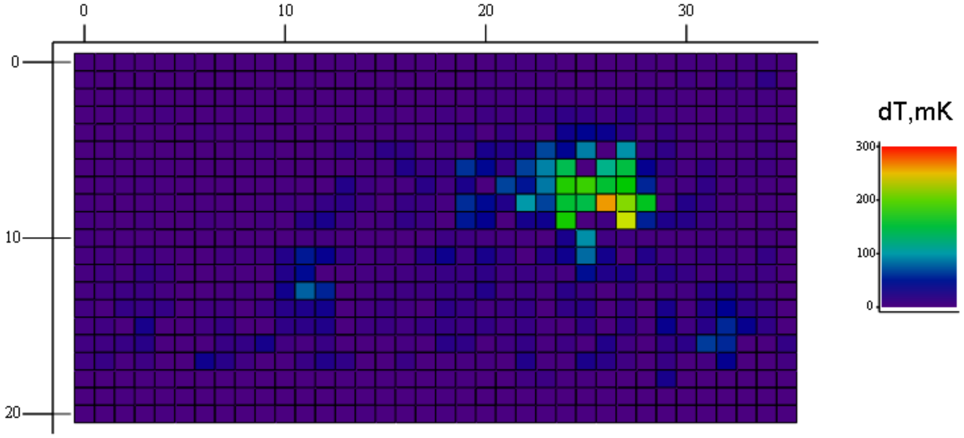

Figure 9.10: Temperature map at B_{peak}=110 mT after the cavity was exposed to ≈ 150 Torr·sec.

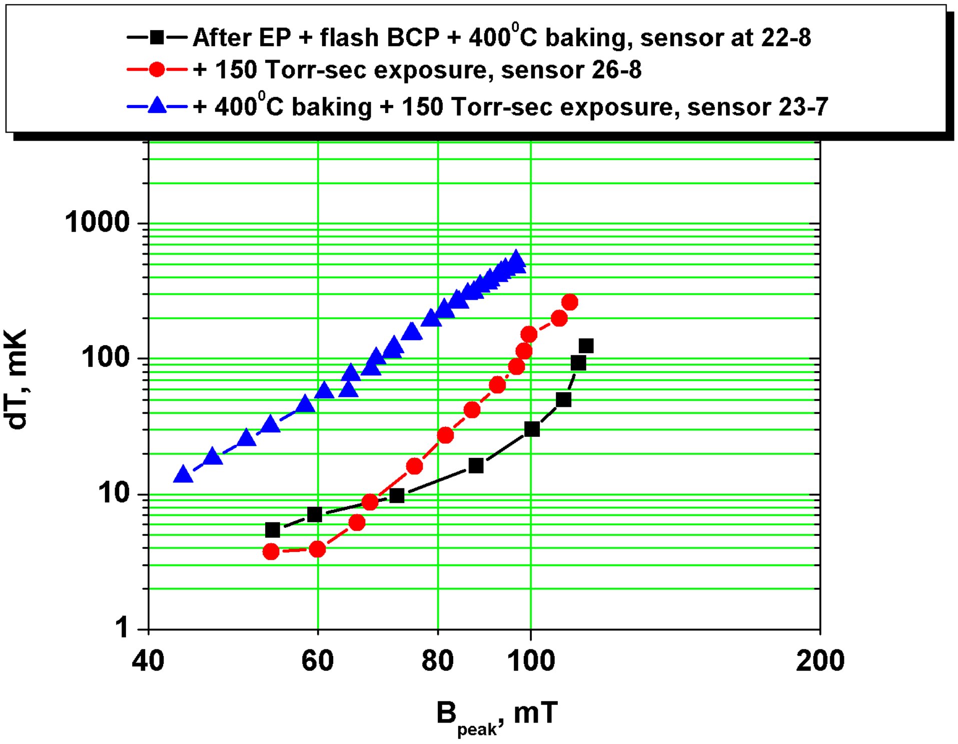

Figure 9.11: Thermometry data from the regions that showed high losses after short exposures: first 400°C baking[squares]; after the cavity was exposed to ≈ 150 Torr·sec[circles], after the cavity was exposed to ≈ 150 Torr·sec following a second 400°C baking[triangles].

Table 9.2: Summary of results for the first set of experiments

	Tbath, K	R_{surf}, nOhm	γ	Limitation
VEP+ 1 min BCP	1.5	8.9±0.1	2.20±0.04	HFS
400^{0}C Baked	1.5	10.6±0.1	1.81±0.03	Quench
air exposure to 2.4 Torr for 1 min	1.5	6.3±.2	N/A	Quench

niobium surface, it was suggested that the strong medium field Q-slope will be removed by the 400°C baking and the cavity performance will be as it was after the first 400°C baking. Thus after the short exposure the cavity was taken out of the cryostat, the thermometry system was removed, the baking setup was arranged and the cavity was baked at 400°C for about two hours. After the baking the cavity was lowered in the cryostat and RF test was performed. In this test the excitation curve was similar to the one after the first 400°C baking, Fig. 9.12[squares]. The cavity had a medium-field Q-slope similar to that after chemistry and after 400°C baking. The limitation was a thermal breakdown at B_{peak} = 115 mT with the quality factor of about 10^{10}, so no high field Q-slope was observed. Temperature maps at high fields show that the lossy region, which appeared after the short exposure, was still present, but substantially improved. The quench site was in the one of the three high-surface-resistance regions, which appeared after the first 400°C baking. Except thermometers from these four regions, all thermometers show the exponential field dependence typical for the high field behavior, Fig. 9.7[triangles].

In order to confirm the strong medium field Q-slope and accordingly high-loss regions, another short exposure, 150 Torr·sec, was done. After the second short exposure the low-field quality factor decreased by a factor of two and was about 10^{10}, Fig. 9.12[circles]. As it was expected from the previous short exposure, the excitation curve exhibits a strong medium field Q-slope. The highest B_{peak}, achieved, was 100 mT due to lack of power. The quality factor of the cavity at B_{peak} = 100 mT was about 10^{9}. The temperature map shows that again a high-loss region was formed in the process of the short exposure. The temperature sensors again shows non-quadratic dependence, Fig. 9.11[triangles].

Because it was suspected that the high-loss regions formed after the short ex-

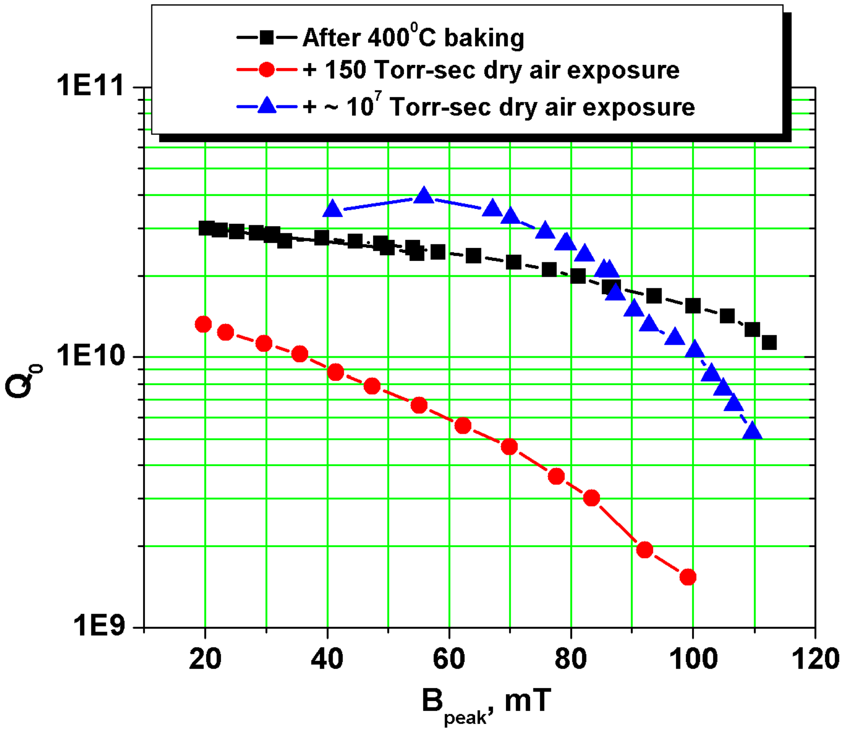

Figure 9.12: Quality factor versus peak magnetic field for the second group of three tests: after the cavity was baked at 400°C, after the cavity was exposed to $\approx$ 150 Torr·sec of dry air, after the cavity was exposed to $\approx 10^7$ Torr·sec

posure are caused by formation of suboxides, the cavity was warmed up and then exposed to 1 atm of dry air for about 12 hours, $\approx 10^7$ Torr·sec, in an attempt to convert possible lossy metallic suboxides to non-lossy dielectric pentoxide. Indeed the low-field quality factor was recovered by the long exposure. The excitation curve in this test has an unusually pronounced low field Q-slope, which was present up to B_{peak} = 60 mT, Fig. 9.12(triangles). After the summit at B_{peak} = 60 mT the quality factor started to decline similarly to the previous experiment. At B_{peak} = 110 mT the experiment was stopped due to lack of power. The temperature maps at high fields show that the anomalous losses, though reduced after long exposure, were still present, Fig. 9.13.

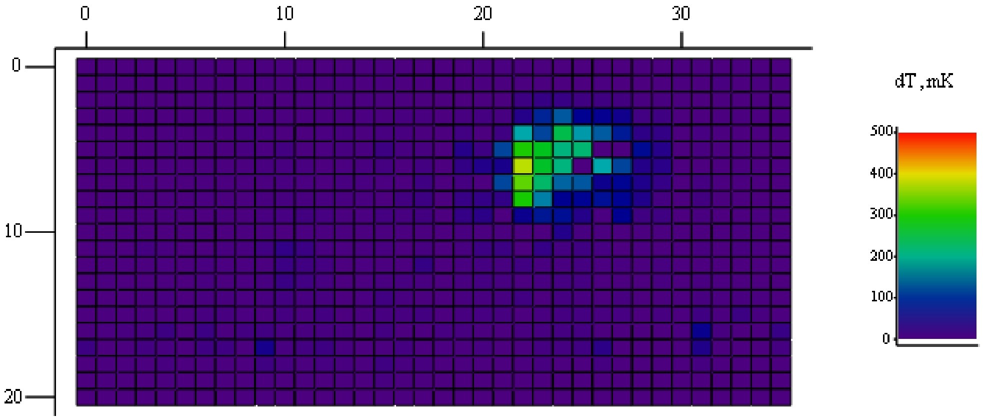

Figure 9.13: Temperature map at B_{peak}=115 mT after the cavity was exposed to ≈ 10^7 Torr·sec.

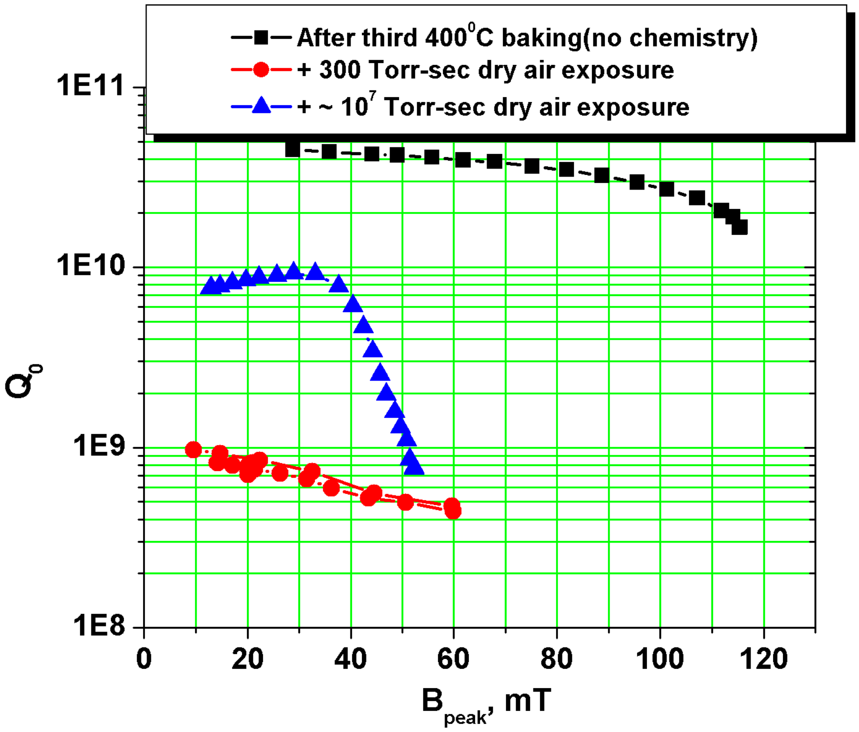

Figure 9.14: Quality factor versus peak magnetic field for the third group of three tests: after the cavity was baked at 400°C, after the cavity was exposed to ≈ 300 Torr·sec of dry air, after the cavity was exposed to ≈ 10^7 Torr·sec

Table 9.3: Summary of results for the second set of experiments

	Tbath, K	R_{surf}, nOhm	γ	Limitation
400^0C Baked	1.5	8.0±0.1	3.49±0.20	Quench
air exposure to 1.0 Torr for 5 min	1.5	15.8±0.4	23.6±1.59	Available power
air exposure to 760 Torr for 12 hours	1.5	2.9±0.6	N/A	Available power

9.4 Third set of experiments

Finally a third set experiments was carried out to confirm findings of the previous experiments. The cavity was taken out of the cryostat, the thermometry system was removed and the cavity was baked at 400°C for an hour, then the temperature was raised to 500^0C and the cavity was kept at this temperature for about half an hour. Then the baking setup was removed, the thermometry system was assembled, the cavity was lowered in the cryostat and tested. In this test there was no strong medium field Q-slope, the Q-slope was similar to those after previous 400 °C bakes, Fig. 9.4. The low-field quality factor was about $4{\cdot}10^{10}$. The cavity was limited by a thermal breakdown at B_{peak} = 117 mT. The analysis of the thermometry data show that all high-loss regions, which appeared after the short and long air exposures, were removed by the 400°C baking.

After the 400°C baking the cavity was warmed up and exposed to about 300 Torr·sec of dry air, then the baking setup was removed, the thermometry system

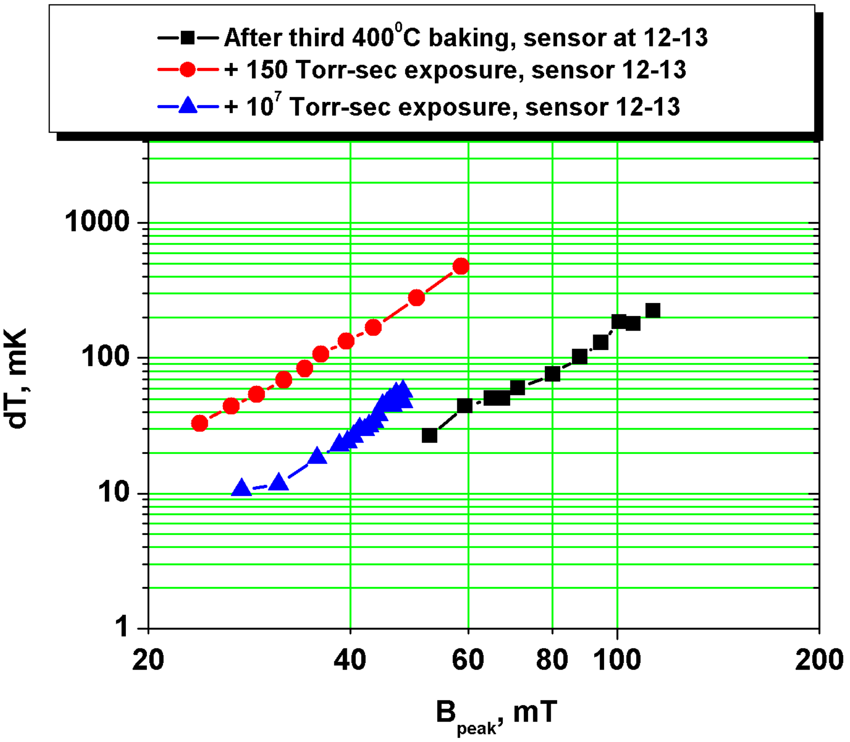

Figure 9.15: Thermometry data for the third set of experiments: after third 400°C baking, after the cavity was exposed to ≈ 150 Torr·sec, after the cavity was exposed to ≈ 10^7 Torr·sec

was assembled, the cavity was lowered in cryostat and tested. The low-field quality factor was 10^9, more than an order of magnitude lower that in previous test! The exposure formed lossy bands on top and bottom half-cell of the cavity as it is shown on the temperature map, Fig. 9.16. These bands did not correspond to the highest-magnetic-field regions, but roughly corresponds to the places, where the heating bands were located during the 400°C baking. The thermometry data shows that both surface resistance and slope were higher in this regions compared to previous test, Fig. 9.15[circles].

To convert suboxides, possibly formed by the short exposure, the cavity was warmed up and exposed to a 1 atm of dry air for 24 hours, ≈ 10^7 exposure. After the long exposure the low-field quality factor improved. The low-field quality factor was about 10^{10}. An interesting feature in this experiment is a pronounced low field Q-slope up to B_{peak}=30 mT. After the summit B_{peak}=30 mT the excitation curve has a strong medium field Q-slope. The measurements were limited by available power at B_{peak} = 50 mT with the quality factor of $8{\cdot}10^8$.

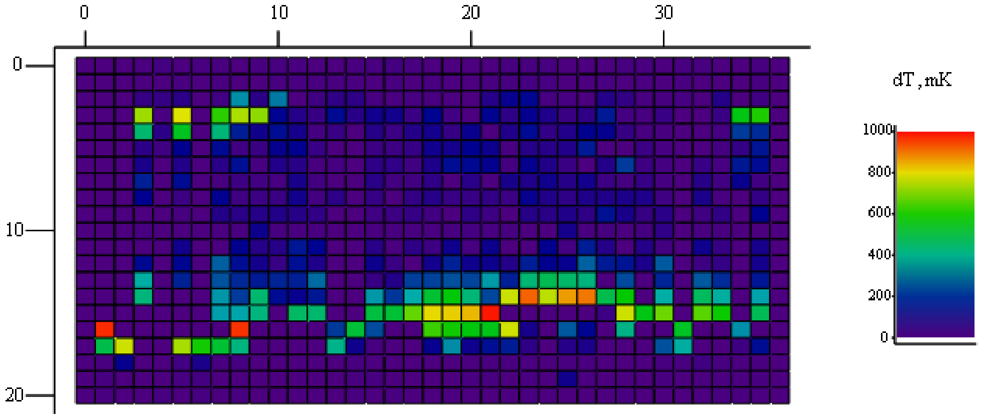

Figure 9.16: Temperature map at B_{peak}=50 mT after the cavity was exposed to $\approx$ 150 Torr·sec

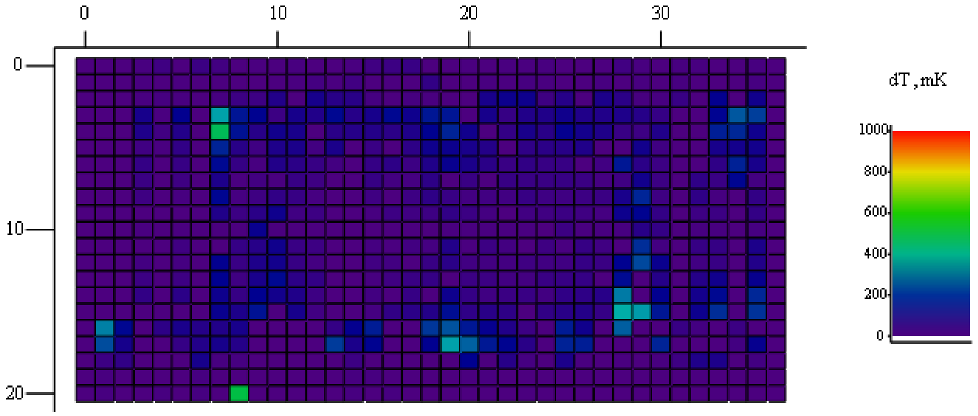

Figure 9.17: Temperature map at B_{peak}=48 mT after $\approx 10^7$ Torr·sec

Table 9.4: Summary of results for the third set of experiments

	Tbath, K	R$_{surf}$, nOhm	γ	Limitation
400^{0}C Baked	1.5	5.4±0.1	2.35±0.14	Quench
air exposure to 1.0 Torr for 5 min	1.5	254.4±7.5	15.8±1.53	Available power
air exposure to 760 Torr for 24 hours	1.5	N/A	N/A	Available power

9.5 Discussion

Clearly these first attempts to eliminate the oxide and to re-grow the oxide in stages has opened a new class of oxide-related phenomena that may shed some light on the Q-slope models. Our study was primarily aimed at the high field Q-slope. The 100°C baking is a common procedure used world-wide to improve the high-field performance of niobium cavities, especially electropolished cavities such as this cavity. To explain the high field Q-slope and the baking effect several models were suggested. This study has addressed two of them: the interface tunnel exchange model, ITE model [60], and the oxygen pollution model [39].

The ITE model attributes the high field Q-slope to losses caused by the natural oxide at high fields. In the ITE model the modification in the niobium pentoxide during the mild baking explains the improvement in the high-field performance. However the 400°C baking, which was done, removes the natural oxide [59], [61] and therefore the high field Q-slope should be removed according to ITE model. This is contrary to what was observed in the first 400 °C baking experiment.

The oxygen pollution model assumes an oxygen pollution layer underneath the oxide. The oxygen-polluted layer has superconducting properties that are worse than those of a pure niobium. Baking of a cavity at 100°C for 48 hours, a typical baking procedure, diffuses the oxygen pollution layer into the bulk. The model however fails to explain the results after baking at higher temperatures, i.e. 150-180°C for 48 hours, in which the high field Q-slope remains unchanged or even degrades. In order to accommodate these results, the oxygen pollution model was modified by G. Ciovati [42]. He suggests that, during baking, the oxide layer dissociates and oxygen atoms from the oxide contribute to the oxygen pollution layer. Due to this enrichment process the oxygen pollution layer is not removed by baking at temperatures higher that 100-120°C. In order to see the predictions of this model for our experiment, we have calculated oxygen depth profile within the model after 400°C baking. From the calculation it follows that the oxygen concentration in the penetration depth should be substantially reduced by 400°C baking, Fig. 9.18. So we expected that the high-field performance will be improved by such baking. Still we observed the high field Q-slope after the first 400 °C baking and it was the same as before baking both from the excitation curve and from the thermometry data. So this model is also contradicted by 400 °C baking experiments.

The presence of the high field Q-slope after 400°C baking can be explained within the ”oxide purifier” model [62]. This model attributes the high field Q-slope to impurities such as carbon and nitrogen, and addresses only the baking effect. In this model a natural oxide is attributed a role of purifier of niobium during the mild baking. During the standard 100°C baking for 48 hours, the

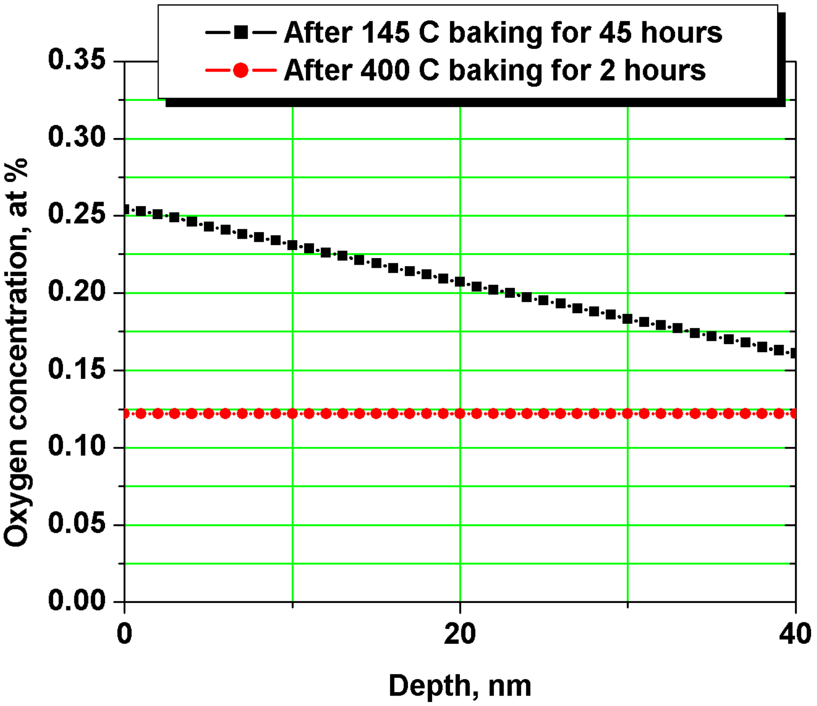

Figure 9.18: Diffusion calculation based on the modified oxygen pollution model proposed by G. Ciovati.

harmful impurities diffuse from niobium into adjacent oxide, thereby improving the superconducting properties of niobium. Even though the diffusion rates of nitrogen and carbon in the bulk niobium are very low, the rates may be elevated near the oxide. The higher temperature baking, i.e. above 150 °C, is less efficient because of a finite capacity of the oxide. Within this model no improvement can be expected after a 400°C baking, because the oxide layer is removed, and therefore the niobium purity is not improved. However recent surface studies suggest that carbon, which was initially proposed as a diffusing impurity in this model, is not responsible for the high field Q-slope. Surface studies have shown that during 300°C baking for 1 hour carbon segregates to the surface [63]. Thus if the carbon were responsible for the high field Q-slope, a degradation in the high field performance would be expected after the 400°C baking due to segregation of the carbon to the surface. But the high field Q-slope did not degrade, so even if the model holds true, carbon is not involved in high-field-Q-slope phenomenon.

Another interesting result in these studies was a strong medium field Q-slope and high surface resistance after short exposures. The strong medium field Q-slope is sometimes observed when the niobium is enriched with hydrogen during chemistry. The excitation curve then has a strong medium field Q-slope, because niobium hydrides are formed during the cooldown if the hydrogen concentration is $\geq$ 6 at. percent [64]. We however suggest that hydrogen contamination is not the cause of the strong medium field Q-slope and a high surface resistance in our experiments. Firstly, because the quality factor was improved by longer exposure, which does not help in the case of the hydrogen Q-disease. Secondly, because the medium field Q-slope was removed by 400°C baking, whereas in order to remove the typical Q-disease, cavities must be treated at 800°C for several hours. We suggest that the reason behind a strong medium field Q-slope and high surface resistance is a formation of niobium suboxides. The idea supported by the fact that performance was improved by longer exposure, which presumably caused conversion of the lossy suboxides to low-loss pentoxide, and then was completely restored by 400°C, which dissolved the pent- and suboxides. Thus these experiments open an interesting question about the contribution of the niobium suboxides to the medium field Q-slope and to the low-field quality factor. As we have mentioned in Chapter 4 the medium field Q-slope does not yet have a convincing explanation.

9.6 Complementary surface studies results

The striking difference in losses, observed for the niobium cavity before and after air exposure, suggests that niobium surface oxide can play an important role in RF losses depending on the stoichiometry. We attributed strong losses after short exposure to formation of niobium suboxides like NbO, i.e. for short exposures niobium pentoxide is not yet formed on the surface, but rather it is NbO, NbO_2 or NbO_x that form first and cause losses, Fig. 9.19.

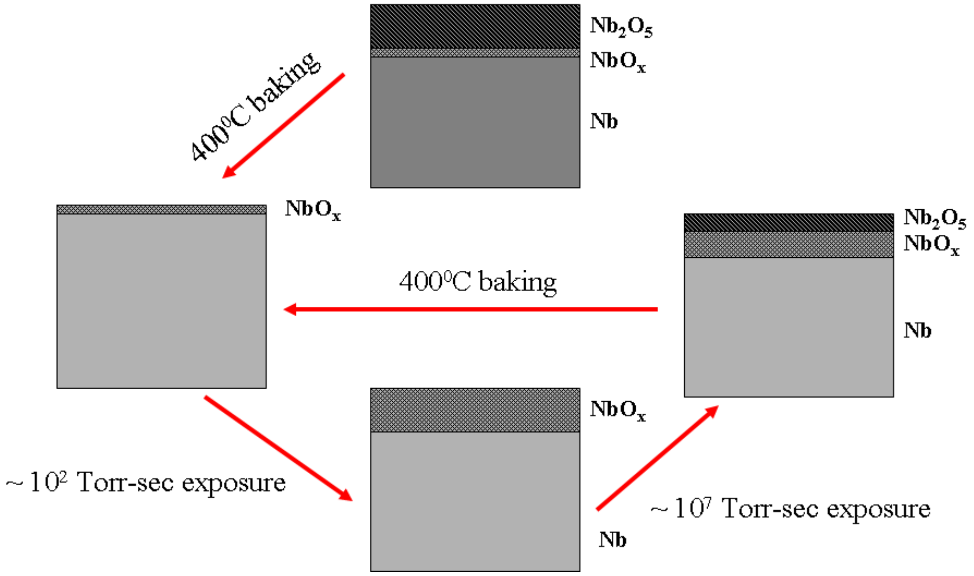

Figure 9.19: A qualitative model that explains results of 400 °C baking and subsequent exposures by modification of oxide.

In order to check the model we performed XPS studies. The studies were done on Kratos Axis Ultra X-ray photoelectron spectrometer at Surface Science Western Center by M. Beisinger. The measurements were performed on single-grain sample, which was chemically etched with BCP, and on small-grain sample, which was electropolished in the setup for vertical electropolishing. In Fig. 9.5 values for position of Nb 3d 5/2 peaks that we used to fit the data, these values are in good agreement with the data form NIST database.

Table 9.5: Data for the center of niobium 3d 5/2 peak at different oxidation state

Species	Position of peak, eV
Nb	202.23
NbO	203.80
NbO_2	205.80
Nb_2O_5	207.75
NbC	203.35

In this study we were surprised to discover formation of niobium carbide on the surface during heating to 400 °C. This formation is unambiguously seen in appearance of a second peak for carbon 1s signal, Fig. 9.20. The identification of formation and presence of carbide is problematic due to close proximity of niobium carbide peak to niobium monoxide peak. So in the niobium 3d spectrum these peaks merge into one and are hard to distinguish. But the 1s carbon peak leaves no room for doubt. Moreover, we were able to determine from angle-resolved study that carbide is formed not on the surface, but rather under residual oxide, on the oxide-niobium interface, Fig 9.21. Angle-resolved study shows that Nb 3d peak that corresponds to NbO/NbC bonding moves to the left as angle of detector becomes more grazing, suggesting that niobium monoxide is on top of niobium carbide.

The studies have been done on two different samples. One sample was a single grain sample. Sample's dimensions were about 1 cm x 1 cm. The sample was cut from large-grain sheet with RRR of 340-420. The sample was polished with BCP prior to analysis. The following sequence of experiments was carried out onto the sample:

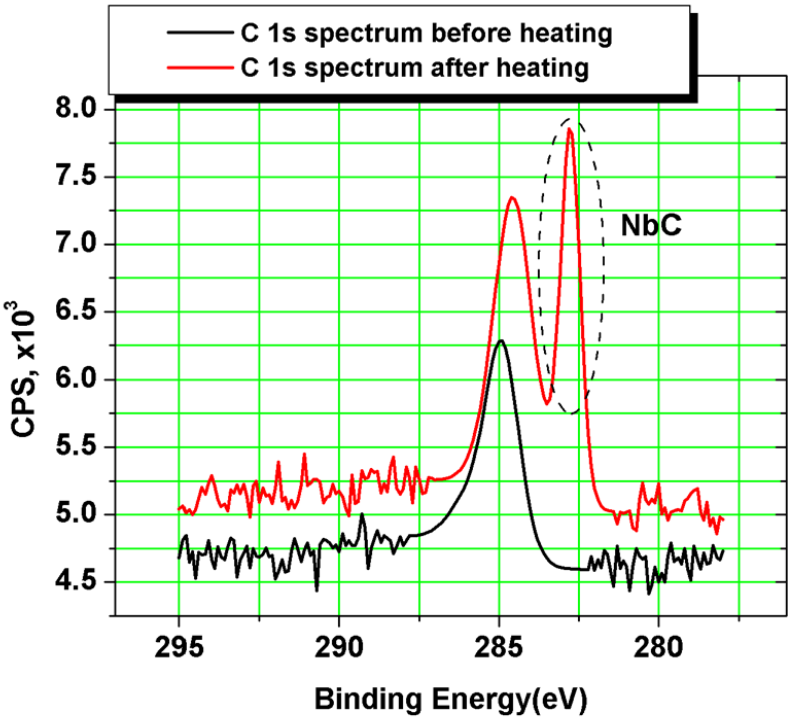

Figure 9.20: Carbon 1s signal proves formation of niobium carbide during 400 - 500 °C baking.

- Sample was chemically etched with BCP. Treatment No.1.
- XPS survey, Nb 3d, O 1s, C 1s spectra were measured.
- Sample was heated to 400 °C for two hours. XPS Nb 3d spectrum was acquired during heating. Treatment No.2.
- XPS survey, Nb 3d, O 1s, C 1s spectra were measured.
- Sample was exposed to 150 Torr-sec of O_2. Treatment No.3.
- XPS survey, Nb 3d, O 1s, C 1s spectra were measured.
- Sample was exposed to air for 24 hours. Treatment No.4.
- XPS survey, Nb 3d, O 1s, C 1s spectra were measured.
- Sample was heated to 400 °C for two hours. Treatment No.5.
- XPS survey, Nb 3d, O 1s, C 1s spectra were measured.

As an example we present a deconvoluted niobium 3d XPS spectrum in

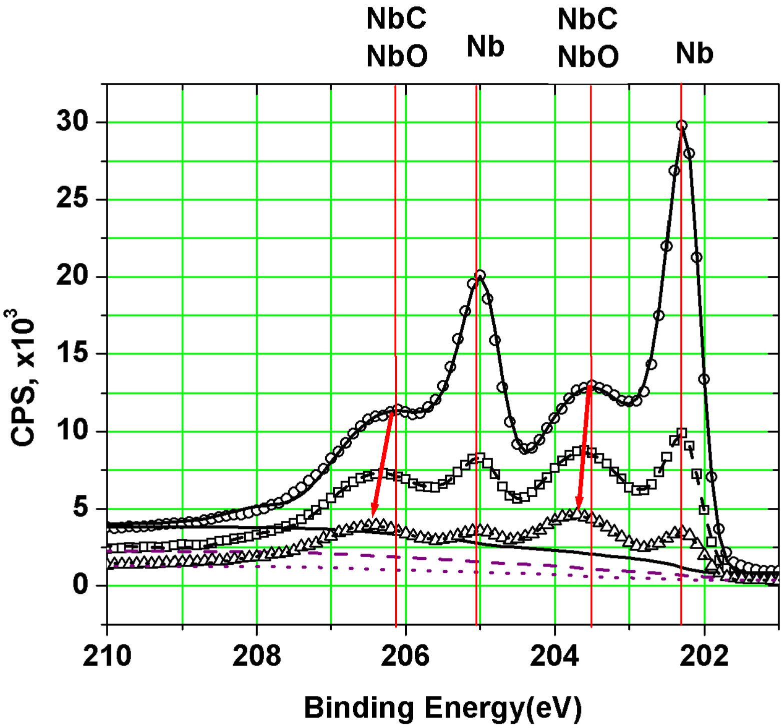

Figure 9.21: Angle-resolved XPS shows that NbO/NbC peak moves to the left as the angle becomes more grazing(peaks at 203.5 eV), whereas Nb peak does not move(peaks at 202.2 eV). This shows that carbide is located underneath the oxide.

Fig. 9.22.

Via deconvolution of niobium 3d spectrum we get an amount of signal coming from each oxidation state of niobium in percent. The results of deconvolution are presented in Fig. 9.23. In order to estimate thickness of corresponding layers, namely, oxide and carbide layers, one has to make an assumption about location of this layer. Angle-resolved study suggests that carbide is formed on the boundary between niobium and oxide, so we assumed a simplified picture of surface composition: the top layer is a composition of niobium oxides, under the oxide there is a uniform layer of niobium carbide, under the carbide resides pure metallic niobium. Assuming exponential decay of signal with depth with the constant λ = 2.725 nm, we estimated the thickness of niobium oxides and

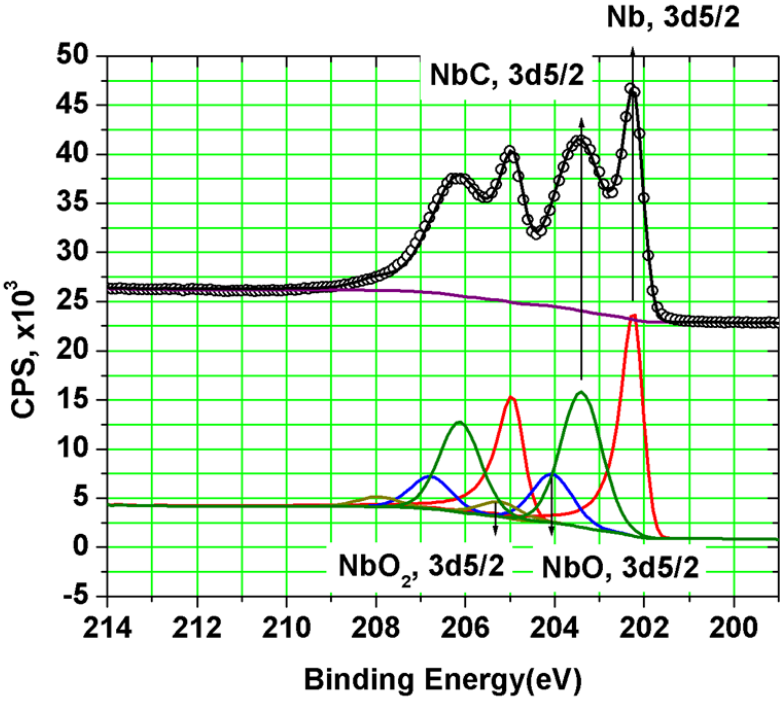

Figure 9.22: An example of niobium 3d spectrum after 400 °C baking for two hours with deconvolution.

carbide. The estimation allowed us to refine our initial picture of process occurring on niobium surface during 400 °C treatment.

XPS measurement of niobium sample as received suggest that niobium had about 4 nm of niobium oxide on top of niobium. During 400 °C baking niobium oxide is destroyed within first 30 min in agreement with Kirby results. But at the same time niobium carbide is being formed on niobium surface. We suggest that carbon is supplied not by ambient CO, generated in vacuum gauge filament, but rather is coming from bulk niobium due to surface attraction. Proposition is supported by Auger studies done J. Kaufmann. In his experiments he found that at elevated temperatures surface concentration of carbon increases with time, Fig. 9.24. So after heat treatment at 400 °C for two hours niobium oxide is destroyed and only one-two monolayers are on the surface, but copious

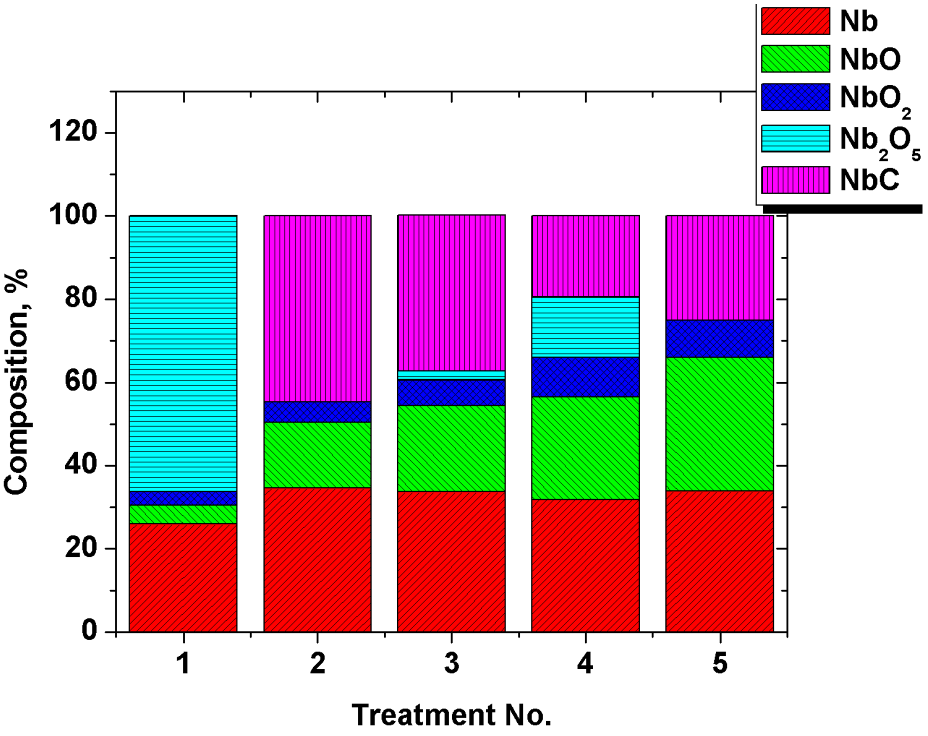

Figure 9.23: Relative percentage of different species after heat treatment.

amounts of carbide are formed.

Air exposure causes destruction of carbide and formation of niobium oxide due to higher binding energy of niobium oxide. Also air exposure causes conversion to high oxidation states. After 24 hours of air exposure there is about 1.5 nm of different niobium oxides and 1 nm of niobium carbide.

Another high temperature treatment destroys niobium oxides once again and cause reconstruction of niobium carbide. The crude picture of surface composition after studied treatments, as inferred from deconvoluted niobium 3d peaks, is presented in Fig. 9.25.

The other sample was a small-grain sample. Sample's dimensions were about 1 cm x 1 cm. The sample was polished with BCP and then electropolished for 50 μm . The following sequence of experiments was carried out onto the sample:

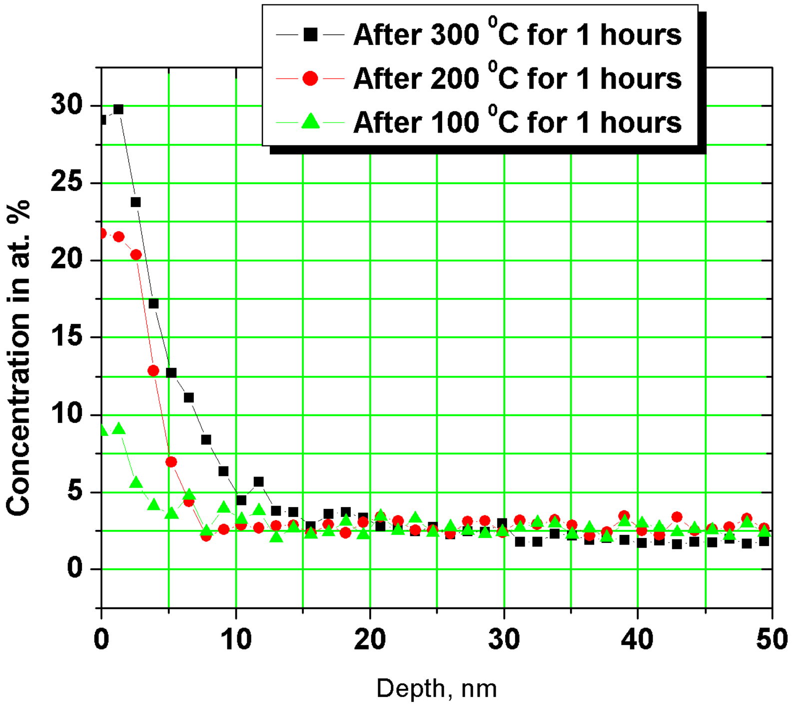

Figure 9.24: Auger studies show that near-surface concentration of carbon increase at elevated temperatures, suggesting migration of carbon to the surface.

- Sample was chemically etched. Treatment No.1.
- XPS survey, Nb 3d, O 1s, C 1s spectra were measured.
- Sample was heated to 450 °C for two hours. XPS Nb 3d spectrum was acquired during heating. Treatment No.2.
- XPS survey, Nb 3d, O 1s, C 1s spectra were measured.
- Sample was exposed to 150 Torr-sec of O_2. Treatment No.3.
- XPS survey, Nb 3d, O 1s, C 1s spectra were measured.
- Sample was exposed to air for 16 hours. Treatment No.4.
- XPS survey, Nb 3d, O 1s, C 1s spectra were measured.
- Sample was heated to 500 °C for two hours. Treatment No.5.
- XPS survey, Nb 3d, O 1s, C 1s spectra were measured.

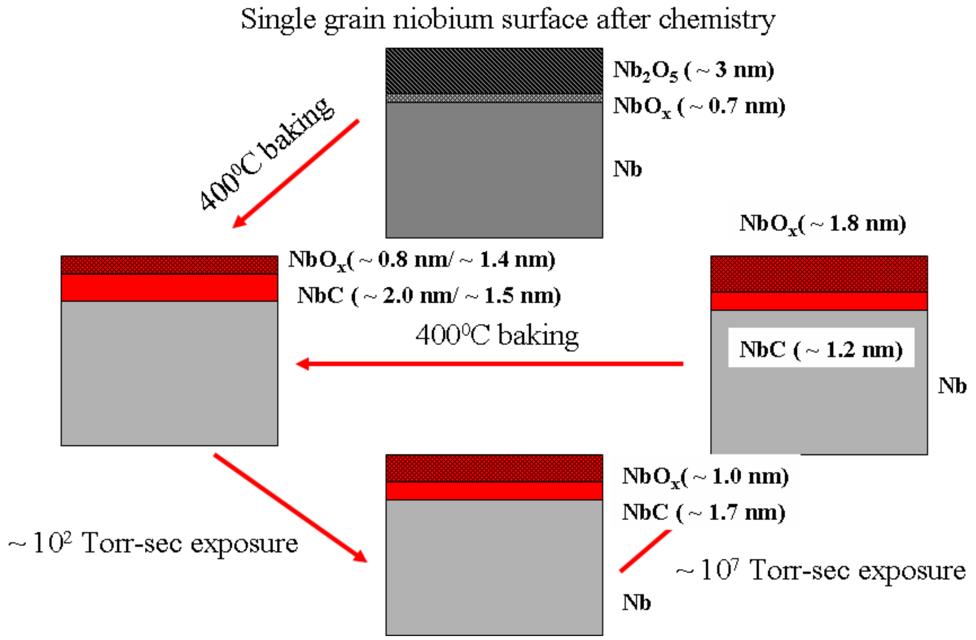

Figure 9.25: Composition of niobium surface after treatments as inferred from XPS results.

The initial composition of the surface for small grain sample was different, because it has a short air exposure and so the oxide-formation process was still going. As the results the sample has thiner oxide as was confirmed by XPS. The results of deconvolution of niobium 3d spectra are presented in Fig. 9.26.

In Fig. 9.27 under the same assumptions as for large-grain sample we present results for small-grain sample.

The XPS results with small-grain and large-grain samples, however, do not give us a hint about a possible cause for a strong degradation of superconducting cavity after short exposure to dry air. Neither NbO, nor NbO_2, NbC seemed to be responsible for such degradation. One question remains open: in the XPS study we noticed that peaks, e.g. for NbO, is not centered always at the same energy, but shifts by a fraction of eV after treatments. On the other hand niobium peak was centered at 202.23±0.05 in all measurements. Therefore we suggest that niobium surface composition is more complex and involves other niobium

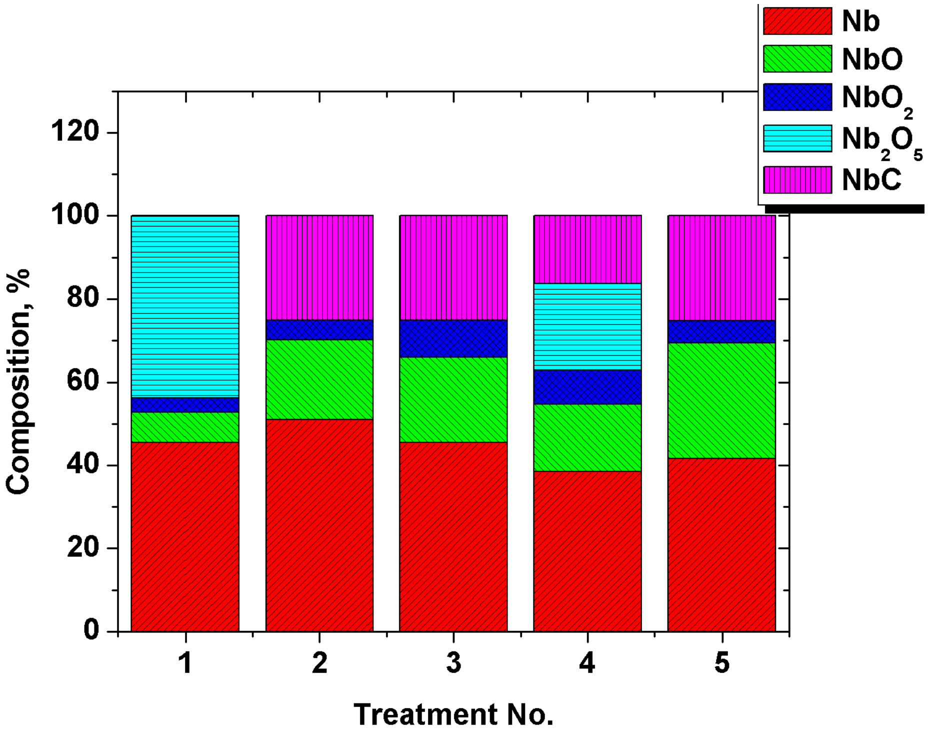

Figure 9.26: The relative intensities of different species as identified by deconvolution of niobium 3d spectrum.

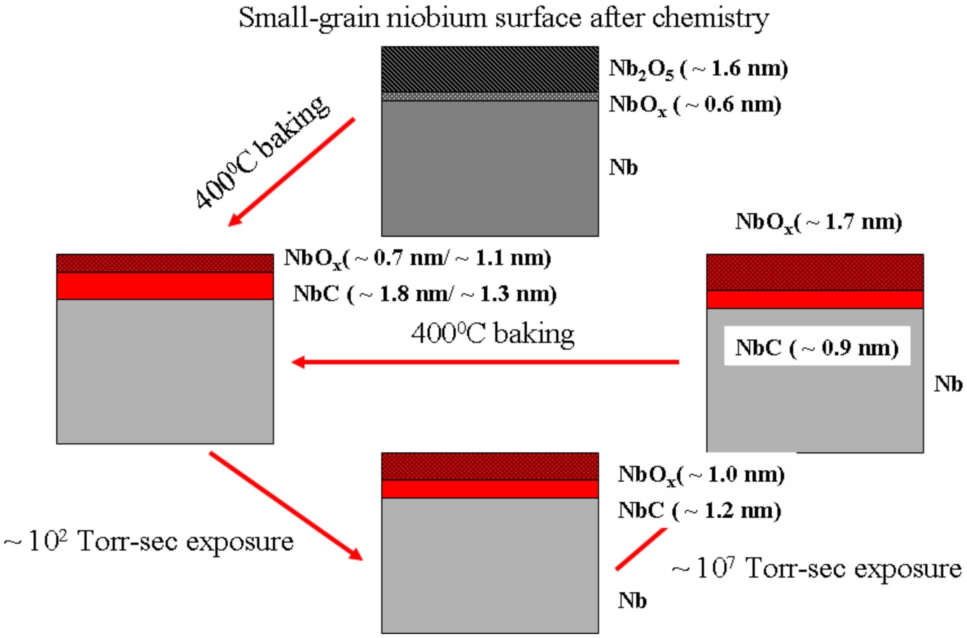

Figure 9.27: Composition of niobium surface after treatments as inferred from XPS results.

oxides. At this point, however, we cannot support this speculation with solid experimental results, as XPS instruments is not sensitive enough to resolve non-stoichiometric niobium oxides.

9.7 Summary

Our surface studies show that baking at 400 °C, which destroys Nb_2O_5 and NbO_2 does not increase residual resistance, but also does not affect medium or high field Q-slope. So we come to conclusion that Nb_2O_5 and NbO_2 are not responsible for degradation of the quality factor at high fields. The oxygen diffusion profile, which was calculated from the modified oxygen pollution model, suggests that amount of oxygen will be reduced after 400 °C baking, which means improvement in the high field performance. Such improvement was not observed in the experiment. So we suggest that the modified oxygen pollution model is wrong.

Following baking at 400 °C, defects are formed in several regions on the cavity surface. We do not understand the origin of these defects, but our surface studies have shown that baking at 400 °C causes diffusion of carbon to the surface and formation niobium carbide. We speculate that the formation of niobium carbide can be the cause for defects.

Air exposures to about 100 Torr-sec cause reduction in quality factor and strong slope with field. Our XPS surface studies show that such exposures will cause an increase in niobium oxide thickness and reduction in niobium carbide thickness. Air exposures to about 10^7 Torr-sec cause improvement in quality factor, but strong slope remains. Our XPS surface studies show that such long exposure will cause further increase in niobium oxide thickness and reduction in niobium carbide. We could not identify any particular species on the surface with change in RF performance. Though we believe that a variety of non-stoichiometric oxides were formed on the surface, some of which may be responsible for changes in RF performance of niobium, XPS is not sensitive enough to distinguish between them.

CHAPTER 10

SUMMARY

The high field Q-slope and the baking effect are some of the outstanding problems in the RF superconductivity. We carried out experiments to study the prevailing models for the high field Q-slope and the baking effect, which are:

- the interface tunnel exchange model, which predicts additional losses in superconducting niobium due to high electric field. In this model mild baking at 100 °C for 48 hours reduces the number of interface states due to changes in the oxide;

- the magnetic field enhancement model, which suggests early quenching at the edges of grain boundaries due to enhanced local magnetic field. The mild baking increases the critical field of the niobium;

- modified oxygen pollution model suggests that a thin($<$ 10 nm) pollution layer of oxygen exists under the oxide layer. The excess of oxygen depending on baking temperature either diffuses away into the bulk niobium or is re-enriched from the dissolution of the oxide layer. The predicted optimum temperature is 140 °C. The pollution layer increases RF losses;

- as an alternative to the modified oxygen pollution model we proposed a oxide-purifier model. In the model the mild baking reduces the impurity level, because impurities diffuse into oxide. Carbon, nitrogen or a similar impurity increases RF losses.

In order to test the magnetic field enhancement at grain boundary steps, losses in a large-grain cavity were measured with the thermometry system. We have not seen any preferential heating near grain boundaries in our test, which is in contradiction with the prediction from magnetic field enhancement model. Interface tunnel exchange is not related to the phenomenon of the high field

Q-slope, since in our experiments we never saw heating due to the high field Q-slope in the high electric field regions. The oxygen pollution model and the modified oxygen pollution model are also found to be in contradiction with anodizing experiments and systematic baking experiments. As a alternative to the modified oxygen pollution model an ″oxide-purified″ model was proposed.

10.1 High field losses

We established that anomalous losses in 1.5 GHz superconducting niobium cavities begin at 105±5 mT in all cavities, which we tested, after chemical treatment. The anomalous losses occur over broad regions of niobium surface with significant spatial variations. The overall slope in a given region depends on strength of magnetic field and is stronger where the overall magnetic field is stronger.

10.2 Mild baking

The anomalous losses at high field are reduced by heating niobium to 100-140 °C, but the effect is not reproducible in fine-grain cavities chemically polished by BCP, i.e. seemingly similar baking conditions produce different amounts of improvement. In our experiments our best result followed 105±5 °C for 48 hours. Baking at the higher temperatures($\sim 130 - 140$°C) has less effect. These results are consistent with the modified pollution model, however re-baking at 100 °C does not restore the baking benefit, which is contradictory to the modified pollution model. Mild baking has a greater effect on cavities polished by electropolishing(EP) method rather than by plain chemical polishing(BCP). Mild baking also has a greater effect on large-grain cavities. This suggests that smoother surfaces respond more strongly to the baking effect.

10.3 Anodizing and depth scale discovery

Our experiments show that a cavity should be anodized for 20-30 Volts in order to remove beneficial effect of heat treatment, which is equivalent to conversion of 15-22 nm of metallic niobium into loss-free pentoxide. Therefore the thickness of the niobium layer benefited by the mild baking at 100°C for 48 hours is between 15 and 22 nm(from the BCP cavity experiments). Increasing the oxide thickness up to 40 nm does not have any effect on the high field Q-slope, which contradicts the interface tunnel exchange model.

This result is consistent with the model that the cause for the change in high field Q-slope during mild baking is oxygen diffusion, though it is not clear within the modified oxygen pollution model, how anodizing re-generates the oxygen pollution layer. As an alternative model we propose oxide-purifier model, in which the oxide purifies adjacent niobium during the mild baking.

10.4 Large grain results

The quenching of the grain boundaries suggested by magnetic-field-enhancement model is rejected. In our experiments we did not observe any preferential heating at the grain boundaries as measured by thermometry system. Hence heating at the grain boundaries cannot explain the high field Q-slope.

10.5 High temperature baking

Our surface studies show that baking at 400 °C, which eliminates Nb_2O_5 and NbO_2 does not change the residual resistance, which is consistent with results by Palmer, but also does not affect medium or high field Q-slope. So we come to conclusion that Nb_2O_5 and NbO_2 are not responsible for degradation of the quality factor at high fields.

The oxygen diffusion profile, which was calculated from modified oxygen pollution model, suggests that amount of oxygen will be reduced after 400 °C baking, which means reduction of the high field Q-slope. Such improvement was not observed in the experiment. So we suggest that modified oxygen pollution model is wrong.

Following baking at 400 °C, defects are formed in several regions on the cavity surface. We do not understand the origin of these defects, but our surface studies have shown that baking at 400 °C causes diffusion of carbon to the surface and formation niobium carbide. We speculate that the formation of niobium carbide can be the cause for defects.

Air exposures to about 100 Torr-sec cause large reductions in quality factor and strong slope with field. Our XPS surface studies show that such exposures will cause increase in niobium oxide thickness and reduction in niobium carbide thickness. Air exposures to about 10^7 Torr-sec restore the low-field quality factor, but the strong slope remains. Our XPS surface studies show that such long exposure will cause further increase in niobium oxide thickness and reduction in niobium carbide. We speculate that a variety of non-stoichiometric oxides were formed on the surface due to the light exposure to oxygen, some of which may be responsible for changes in RF performance of niobium. XPS is not sensitive enough to distinguish between them.

BIBLIOGRAPHY

[1] H. Kamerlingh Onnes, ”Communications from the Physical Laboratory at the University of Leiden by Prof. Dr. H. Kamerlingh Onnes”, 108, 1908.

[2] H. Kamerlingh Onnes, ”Communications from the Physical Laboratory at the University of Leiden by Prof. Dr. H. Kamerlingh Onnes”, 119, 1908.

[3] H. Kamerlingh Onnes, ”Communications from the Physical Laboratory at the University of Leiden by Prof. Dr. H. Kamerlingh Onnes”, 124c, 1911.

[4] H. Kamerlingh Onnes, ”Communications from the Physical Laboratory at the University of Leiden by Prof. Dr. H. Kamerlingh Onnes”, 133d, 1913.

[5] H. Kamerlingh Onnes, ”Communications from the Physical Laboratory at the University of Leiden by Prof. Dr. H. Kamerlingh Onnes”, 139f, 1914.

[6] H. Kamerlingh Onnes, ”Communications from the Physical Laboratory at the University of Leiden by Prof. Dr. H. Kamerlingh Onnes”, 140b, 1914.

[7] W. Meissner and H. Franz, Messungen mit Hilfe von flussigen Helium. VIII. Supraleitfahigkeit von Niobium, Physikalisch-Technische Reichsanstalt, Mitteilung: 558-559, 1930.

[8] A. Inoue et al., J. Phys., Colloque-8. 41, 758, 1980.

[9] V. Novotny et al., J. Low Temp. Phys. 18, 147, 1975.

[10] W. Meissner and R.Ochsenfeld, ”Ein neuer Effekt bei Eintritt der Supraleitfahigkeit”, Naturwiss.,21, 787, 1933.

[11] C.J.Gorter and H.Casimir,”Zur Thermodynamik des supraleitenden Zustandes”, Zeitschr.f.techn.Physik, 15, 539, 1934.

[12] French, R.A., Cryogenics 8, 301, 1968.

[13] Alekseevskii, N.E. et al., Phys. Met. Metallogr. USSR, 37, 53, 1974.

[14] A.A.Abrikosov, On the Magnetic Properties of Superconductors of the Second Group, Soviet physics JETP, Volume 5, Number 6, December 15, 1957.

[15] D. Saint-JamesP. G.De Gennes, Onset of superconductivity in decreasing fields, Physics Letters, Volume 7, Issue 5, 15, Pages 306-308 December 1963.

[16] J. Bardeen, L.N. Cooper, and J.R. Schrieffer, Phys. Rev. 108, 1175 (1957).

[17] D.C. Mattis and J. Bardeen, Phys. Rev.,111:412,1958.

[18] H. Padamsee, J. Knobloch, T. Hays, RF Superconductivity for Accelerators, John Wiley and Sons, 1998.

[19] B. Bonin and R.W. Roeth, in Proceedings of the 5th Workshop on RF Superconductivity, DESY, Hamburg, Germany, 1991.

[20] T. Yogi, G.J. Dick and J.E. Mercereau, Critical rf Magnetic Fields for Some Type-I and Type-II Superconductors, Phys. Rev. Let., vol. 39, num. 13, 826-829, 1977

[21] T.Hays et al., in Proceedings of the 7th Workshop on RF Superconductivity, Gif-sur-Yvette, France, p.437(1995).

[22] R.L.Geng et al., Proceedings of PAC07, Albuquerque, New Mexico, USA, 2007.

[23] U. Kelin and D. Proch, in Proceedings of the Conference of Future Possibilities for Electron Accelerators, Charlottesville, 1979.

[24] P. Kneisel et al., Nucl. Instrum. Methods Phys. Res., 188:669, 1981.

[25] J.Knobloch, PhD Thesis, Cornell University, 1997.

[26] Rao C.N.R., Rao G.V. Subba, Transition metal oxides, Wash., 1974, 92-99(National Standard reference date system, v. 49)

[27] H. Diepers et al., Phys. Let., 37A, 139, 1971.

[28] K. Saito et al., SRF'1990,Tsukuba.

[29] R. Geng et al., In the Proceedings of Particle Accelerator Conference, Portland, Oregon, 2003.

[30] R. L. Geng, J. Knobloch, and H. Padamsee, Microstructures of rf surfaces in the electron-beam-weld regions of niobium, 9th Workshop on RF Superconductivity, 1999.

[31] K.Kovacs, G.Kiss, M. Stenzel and H. Zillgen, Jour. Elect. Soc., 150(8) B361-B366(2003).

[32] H. Martens, H. Diepers and R.K. Sun, Phys. Let. 34A, 439, 1971.

[33] K.C.Kalra, K.C.Singh and M.Singh, Ind. Jour. Chem., 36A 216-218, 1997.

[34] L. Young, Can. Jour. Chem., 38 1141-1146, 1960.

[35] P. Bauer et al., Physica C, 44, (2006).

[36] J. Vines et al., Systematic Trends for the Medium Field Q-Slope, 13th Workshop on RF Superconductivity, 2007.

[37] J.Knobloch, R.L.Geng, M.Liepe, and H.Padamsee, High field Q-slope in Superconducting Cavities Due to Magnetic Field Enhancement at Grain Boundaries, 9th Workshop on RF Superconductivity, 1999.

[38] B. Visentin et al.,EPAC 1998, Sweden, 1998.

[39] H. Safa, 9th Workshop on RF Superconductivity, 1999.

[40] W. DeSorbo, Phys. Rev., 132, 1, 107(1963).

[41] C.C. Koch et al., Phys. Rev. B, 9, 3, 888(1974).

[42] G. Ciovati, Applied Physics Letters 89,022507, 2006.

[43] L.Lilje, PhD Thesis, Universitaet Hamburg, 2001.

[44] G. Ciovati, Journal of Applied Physics, Vol. 96, Num. 3, 2004.

[45] P. Kniesel, 8th Workshop on RF Superconductivity, 1999.

[46] G. Ciovati et al., Phys. Rev. ST Accel. Beams 10, 062002, 2007.

[47] B. Visentin et al., Physica C vol.441, Issue 1-2, p.66-69, 2006.

[48] I. Arfaoui et al., J. Appl. Phys. 91, 9319,2002.

[49] H.Tian, SRF Material Workshop, 2007.

[50] R.W.Powers amd M.V.Doyle, J. Appl. Phys., 30 ,514, 1959.

[51] C.A.Wert, J. Appl. Phys., 21 ,1196, 1950.

[52] B. Bonin and H. Safa, Supercond. Sci. Technol. 4, 257 (1991).

[53] P.J. Lee et al., Physica C vol.441, Issue 1-2, p.126-129, 2006.

[54] P. Kneisel et al., Single Crystal Workshop, Brasil, 2006.

[55] J.C.Amato, SRF-840506, 1984.

[56] H.Padamsee, CLNS 80/469, 1980.

[57] F.L. Palmer, IEEE TRANSACTIONS ON MAGNETICS, VOL. MAG-23, NO. 2, MARCH 1987.

[58] F. Palmer and M. Tigner, IEEE TRANSACTIONS ON MAGNETICS, VOL. MAG-21, NO. 2,1011, 1985.

[59] Q. Ma et al., J. Appl. Phys., Volume 96, Issue 12, 2004.

[60] J. Halbritter, 10th Workshop on RF Superconductivity, 2001.

[61] R. Kirby et al., SLAC-TN-05-049, 2005.

[62] G.Eremeev et al., 12th Workshop on RF Superconductivity, 2005.

[63] J.Kaufman, personal communications.

[64] T.Schober and H. Wenzl, Hydrogen in Metals II, Topics in Applied Physics, Vol.29, p.32, 1978.